RAB5 ACTIVATION BY THE VPS9 DOMAIN

APPROVED BY SUPERVISORY COMMITTEE

Bruce Horazdovsky, Ph. D. _____

Michael Roth, Ph. D. _____

Melanie Cobb, Ph. D. _____

Stephen Sprang, Ph. D. _____

This dissertation is dedicated to my family,
without whose support and encouragement its
completion would not have been possible.

ACKNOWLEDGMENTS

I'd like to thank my committee members, Michael Roth, Melanie Cobb, Stephen Sprang and Bruce Horazdovsky. Though they were largely unaware of what they signed up for, in both content and duration, their commitment to the completion of these studies is appreciated. Within the Horazdovsky Lab, I am most indebted to Brian Davies for sharing his ideas, discussions, technical assistance, time and friendship. I also owe many thanks to Brad Bellin and Bob Sikkink for construct generation, protein expression and purification, and more. I thank these and other past and present members of the Horazdovsky Lab, especially Greg Tall, Andrew Friedberg, Justin Topp, Guo Chen, and Sandy Severson, and members of the David Katzmann Lab, especially Jackie Lee and Johanna Payne, for everything from scientific discussion and assistance to babysitting and general camaraderie. I thank Sherry Linander for all that she does for the lab and Shay Criss for coordinating the completion of my degree in absentia. I'd also like to thank my scientific collaborators, including Stephen Sprang, Brian Vash, and Xinlin Du for crystallization trials; Kevin Gardner for helping initiate NMR studies; Nenad Juranic and the Mayo Clinic NMR facility; and, most notably, Brian Volkman and Francis Peterson at the Medical College of Wisconsin for the bulk of our NMR data acquisition and continual assistance in analysis of this data. Most importantly, I thank Bruce Horazdovsky for teaching me about science, from yeast and lab techniques to business and political aspects, for allowing me to pursue areas of interest outside the established realm of the lab, for his patience and understanding during times of scientific and personal trials, for creating and maintaining a laboratory environment that was a pleasure in which to work, and for all the fantastic food and drink.

Personally, I thank my teachers and professors over the years, especially Paul Baur of Dickinson High School and Robert Blystone of Trinity University, for their part in shaping my interest in biology and research. I am lucky to have had friends like Tiffany, Joe, Amelia, the rest of the KYL crew, Bob, Jon, and Katie during my time in graduate school. I thank my family for their continuous support and encouragement, especially my brother and my parents, on whom I relied more than I ever expected I would. Finally, I thank Jessica for giving me the best gift I ever received, our wonderful son Landon.

RAB5 ACTIVATION BY THE VPS9 DOMAIN

by

DARREN SCOTT CARNEY

DISSERTATION

Presented to the Faculty of the Graduate School of Biomedical Sciences

The University of Texas Southwestern Medical Center at Dallas

In Partial Fulfillment of the Requirements

For the Degree of

DOCTOR OF PHILOSOPHY

The University of Texas Southwestern Medical Center at Dallas

Dallas, Texas

April, 2007

ABSTRACT

DARREN SCOTT CARNEY, Ph. D.

The University of Texas Southwestern Medical Center at Dallas, 2007

Supervising Professor: BRUCE F. HORAZDOVSKY, Ph. D.

The movement of proteins through the endocytic pathway is a complex and highly regulated process. Not only is this pathway used to internalize cellular nutrients, but it is also used to modulate a cell's response to extracellular stimuli. Internalization and subsequent trafficking of transmembrane receptor proteins that receive these signals from the external milieu play an essential role in establishing and maintaining cellular homeostasis. As key regulators of the early stages the endocytic pathway, the small GTPases of the Rab5 family serve an essential function in integrating intracellular protein traffic and these cell signaling events.

Rab5 proteins exert their influence on protein trafficking only when bound to GTP. A large family of proteins containing a conserved domain (Vps9) activate Rab5 by promoting the release of GDP and reloading of GTP. These nucleotide exchange factors contain additional domains which link them to specific cellular locations or signaling cascades. The multiplicity of these Rab5 proteins and exchange factors raises the question of how these proteins specifically interact to regulate individual trafficking events.

To investigate this specificity, the three Rab5 proteins of *Saccharomyces cerevisiae*, Vps21, Ypt52 and Ypt53, and the two yeast Vps9 domain-containing proteins, Vps9 and Muk1, were analyzed. This analysis identified previously unappreciated roles for Ypt53 and Muk1 in a relatively late stage of endocytosis. A mutational analysis of Vps9 identified several residues important for Vps9 domain function and shed light on a possible intramolecular regulation of this domain by the carboxy-terminal ubiquitin-binding CUE domain. Finally, structural studies of the Rab5/Vps9 domain complex were initiated to gain a better understanding of the molecular mechanisms by which Rab5 proteins interact with and are activated by the Vps9 domain.

TABLE OF CONTENTS

PUBLICATIONS

Relating to this dissertation:
Davies, B.A., J.D. Topp, A.J. Sfeir, D.J. Katzmann, **D.S. Carney**, G.G. Tall, A.S. Friedberg, L. Deng, Z. Chen, and B.F. Horazdovsky. (2003). Vps9p CUE domain ubiquitin binding is required for efficient endocytic protein traffic. J. Biol. Chem., 278, 19826-19833.

Davies, B.A., **D.S. Carney**, and B.F. Horazdovsky. (2005). Ubiquitin regulation of the Rab5 family GEF Vps9p, in Methods in Enzymology, GTPases Regulating Membrane Targeting and Fusion, Balch, Der, Hall, Editors. Elsevier Life Sciences, Vol. 403, Chapter 49, Pages 561-583.

Carney, D.S., B.A. Davies, and B.F. Horazdovsky. (2006). Vps9 domain-containing proteins: activators of Rab5 GTPases from yeast to neurons. Trends Cell Biol. 16, 27-35.

Davies, B.A., **D.S. Carney**, and B.F. Horazdovsky. (2007). Evaluating yeast biosynthetic vacuolar transport, in Methods in Cell Biology: Protein Targeting. Humana Press, Chapter 22.

Relating to this dissertation, in preparation:
Carney, D.S., B.A. Davies, B.J. Bellin, R.A. Sikkink, and B.F. Horazdovsky. Specificity of the yeast Rab5 family and their exchange factors.

Carney, D.S., F.C. Peterson, R.A. Sikkink, B.F. Volkman and B.F. Horazdovsky. NMR analysis of the Rab5 family/Vps9 domain interaction.

Davies, B.A., **D.S. Carney**, and B.F. Horazdovsky. Interdependence between Vps9 GEF and CUE domains.

Other publications:
Topp, J.D., **D.S. Carney**, and B.F. Horazdovsky. (2005). Biochemical characterization of Alsin, a Rab5 and Rac1 guanine nucleotide exchange factor, in Methods in Enzymology, GTPases Regulating Membrane Targeting and Fusion, Balch, Der, Hall, Editors. Elsevier Life Sciences, Vol. 403, Chapter 22, Pages 261-276.

Kim, K., D.A. Fancy, **D.S. Carney**, and T. Kodadek. (1999). Photoinduced Protein Cross-Linking Mediated by Palladium Porphyrins. J. Am. Chem. Soc., 121, 11896-11897.

FIGURES

Chapter 1

Chapter 2

Chapter 3

Chapter 4

TABLES

ABBREVIATIONS AND SYMBOLS

°	degree
Δ	gene deletion
2D	two-dimensional
3D	three-dimensional
aa	amino acid
AEBSF	4-(2-aminoethyl) benzenesulfonyl fluoride
BSA	bovine serum albumin
C	Celsius
CARA	Computer Aided Resonance Assignment
CD	circular dichroism
CPS	Carboxypeptidase S
CPY	Carboxypeptidase Y
CUE	coupling of ubiquitin ER to degradation domain
DH	Dbl homology
DNA	deoxyribonucleic acid
DTT	dithiothreitol
E.	*Escherichia*
EDTA	ethylenediaminetetraacetic acid
EEA1	early endosome antigen 1
ER	endoplasmic reticulum
ESCRT	endosomal sorting complex required for transport
FPLC	fast protein liquid chromatography
g	gram
g	force of gravity
GAP	GTPase activating protein
GARANT	General Algorithm for Resonance Assignment
GDP	guanosine-5'-diphosphate
GEF	guanine nucleotide exchange factor
GFP	green fluorescent protein

GGA	Golgi-localizing, γ-adaptin ear homology domain, ARF-binding proteins
GppNHp	5'-guanylylimidodiphosphate
GST	glutathione S-transferase
GTP	guanosine-5'-triphosphate
HA	influenza hemagglutinin epitope
HOPS	homotypic fusion and vacuole sorting
HRP	horseradish peroxidase
HSQC	heteronuclear single quantum correlation
IPTG	isopropyl β-d-thiogalactoside
kDa	kilodalton
L	liter
LB	Luria-Bertani
M	molar
mant	*N*-methylanthraniloyl
MBP	maltose binding protein
mCPS	mature vacuolar CPS
mCPY	mature vacuolar CPY
mg	milligram
MHCI	major histocompatibility complex class I
ml	milliliter
mM	millimolar
Muk	computationally linked to Kap95
MVB	multivesicular body
nm	nanometer
NMDA	N-methyl-D-aspartate
NMR	nuclear magnetic resonance
OD_{600}	optical density (absorbance) at 600nm
p1CPY	ER-modified CPY precursor
p2CPY	Golgi-modified CPY precursor
PAGE	polyacrylamide gel electrophoresis
PBS	phosphate buffered saline

PBST	phosphate buffered saline with Tween-20
pCPS	precursor CPS
PCR	polymerase chain reaction
Pep	carboxypeptidase Y-deficient
PH	Pleckstrin homology
RA	Ras association
Rabex5-T	trypsin fragment of Rabex-5
S.	*Saccharomyces*
SDS	sodium dodecyl sulfate
SH2	Src homology 2
SMART	Simple Modular Architecture Research Tool
SNARE	soluble N-ethylmaleimide-sensitive factor attachment protein receptor
Ste	Sterile
TEV	tobacco etch virus
Ub	ubiquitin
UBA	Ubiquitin associated
uv	ultraviolet
VPS	vacuolar protein sorting
XEASY	ETH Automated Spectroscopy for X Windows
Ypt	yeast protein (requred for transport)
μg	microgram
μM	micromolar

CHAPTER ONE

Introduction and Literature Review

Overview

Endocytosis of cell surface receptors plays an important role in regulating cell signaling cascades. Regulating the movement of receptors and other signaling proteins through the endocytic pathway, therefore, has a direct impact on cellular homeostasis. The small GTPase Rab5 is a crucial regulatory component of the endocytic pathway. Activation of Rab5 is mediated by guanine nucleotide exchange factors (GEFs) that generate the Rab5•GTP complex. A large number of proteins have been identified that contain a specific, highly conserved domain (Vps9) that catalyzes nucleotide exchange on Rab5, linking the regulation of cell signaling cascades with intracellular receptor trafficking through the endocytic pathway.

Vacuolar protein sorting and endocytosis

The yeast vacuole is the structural and functional analog of the mammalian lysosome (Klionsky, Herman et al. 1990), and the study of vacuolar protein delivery has played a key role in our understanding of the trans-acting

cellular machinery involved in the process in both yeast and mammalian cells. Among other functions, this large acidic organelle is responsible for degradation of proteins. Biosynthetic delivery of resident hydrolases to the vacuole begins as part of the secretory pathway, with proteins entering the endoplasmic reticulum (ER) and progressing through the Golgi (Stevens, Esmon et al. 1982). Here vacuolar cargo must be actively diverted from the secretory pathway. Importantly, defects in sorting from the Golgi to the vacuole result in an accumulation of vacuolar cargo in this organelle which is then delivered to the cell surface via the secretory pathway. This unintended delivery of hydrolases, especially carboxypeptidase Y (CPY), to the cell surface was the basis of several genetic selections (Bankaitis, Johnson et al. 1986; Rothman and Stevens 1986) that identified thousands of mutants that were then gathered into over 50 vacuolar protein sorting (*vps*) complementation groups. The examination of these mutants has helped identify much of the machinery involved in delivery to the vacuole and, by analogy, the lysosome.

The *vps* mutants were originally classified into six classes (A through F) according to their vacuolar morphology by electron microscopy, and further scrutiny has revealed that these classes correlate well with their sites of action (Figure 1). Class D *vps* mutants display an enlarged vacuole and affect transport of vesicles from the Golgi to endosomes. Proteins defective in Class D mutants include the yeast Rab5 ortholog Vps21 (Horazdovsky, Busch et al. 1994) and its

exchange factor Vps9 (Burd, Mustol et al. 1996; Hama, Tall et al. 1999) and the SNARE (soluble N-ethylmaleimide-sensitive factor attachment protein receptor) Pep12 (Vps6) (Becherer, Rieder et al. 1996). Class B *vps* mutants display a fragmented vacuole and affect retrograde trafficking from the endosome to the Golgi. Proteins defective in Class B mutants include a complex known as the retromer which consists of two subcomplexes (Vps5/Vps17, and Vps26/Vps29/ Vps35) and is responsible for recycling the CPY receptor, Vps10 (Horazdovsky,

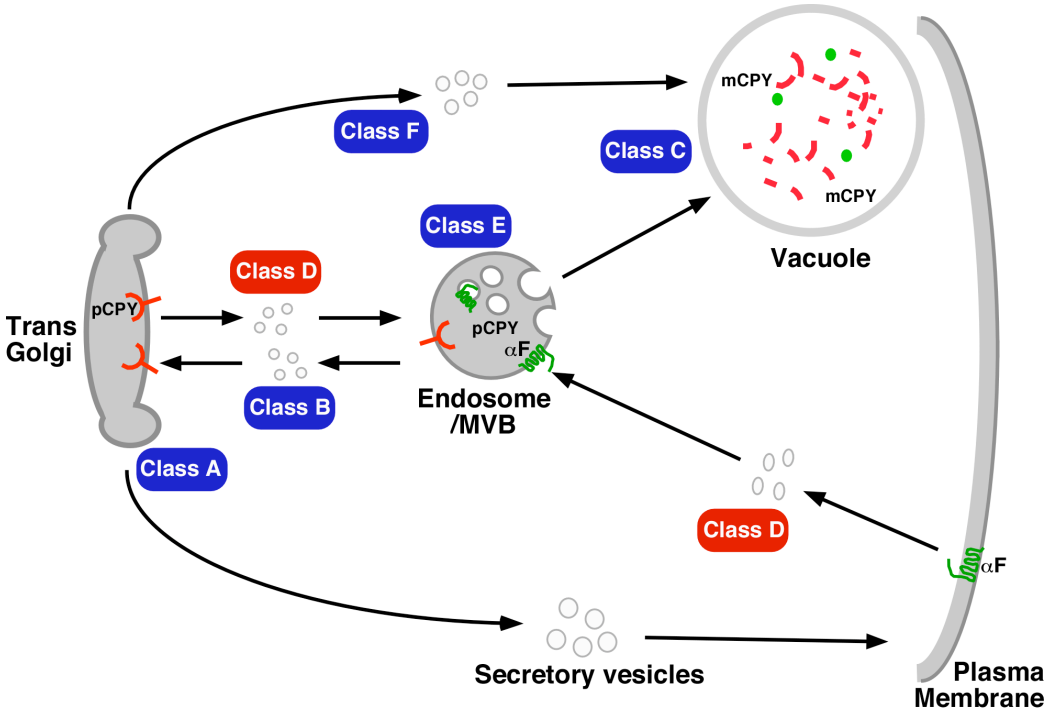

Figure 1. Vacuolar protein sorting and endocytosis. Vacuolar protein sorting (*vps*) mutants are grouped according to vacuolar morphology and the protein's site of action, as described in the text. Class D Vps proteins (red), including the yeast Rab5 protein Vps21 and its GEF Vps9, coordinate the intersection of the biosynthetic pathway used to sort vacuolar hydrolases like CPY (precursor, pCPY, and mature, mCPY) and the endocytic pathway used to endocytose receptors like the mating factor (α-factor, αF) receptor Ste2.

Davies et al. 1997; Seaman, McCaffery et al. 1998). Class A mutants exhibit wild-type morphology and appear to be primarily involved in vacuolar protein recognition events.

Class E *vps* mutants display a unique perivacuolar compartment and many affect the formation of multivesicular bodies (MVBs), the process by which membrane-associated proteins can be delivered to the lumen of the vacuole, and not the limiting membrane. Proteins defective in Class E mutants include the subunits of three ESCRT (endosomal sorting complex required for transport) complexes (Katzmann, Babst et al. 2001; Babst, Katzmann et al. 2002; Babst, Katzmann et al. 2002). The sequential action of the ESCRTs recognize ubiquitinated cargo proteins trafficked from either the Golgi (carboxypeptidase S, CPS) or the plasma membrane (mating factor receptors Ste2 and Ste3) and incorporate this cargo into vesicles that bud into the lumen of the MVB. The MVB is likely the compartment where the Golgi derived biosynthetic pathway and the endocytic pathways merge.

Class C *vps* mutants display no identifiable vacuole and affect the final transport step, delivery of the MVB to the vacuole. Most of the proteins defective in Class C mutants make up the HOPS (homotypic fusion and vacuole sorting) complex, which acts through Vps39 as a GEF for the Rab Ypt7 that directs the targeting and fusion of the MVB with the vacuole (Seals, Eitzen et al. 2000; Wurmser, Sato et al. 2000). Finally, Class F *vps* mutants display an intermediate

morphology and affect a pathway that bypasses endosomal intermediates and sorts vesicles directly from the Golgi to the vacuole (Odorizzi, Cowles et al. 1998).

It is quite clear that the vacuolar protein sorting pathway and the endocytic pathway are intertwined. After transport to the plasma membrane via the secretory pathway, the α-factor receptor Ste2 and the a-factor receptor Ste3 are ubiquitinated by Rsp5 in a ligand-dependent and constitutive manner, respectively (Rotin, Staub et al. 2000). After ubiquitination, they are transported to an early endocytic compartment, which is ill-defined in yeast but may be marked by the t-SNARE Tlg1 (Prescianotto-Baschong and Riezman 2002), and transported to the late endosome/MVB in a process dependent on Class D Vps proteins, including Vps21 and Vps9, and internalized as mentioned above by Class E Vps proteins for delivery to the vacuole by Class C Vps proteins.

The Rab5 Family

Rab proteins comprise the largest class within the Ras GTPase superfamily of small GTPases. Yeast contain eleven Rabs, and more than 60 have been identified in mammals (Bock, Matern et al. 2001). Rab proteins generally act as specific regulators of intracellular protein and membrane trafficking events. Rab5 has long been known to orchestrate the initial trafficking steps of the endocytic pathway. It is required for targeting and fusion of endocytic vesicles to

early endosomes and also for homotypic fusion of these endosomes (Gorvel, Chavrier et al. 1991; Bucci, Parton et al. 1992). Furthermore, Rab5 can stimulate motility of early endosomes along microtubules (Nielsen, Severin et al. 1999) and has even been shown to direct signaling from the endocytic pathway to the nucleus (Zerial and McBride 2001).

In mammalian systems, three isoforms of Rab5 (a, b, and c) have been documented (Bucci, Lutcke et al. 1995), and several specific functions have been attributed to distinct isoforms. For example, Rab5a can potentiate EGFR endocytosis, but Rab5b and Rab5c cannot (Barbieri, Roberts et al. 2000). In contrast, Rab5b alone has been implicated in neuroprotection against N-methyl-D-aspartate (NMDA) excitotoxicity (Arnett, Bayazitov et al. 2004). The Rab5 isoforms may also be differentially regulated through signaling kinase-dependent phosphorylation, though the functional significance of these phosphorylation events is unknown (Chiariello, Bruni et al. 1999). The yeast *Saccharomyces cerevisiae* similarly contains three Rabs that show strong homology with Rab5: Vps21 (also called Ypt51), Ypt52, and Ypt53 (Singer-Kruger, Stenmark et al. 1994). Like Rab5, Vps21 is required for endocytic transport (Gerrard, Bryant et al. 2000); however, Vps21 is also responsible for delivery of biosynthetic cargo from the Golgi to endosomes (Horazdovsky, Busch et al. 1994; Singer-Kruger, Stenmark et al. 1994; Gerrard, Bryant et al. 2000). While disruption of Vps21 function has the most severe consequences, studies suggest that Ypt52 and Ypt53

function may be partially redundant with Vps21 (Singer-Kruger, Stenmark et al. 1994).

Phylogenetic analysis of the human Rab family suggests that Rab21, Rab22a and Rab22b may also be grouped with the Rab5 proteins (Pereira-Leal and Seabra 2001). All three have been colocalized with Rab5 and its effectors on early endocytic compartments (Mesa, Salomon et al. 2001; Rodriguez-Gabin, Cammer et al. 2001; Kauppi, Simonsen et al. 2002; Simpson, Griffiths et al. 2004), and mutants of these Rabs disrupt traffic through the endocytic pathway (Mesa, Salomon et al. 2001; Kauppi, Simonsen et al. 2002; Simpson, Griffiths et al. 2004; Mesa, Magadan et al. 2005). However, unlike the Rab5 proteins, Rabs 21, 22a and 22b have also been localized to the trans-Golgi (Rodriguez-Gabin, Cammer et al. 2001; Kauppi, Simonsen et al. 2002; Simpson, Griffiths et al. 2004), and Rabs 22a and 22b have been implicated in regulating endosome-to-Golgi and Golgi-to-endosome traffic, respectively (Rodriguez-Gabin, Cammer et al. 2001; Mesa, Magadan et al. 2005). Additionally, a role for Rab22a in recycling major histocompatibility complex class I (MHC1) from endosomes to the plasma membrane has been indicated (Weigert, Yeung et al. 2004). While definitive roles for these Rabs are yet to be completely established, the common thread of these observations is that Rab21, Rab22a and Rab22b can associate with endosomal compartments that also contain Rab5. Additional studies will be needed to better define the functional relationships between these six closely related proteins.

The Vps9 Domain

Rab proteins are regulated through the binding of guanine nucleotides and are active when bound to GTP. Rab5 activation by GTP binding is required to complete vesicle targeting and fusion events. Expression of a Rab5 mutant with decreased affinity for GTP (S34N; dominant negative allele) inhibits endocytic fusion events; moreover, expression of a mutant form of the protein with a decreased intrinsic rate of GTP hydrolysis (Q79L; constitutively active allele) promotes endosome fusion events (Stenmark, Parton et al. 1994).

How then is the Rab5 nucleotide state modulated? The activity of Rabs, as with all small GTPases, can be negatively regulated by GTPase-activating proteins (GAPs), which accelerate the intrinsic rate of GTP hydrolysis, and positively regulated by guanine nucleotide exchange factors (GEFs), which stimulate the release of GDP allowing GTP to bind anew. GEFs act upon very specific Rab proteins or Rab protein subfamilies and show very little sequence similarity or functional overlap. In contrast, most GEFs for the Ras, Rho, and Arf families of small GTPases contain easily identifiable nucleotide exchange domains -- Cdc25, Dbl homology (DH)/Pleckstrin homology (PH), and Sec7 domains respectively (Cherfils and Chardin 1999).

In the case of the Rab5 family, Rabex5 and Vps9 were identified as GEFs for Rab5 and Vps21 and found to share a region of homology now known as the

Vps9 domain (Burd, Mustol et al. 1996; Horiuchi, Lippe et al. 1997; Hama, Tall et al. 1999). This domain was also found in another protein, Rin1, which was shown to exhibit Rab5-specific GEF activity as well, establishing this region of homology as the modular Rab5 GEF domain (Burd, Mustol et al. 1996; Han, Wong et al. 1997; Horiuchi, Lippe et al. 1997; Tall, Barbieri et al. 2001). The SMART and Pfam databases (Bateman, Coin et al. 2004; Letunic, Copley et al. 2004) now show that Vps9 domain-containing proteins are widely conserved in eukaryotes, including two *S. cerevisiae* proteins (Vps9 and Muk1), three *C. elegans* proteins (RME-6, RABX-5 and CE23604), four *D. melanogaster* proteins (Sprint, CG9139-PA, CG1657-PA, and CG7158-PA) and at least nine different human proteins (Figure 2). Currently, Rab5 GEF activity has been demonstrated

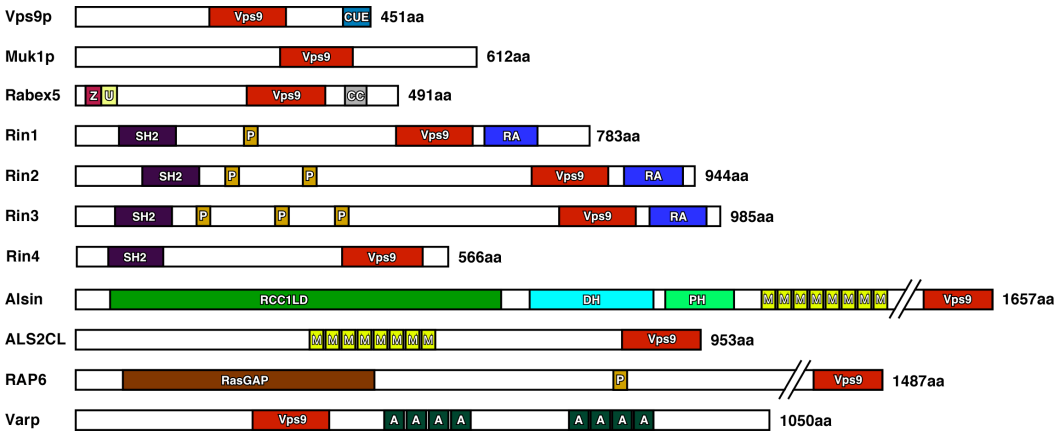

Figure 2. Vps9 domain-containing proteins. Shown are the known *Saccharomyces cerevisiae* and human proteins that contain Vps9 domains. These proteins contain additional functional domains including: coupling of ubiquitin conjugation to ER degradation (CUE), A20 zinc finger (Z), motif interacting with ubiquitin (MIU, U), coiled coil (CC), Src-homology 2 (SH2), Proline-rich (P), Ras Association (RA), RCC1-like (RCC1LD), Dbl Homology (DH), pleckstrin homology (PH), Membrane Occupation and Recognition Nexus (MORN, M), RasGAP and ankyrin (A).

for nine of these Vps9 domain-containing proteins (Horiuchi, Lippe et al. 1997; Hama, Tall et al. 1999; Tall, Barbieri et al. 2001; Saito, Murai et al. 2002; Kajiho, Saito et al. 2003; Otomo, Hadano et al. 2003; Hadano, Otomo et al. 2004; Zhang, He et al. 2006; Lodhi, Chiang et al. 2007).

The recent biochemical analysis of the Vps9 domain of Rabex5 has further demonstrated the specificity of the Vps9 domain. Tested against 31 different mammalian Rabs, the Vps9 domain of Rabex5 showed GEF activity on only Rab5, Rab21, and more weakly Rab22 (Delprato, Merithew et al. 2004). The differential activities toward Rab21 and Rab22 were unexpected as phylogenetic analysis suggests that Rab22 is more closely related to Rab5 than is Rab21 (Pereira-Leal and Seabra 2001); however, the ability of the Rabex5 Vps9 domain to activate both Rab21 and Rab22 supports the concept that Rab21 and Rab22 represent more highly diverged members of the Rab5 family rather than entirely distinct Rab groups.

Detailed kinetic studies of Vps9 and Rabex5 indicate that these proteins have lower exchange activity than GEFs for other small GTPases (Esters, Alexandrov et al. 2001). Interestingly, the Vps9 domain of Rabex5 has a significantly higher activity than full-length Rabex5 (Delprato, Merithew et al. 2004), and the activity of full-length Rabex5 is enhanced when in complex with Rabaptin5 (Lippe, Miaczynska et al. 2001) (see below). These observations suggest that the Vps9 domain may be prone to intramolecular modulation to allow

for robust and appropriate Rab5 activation. Moreover, the presence of other signaling domains within Vps9 domain-containing proteins suggests that these GEFs may serve to integrate Rab5 activation with signal transduction cascades, as discussed below.

Ubiquitin-dependent regulation of Vps9

The yeast *S. cerevisiae* offers a model system for understanding the regulation of these Rab5 GEFs through the study of Vps9. A 42 residue motif (CUE domain) was identified in the carboxy-terminus of Vps9 (Ponting 2000) and was found to be necessary and sufficient for Vps9 binding to ubiquitin (Davies, Topp et al. 2003; Donaldson, Yin et al. 2003; Shih, Prag et al. 2003). The CUE domain of Vps9 binds ubiquitin more strongly than other ubiquitin binding domains (Prag, Misra et al. 2003; Shih, Prag et al. 2003), and structural analyses of the CUE domains of Vps9 and Cue2 shed light on this disparity. The CUE domains of Cue2 bind ubiquitin as monomers similar to the interaction of the ubiquitin associated (UBA) domain with ubiquitin (Kang, Daniels et al. 2003). In contrast, crystal structure determination of the Vps9 CUE domain in complex with ubiquitin revealed that the Vps9 CUE domain dimerizes to form an additional higher affinity ubiquitin binding pocket (Prag, Misra et al. 2003).

Ubiquitin was previously known to play an important role in the yeast endocytic pathway, serving roles both early in the process as a signal for receptor

internalization as well as late in the pathway as a tag for sorting into multivesicular bodies (reviewed in (Haglund, Di Fiore et al. 2003; Hicke and Dunn 2003)). However, Vps9 was thought to function at another stage in the pathway, regulating fusion of the endocytic vesicles with the early endosome (Burd, Mustol et al. 1996; Hama, Tall et al. 1999). To address the requirement for Vps9 ubiquitin binding in endocytic transport, the trafficking of pheromone receptors (Ste2 and Ste3) was examined in yeast with point mutations in or lacking the Vps9 CUE domain. These analyses identified defects in pheromone receptor transport to the vacuole, indicating that the CUE domain positively regulates Vps9 function in the endocytic pathway (Davies, Topp et al. 2003; Donaldson, Yin et al. 2003). Furthermore, mutations that specifically interfere with the CUE dimer ubiquitin binding, but not CUE monomer ubiquitin binding, demonstrate the requirement for the high affinity ubiquitin binding pocket of the Vps9 dimer in efficient vacuolar transport of receptors (Prag, Misra et al. 2003). Ubiquitin binding appears to regulate Vps9 by localizing the GEF to internalized ubiquitinated receptors (Figure 3).

A second level of Vps9 regulation may occur through the covalent modification of this ubiquitin binding protein with ubiquitin. A portion (~10 percent) of the Vps9 pool is covalently modified with ubiquitin, with monoubiquitination the predominant form (Davies, Topp et al. 2003; Shih, Prag et al. 2003). Moreover, ubiquitin binding by the CUE domain is required for Vps9

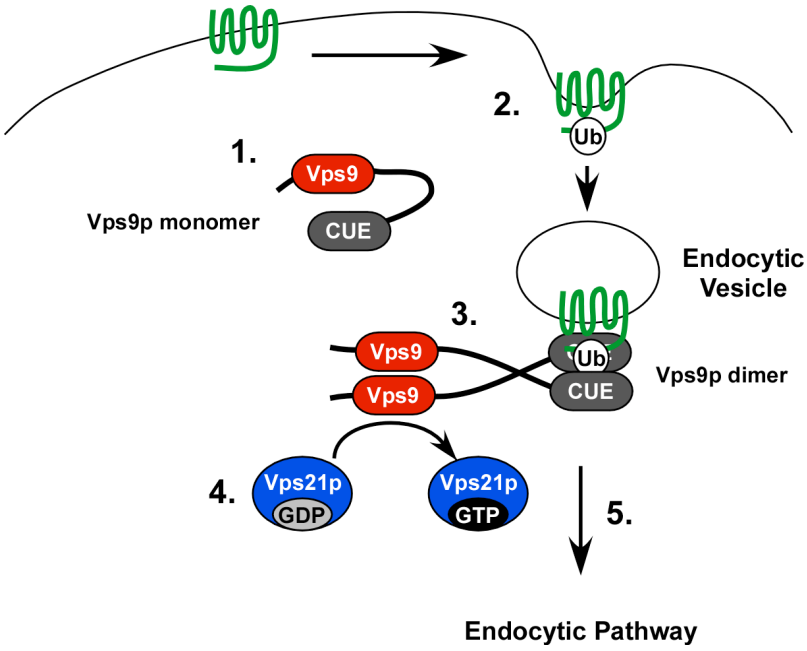

Figure 3. Ubiquitin Regulates Vps9 endocytic function. Ubiquitin binding potentiates Vps9 endocytic function in yeast. (1) The yeast Rab5 family GDP–GTP exchange factor (GEF) Vps9 harbors both the Vps9 domain and the ubiquitin-binding CUE domain. Vps9 predominantly exists as a monomer in the cytoplasm. (2) Ubiquitination of yeast pheromone receptors (green) promotes internalization and results in local concentration of ubiquitin on the endocytic vesicle. (3) Vps9 forms a dimer to bind to these ubiquitinated receptors by means of the CUE domain. (4) The recruitment of Vps9 leads to enhanced activation of the Rab protein Vps21 by means of the Vps9 domain, thereby promoting fusion with the early endosome (5). Thus, ubiquitin binding by the CUE domain potentiates Vps9 function in endocytosis to facilitate pheromone receptor degradation.

ubiquitination (Davies, Topp et al. 2003; Prag, Misra et al. 2003; Shih, Prag et al. 2003). Importantly, the levels of Vps9 in cells are unaffected by its ability to be covalently modified with ubiquitin. Monoubiquitination may be regulating Vps9's guanine nucleotide exchange or ubiquitin binding activities rather than modulating protein turnover. Ubiquitination was found to be dependent on Rsp5, a HECT domain ubiquitin ligase that modifies both cargoes and machinery of the

endocytic and biosynthetic pathways to the vacuole. The CUE domain of Vps9 may mediate an association with Rsp5 to promote an intramolecular ubiquitination event (Shih, Prag et al. 2003); a second possibility is that the CUE domain serves to localize Vps9 to an endocytic compartment containing ubiquitinated receptors whereon ubiquitination of the exchange factor itself occurs. While the ubiquitination of Vps9 appears to be significant, the issue yet to be addressed is if the Vps9 ubiquitination alters either its ability to bind ubiquitinated cargoes or its exchange activity toward Vps21. A third allosteric mechanism involving the CUE domain also appears to be regulating Vps9, and will be the focus of the latter half of Chapter 3.

Rabex5 and Rabaptin5

In mammalian systems, Rabex5 is a potent Rab5 exchange factor. Unlike the ubiquitin-dependent modulation of Vps9, Rabex5 is modulated by the Rab5 effector Rabaptin5. Rabaptin5 interacts with GTP-bound Rab5 via its carboxy terminus and has been shown to homo-oligomerize in solution (Vitale, Rybin et al. 1998). Structural studies revealed that Rabaptin5 forms a dimer that binds two Rab5•GTP molecules (Zhu, Zhai et al. 2004). Rabaptin5 has also been demonstrated to bind Rabex5 (Horiuchi, Lippe et al. 1997). What are the ramifications of this Rabex5/Rabaptin5 complex? First, Rabaptin5 potentiates Rabex5 guanine nucleotide exchange activity towards Rab5 (Lippe, Miaczynska

et al. 2001), though the mechanism generating this enhanced activity is unclear. Second, Rabex5 and Rabaptin5 may be part of the effector machinery that docks and fuses Rab5 vesicles with the endosome. For example, the association of Rabaptin5 with endosomes is dependent on the presence of Rabex5 (Lippe, Miaczynska et al. 2001). Rabaptin5 has also been found in an endosomal complex that includes another Rab5 effector, early endosome antigen 1 (EEA1), as well as NEM-sensitive factor (NSF) (McBride, Rybin et al. 1999). In addition, Rabaptin5 associates with the GGAs (Golgi-localizing, γ-adaptin ear homology domain, ARF-binding proteins) and the γ1-adaptin and γ2-adaptin subunits of AP-1 (adaptor protein 1) complex (Hirst, Lui et al. 2000; Zhu, Doray et al. 2001; Shiba, Takatsu et al. 2002; Mattera, Arighi et al. 2003), suggesting that Rabaptin5 may also direct the Rabex5/Rabaptin5 complex to vesicles from the trans-Golgi network destined to fuse with the endosome (reviewed in (Bonifacino 2004)). And finally, Rabaptin5 has been found to bind a subset of other GTP-bound Rab proteins, including Rab4, Rab1, Rab3 and Rab33b (Vitale, Rybin et al. 1998; Valsdottir, Hashimoto et al. 2001). Whereas Rab5 regulates traffic into the early endosome, Rab4 has been implicated in recycling receptors from the endosome to the plasma membrane (van der Sluijs, Hull et al. 1992); thus, Rabaptin5 may also serve to link Rab5 with consecutively functioning Rab proteins. The variety of interactions suggest that the Rabex5/Rabaptin5 complex may function to initiate and propagate microdomains of activated Rab5 for both biosynthetic and

endocytic trafficking to the endosome in mammals, analogous to the role of Vps9 as the activator of Vps21 in both biosynthetic and endocytic pathways in yeast.

Rin1, Ras and the EGF Receptor

In contrast to the general role ascribed to Rabex5, the Rab5 GEFs of the Rin (Ras interaction/interference) family appear to regulate the trafficking of specific proteins to the endosome in response to external stimuli. The best characterized is Rin1, which impacts the intracellular trafficking of the epidermal growth factor receptor (EGFR). In addition to its Rab5 GEF activity, Rin1 can directly associate with both activated EGFR through its amino-terminal SH2 domain(Barbieri, Kong et al. 2003)and GTP-bound H-Ras through its carboxy-terminal Ras Association (RA) domain (Han and Colicelli 1995; Wang, Waldron et al. 2002). Binding activated Ras potentiates Rin1 GEF activity (Tall, Barbieri et al. 2001)and may contribute to the membrane recruitment of Rin1. These properties appear to link the activation of EGFR with its subsequent endocytosis and down-regulation (Figure 4).

The endocytosis of EGFR has long been known to be stimulated by activated Ras and is dependent on Rab5 activation (Bar-Sagi and Feramisco 1986; Li, D'Souza-Schorey et al. 1997; Barbieri, Kohn et al. 1998; Barbieri, Roberts et al. 2000). While overexpression of either Rin1 or activated Ras increases EGF uptake, coexpression of these two potentiates the endocytosis enhancement (Tall,

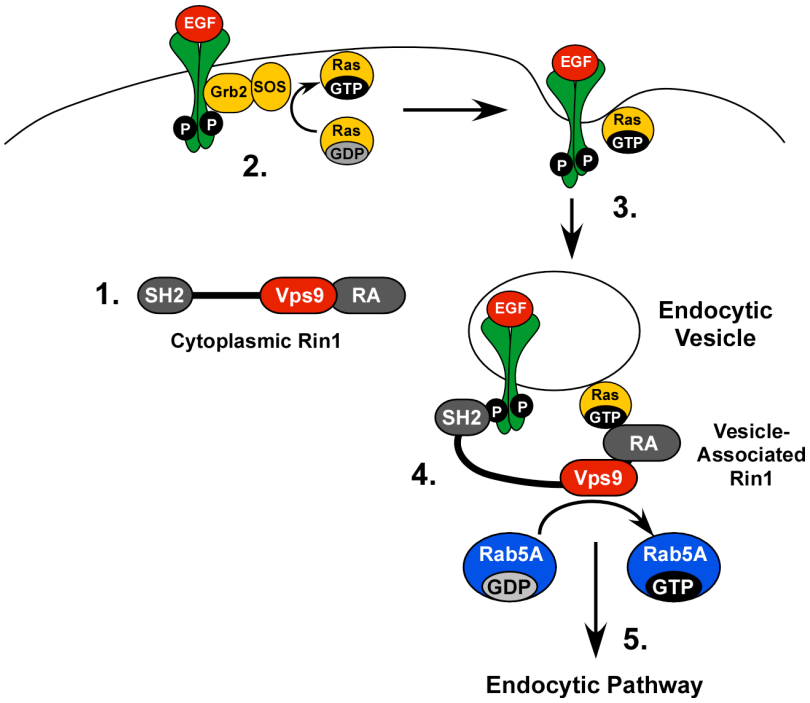

Figure 4. Rin1 regulates endocytosis of EGFR. Rin1 potentiates endocytosis of the epidermal growth factor receptor (EGFR). (1) The Rab5 family GDP–GTP exchange factor (GEF) Rin1 harbors both Src homology 2 (SH2) and Ras Association (RA) domains in addition to the Vps9 domain. (2) Activation of the EGFR receptor occurs through receptor phosphorylation and leads to activation of Ras by means of Grb2 and SOS. (3) Receptor phosphorylation also results in internalization although the clathrin pathway. (4) Rin1 binds to the internalized phosphorylated receptor by means of its SH2 domain. In addition, the Rin1 RA domain binds activated Ras. (5) Interactions through these SH2 and RA domains potentiate Rin1 activation of Rab5A by the Vps9 domain, thereby promoting fusion with the early endosome. These events facilitate the degradation of the activated receptor and promote attenuation of the EGF signal transduction cascade.

Barbieri et al. 2001). Conversely, coexpression of a dominant negative Rin1 (Rin1Δ, a naturally occurring splice variant defective for Rab5 guanine nucleotide exchange activity) with activated Ras can block the Ras-effect on EGF uptake (Han, Wong et al. 1997; Tall, Barbieri et al. 2001). Thus, Rin1 functions downstream of Ras to stimulate EGFR endocytosis through the activation of Rab5.

Is this enhanced endocytosis important for modulating the EGF signaling pathway? Rin1 overexpression diminishes Erk phosphorylation after EGF stimulation (Tall, Barbieri et al. 2001). This could be due to enhanced EGFR endocytosis more rapidly downregulating the receptor signal. Alternatively Erk activation may be blocked by Rin1 competing with Raf for binding to activated Ras. Overexpression of dominant negative Rin1Δ, which is unable to activate Rab5, enhances Erk activation after EGF stimulation (Tall, Barbieri et al. 2001). The downstream effects of Rin1 correlate with its ability to activate Rab5 and EGF uptake; thus, Rin1 likely stimulates EGFR endocytosis to attenuate the signal transduction cascade. Rin1 expression also suppresses the transforming ability of activated Ras (Wang, Waldron et al. 2002), consistent with Rin1 functioning as a negative regulator of Ras signaling. Rin1 has also been identified as an activator of ABL2 and has been demonstrated to potentiate BCR-ABL induced lukemias (Afar, Han et al. 1997). While these findings appear to contradict Rin1's ability to suppress Ras-mediated cell transformation, these functions of Rin1 appear to be distinct from its Ras-binding and Rab5 GEF activities.

What is the consequence of loss of Rin1 function in an animal? Dhaka et al. have generated *Rin1*$^{-/-}$ mice, which develop normally with no gross morphology defects (Dhaka, Costa et al. 2003). However, these knockout mice do show an abnormality in aversive memory formation linked to the amygdala,

where Rin1 expression would normally be elevated (Dhaka, Costa et al. 2003). *Rin1*$^{-/-}$ mice exhibit enhanced amygdala-associated learning behaviors and long term potentiation (LTP), a process in which Ras has previously been implicated (reviewed in (Orban, Chapman et al. 1999)). These phenotypes are consistent with Rin1 negatively regulating Ras function and correlate well with the opposite effects on LTP and amygdala-dependent learning observed upon loss of the Ras activator, GRF1 (Brambilla, Gnesutta et al. 1997). The mechanism by which Rin1 downregulates Ras activity in the amygdala has not yet been addressed, but it is intriguing to speculate that increased endocytosis of a yet to be identified receptor may be involved in this process. The elucidation of these specific learning defects in the *Rin1*$^{-/-}$ mice and the ability of Rin1 overexpression to block Ras-mediated cell transformation support a role for Rin1 as a negative regulator of Ras signaling.

While Rin1 has been well characterized, other members of the Rin family have been less well explored. Nematode and fruit fly genomes appear to contain only single members of the Rin family (CE23604 and Sprint, respectively) (Szabo, Jekely et al. 2001), but mammals contain at least two additional proteins related to Rin1. Similar to Rin1, Rin2 and Rin3 have been demonstrated to possess Rab5 GEF activity (Saito, Murai et al. 2002; Kajiho, Saito et al. 2003); however, Rin2 and Rin3 can bind amphiphysin II, while Rin1 cannot (Kajiho, Saito et al. 2003). In addition to this distinct interaction, Rin1, -2 and -3 exhibit

distinct expression patterns. While Rin1 expression is highest in the brain and pancreas (Han, Wong et al. 1997; Dhaka, Costa et al. 2003), Rin2 expression is elevated in the heart, kidney, and lung (Saito, Murai et al. 2002), and Rin3 expression is most prominent in peripheral blood cells (Kajiho, Saito et al. 2003). The importance of this differential expression pattern is not yet known but may yield insights into the involvement of these Rin proteins in different signal transduction pathways.

Alsin and Juvenile ALS

Mutations in the gene *ALS2* (amyotropic lateral sclerosis 2) have been linked to juvenile-onset forms of the neurodegenerative diseases amyotropic lateral sclerosis (ALS2), primary lateral sclerosis (PLSJ) and hereditary spastic paraplegia (IAHSP) (Hadano, Hand et al. 2001; Yang, Hentati et al. 2001; Eymard-Pierre, Lesca et al. 2002; Devon, Helm et al. 2003; Gros-Louis, Meijer et al. 2003). These rare autosomal recessive conditions present early in life and gradually progress toward para- or tetraplegia (Devon, Helm et al. 2003). Alsin is the gene product of *ALS2* and is a member of the family of Vps9 domain containing proteins. In addition to its carboxy-terminal Vps9 domain, Alsin contains a region similar to the beta-propeller of the Ran GEF RCC1 (RCC1-like domain), tandem DH and PH domains indicative of a Rho family GEF, and a number of MORN (membrane occupation and recognition nexus) motifs.

The Vps9 domain of Alsin activates Rab5 and stimulates endosome fusion in vivo (Otomo, Hadano et al. 2003; Topp, Gray et al. 2004), and the DH/PH domain has been shown to bind and activate Rac1 (Topp, Gray et al. 2004; Kanekura, Hashimoto et al. 2005). Alsin's RCC1-like domain may function as a third GEF domain (Hadano, Hand et al. 2001); however, this domain more likely serves to mediate some other protein:protein interaction. In fact, while expression of the Alsin Vps9 domain alone or constructs containing both the DH/PH and Vps9 domains localize to endosomal compartments, full-length Alsin constructs are largely seen in the cytosol (Otomo, Hadano et al. 2003; Topp, Gray et al. 2004). This dichotomy suggests the RCC1-like domain may regulate the Vps9 domain-mediated endosomal localization, either by binding a sequestering molecule in the cytosol or via an intramolecular inhibition of Rab5 binding.

All known disease-associated mutations result in truncation of Alsin, including a short 83 amino acid deletion eliminating the carboxy-terminal portion of the Vps9 domain. This observation suggests that the loss of Alsin's Rab5 GEF activity correlates with the disease state. How might a deficiency in Rab5 activation lead to decreased motor neuron viability? One model is that defects in turnover of a receptor might exacerbate a signaling system, similar to defects in EGFR trafficking and signaling seen upon overexpression of a dominant negative version of Rin1 (Tall, Barbieri et al. 2001). Alternatively, the Rab5 GEF activity of Alsin may facilitate neurotrophic receptor signaling by contributing to the

formation of signaling endosomes. In the case of nerve growth factor (NGF), the formation and retrograde transport of endosomal structures containing activated receptors (TrkA) to neuron cell bodies is thought to facilitate NGF-mediated signaling (Riccio, Pierchala et al. 1997; Howe, Valletta et al. 2001). The Rab5 GEF activity of Alsin may be critical for the trafficking of activated receptor complexes to these endosomal structures before they begin their journey to the cell body. Alsin may also promote neuronal survival and maintenance via activating Rac1. Recently, Alsin overexpression has been demonstrated to inhibit superoxide dismutase 1 (SOD1) mutant-induced neurotoxicity in a cellular model of familial ALS; moreover, this protection was dependent on a functional Rac1 GEF domain (Tall, Barbieri et al. 2001). Alsin overexpression also can potentiate neurite outgrowth, and this effect is dependent on Rac1 activation (Tudor, Perkinton et al. 2005). These results suggest that coordinating activation of Rac1 and Rab5 may be critical for Alsin's role in receptor trafficking, although the mechanism by which the Rac1 and Rab5 GEF activities of Alsin may function synergistically to promote motor neuron maintenance and survival has yet to be determined.

Recently, ALS2CL, a protein homologous to the carboxy-terminal 60% of Alsin has been identified (Hadano, Otomo et al. 2004; Devon, Schwab et al. 2005). ALS2CL lacks the RCC1-like domain, and while the alignment of these proteins spans from just before the DH/PH region of Alsin through the end of the

protein, SMART and Pfam were unable to identify a DH or PH domain in the corresponding region of ALS2CL (Bateman, Coin et al. 2004; Letunic, Copley et al. 2004), suggesting that it may not possess Rac GEF activity. In addition, the Rab5 GEF activity of the ALS2CL Vps9 domain, while present, is far weaker than that of Alsin in vitro, and overexpression of ALS2CL shows a different localization pattern and has a different effect on endosomal morphology compared to Alsin (Hadano, Otomo et al. 2004). Finally, RT-PCR suggests that ALS2CL's expression pattern may be widespread or even ubiquitous, as opposed to Alsin's pronounced enrichment in the CNS (Hadano, Otomo et al. 2004; Devon, Schwab et al. 2005). Together these differences indicate that, although Alsin and ALS2CL are similar, they may have significantly different functions.

Other Proteins with Vps9 Domains

RAP6, which contains an amino-terminal RasGAP domain and a carboxy-terminal Vps9 domain, is the only other Vps9 domain-containing protein characterized to date. Recent studies in *C. elegans* indicate that RAP6 associates with clathrin-coated pits and there directs endocytosis (Sato, Sato et al. 2005). Further functional and biochemical studies will be needed to address how this conserved Rab5 GEF/Ras GAP potentially integrates with the Rab5 GEF/Ras effector Rin1.

In addition to the proteins discussed above, the SMART and Pfam databases currently list a number of uncharacterized Vps9 domain-containing proteins (Bateman, Coin et al. 2004; Letunic, Copley et al. 2004) (Figure 2). The second yeast Vps9 domain-containing protein, Muk1, is examined for the first time here in Chapter 2. While the absence of additional conserved domains in Muk1 yields few clues to its cellular function, two uncharacterized mammalian Vps9 domain proteins do contain such domains. Like the members of the Rin family, Rin4 (XP_059046) has an amino-terminal SH2 domain and a proline rich sequence; but unlike these others, it has no carboxy-terminal Ras Association domain. Finally, Varp contains a Vps9 domain followed by 2 sets of 4 ankyrin repeats that may direct its association with another protein or complex. Interestingly, a novel Rab5 effector containing 21 ankyrin repeats has also been recently described with a role in macropinocytosis (Schnatwinkel, Christoforidis et al. 2004).

Research Aims

Rab5 family members and their Vps9 domain-containing GEFs have been implicated in a diverse array of cell signaling and protein trafficking events. I have been interested in the specificity involved in Rab5/Vps9 domain protein interactions and the mechanism by which the Vps9 domain activates Rab5 proteins.

Saccharomyces cerevisiae provides a conserved yet less complex model system for analyzing these interactions. I will first determine whether Vps9 or the uncharacterized Vps9 domain-containing protein, Muk1, stimulate nucleotide exchange of the three yeast Rab5 proteins Vps21, Ypt52 and Ypt53. I will then examine the functional significance of lacking each of these proteins to uncover differential phenotypes that will indicate specific roles for these proteins.

I will first use a mutational analysis to identify residues within the Vps9 domain that are involved in catalyzing nucleotide exchange of Vps21. Mutants will be tested for their capacity to interact with and stimulate nucleotide release from Rab protein and their capacity to complement a deletion of the *VPS9* gene.

Finally, I will initiate structural studies to determine the mode of interaction between Rab5 proteins and the Vps9 domain by either crystallography or NMR. From these studies I hope to infer a model for the mechanism of Rab5 nucleotide exchange that will then be tested by additional mutagenesis.

CHAPTER TWO

Functional Specificity of the Yeast Rab5 Family and their Exchange Factors

Overview

The yeast *Saccharomyces cerevisiae* contains three members of the Rab5 family, Vps21, Ypt52 and Ypt53. Vps21 is essential for proper biosynthetic and endocytic protein transport to the vacuole, and the only prior investigation into Ypt52 and Ypt53 function concluded that these proteins may be redundant to Vps21. *S. cerevisiae* also contains two Vps9 domain-containing proteins, Vps9 and Muk1. While Vps9 is a guanine nucleotide exchange factor (GEF) for Vps21 and is also required for both biosynthetic and endocytic vacuolar protein sorting, neither the GEF activity nor the in vivo function of Muk1 has been previously characterized. Here we extend the known GEF activity of Vps9 to include the Rabs Ypt52 and Ypt53 and establish Muk1 as a Rab5 family GEF. Furthermore we identify a unique role for Muk1 and Ypt53 in the endocytic pathway distinct from that of Vps9 and Vps21.

Introduction

In mammals, the Rab5 family has a well established role in regulating the complex process of endocytosis. Rab5a was originally shown to regulate targeting and fusion of endocytic vesicles to early endosomes and promote homotypic fusion of these endosomes (Gorvel, Chavrier et al. 1991; Bucci, Parton et al. 1992). Since the initial work on Rab5a, two additional Rab5 isoforms, Rab5b and Rab5c were identified(Bucci, Lutcke et al. 1995), though few functional differences have been uncovered. First phylogenetic (Pereira-Leal and Seabra 2001) and then experimental (Delprato, Merithew et al. 2004)analyses suggested that Rab21, Rab22a and Rab22b (also called Rab31) be grouped with the Rab5 isoforms into a larger subfamily. The newer members of this family are more diverse in their localization as well as the trafficking events they regulate (reviewed in (Simpson and Jones 2005)), but all members of the Rab5 family impact transport through endocytic compartments.

The yeast Rab5 ortholog Vps21 (also called Ypt51) regulates traffic from the plasma membrane to endosomes as well (Singer-Kruger, Stenmark et al. 1994; Singer-Kruger, Stenmark et al. 1995; Gerrard, Bryant et al. 2000). Unlike Rab5, Vps21 is also required for biosynthetic sorting of cargo such as vacuolar hydrolases from the Golgi to endosomes en route to the vacuole (Horazdovsky, Busch et al. 1994; Singer-Kruger, Stenmark et al. 1994; Gerrard, Bryant et al.

2000). It is not yet clear if one or more of the newer additions to the mammalian Rab5 family has a role in the analogous pathway in mammalian cells. In addition to Vps21, yeast contain two other proteins homologous to Rab5, Ypt52 and Ypt53 (Figure 5). In the only previous study of the yeast Rab5 family, these proteins were found to have overlapping if not redundant function (Singer-Kruger, Stenmark et al. 1994). Whereas, the loss of Vps21 significantly impacted both biosynthetic and endocytic trafficking, the loss of Ypt52 or Ypt53 alone had no effect. Loss of Ypt52 and Vps21 together had a more deleterious effect on these pathways, though the same was not true for the Ypt53 and Vps21 combination. A marginal effect for the loss of Ypt53 on these pathways was only seen upon formation of the *Δvps21Δypt52Δypt53* triple mutant (Singer-Kruger, Stenmark et al. 1994). These results suggested that some level of redundant function exists for these proteins, with Vps21 contributing most significantly.

As GTPases, members of the Rab5 family cycle between an active GTP-bound form and an inactive GDP-bound form. The reactivation of the inactive form is accelerated by GEFs, which show specificity for a given Rab or family of Rab proteins. Rab5 GEFs contain a Vps9 domain, a region of homology to the yeast Vps21 GEF of the same name. There are now nine mammalian Vps9 domain-containing proteins that contain numerous signaling and protein-protein interaction domains. Eight of these proteins have been shown to have GEF activity for at least one Rab5 family member, and these Rab/GEF pairings are

being linked to increasingly specific functions. In yeast, Vps9 has been shown to be required for both biosynthetic (Burd, Mustol et al. 1996)and endocytic (Donaldson, Yin et al. 2003; Davies, Carney et al. 2005) transport to the vacuole. Until now, the second Vps9 domain-containing protein has gone unexamined.

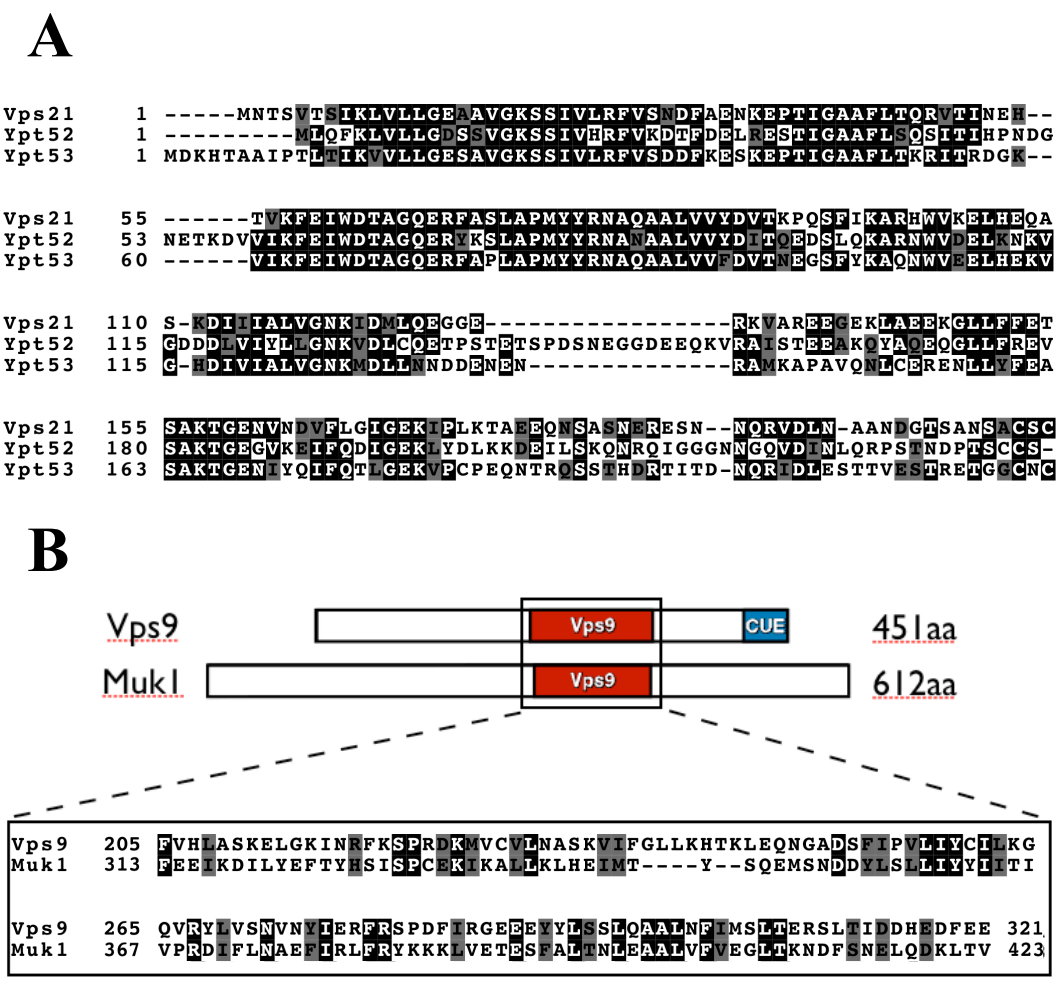

Figure 5. The yeast Rab5 family and Vps9 domain-containing proteins. The sequence alignments between (A) the yeast Rab5 family members and (B) the Vps9 domains of Vps9 and Muk1 obtained using ClustalW 1.8 from the Baylor College of Medicine Search Launcher and the BOXSHADE server are shown. Black boxes indicate amino acid identity, and shaded boxes indicate conservative amino acid substitutions.

We have undertaken a comprehensive analysis of the yeast Rab5 family and Vps9-domain containing proteins. We show that both Vps9 and Muk1 can interact with and have exchange activity for all three yeast Rabs. We confirm a minor contribution from Ypt52 in biosynthetic vacuolar sorting but see no such contribution from Muk1 and Ypt53. Conversely, while not observing any role for Ypt52 in endocytosis, we identify a role for Muk1 and Ypt53 in endocytosis distinct from that of Vps9 and Vps21.

Results

Interaction of Vps9 and Muk1 with Vps21, Ypt52 and Ypt53

Vps9 has been demonstrated to activate Vps21 in vitro and their similarity of phenotypes indicates that Vps9 and Vps21 act together to mediate biosynthetic and endocytic trafficking to the vacuole. However, the contributions of the additional Rab5 proteins, Ypt52 and Ypt53, as well as the additional Vps9 domain-containing protein, Muk1, in these processes is unclear. To begin to resolve this question, the ability of Vps9 and Muk1 to associate with the yeast Rab5 proteins was assessed.

Rab proteins exhibit a conserved a Ser or Thr residue at a position corresponding to Ras S17 for the coordination of a Mg^{2+} ion associated with guanine nucleotide binding. As seen in Ras (Feig and Cooper 1988; Farnsworth

and Feig 1991), mutating the corresponding residue in Vps21, Ser21, to glutamine has been shown to significantly reduce the protein's affinity for GTP (Hama, Tall et al. 1999), resulting in either GDP-bound or nucleotide free Rab. Rab GEFs are unique in their preferential recognition of GDP-bound or nucleotide-free Rabs. Our laboratory has previously shown that the Vps21 GEF Vps9 binds Vps21^{S21N}, but not wild-type Vps21 using the yeast two-hybrid system (Hama, Tall et al. 1999). We expanded that analysis to include another yeast Vps9 domain-containing protein, Muk1, as well as two additional Rab5 family members Ypt52 and Ypt53. Full length Muk1, Ypt52 and Ypt53 were cloned from wild-type yeast DNA, and Ypt52^{S17N} and Ypt53^{S26N} point mutants were generated by site-directed mutagenesis. Prey plasmids encoding LexA DNA binding domain-fusions of Vps9 and Muk1 were cotransformed into L40 yeast cells with bait plasmids encoding Gal4 activation domain-fusions of wild-type or S/N Vps21, Ypt52 and Ypt53. The ability of these bait/prey pairs to interact was determined by their ability to drive the *HIS3* (Figure 6a) and *lacZ* (Figure 6b) genes in the L40 yeast reporter strain. All baits were tested against empty pGADGH and all preys were tested against empty pVJL11 to insure that auto-activation did not occur. As seen previously with Vps21^{S21N}, Vps9 interacted with Ypt52^{S17N} and Ypt53^{S26N}, as seen by the ability of these transformants to grow on media lacking histidine (Figure 6a) and also by their ability to produce β-galactosidase (Figure 6b). The wild-type forms of these Rabs did not interact with Vps9 in this assay. Muk1 interacted with

Ypt53^{S26N} and Vps21^{S21N} based on expression of β-galactosidase and growth on media lacking histidine. (While not obvious in the figure, visual inspection of the his^{-} plate revealed a level of growth higher than background for the Muk1/ Vps21^{S21N} pair. B. Bellin, personal communication) In contrast, Muk1 interaction with Ypt52^{S17N} was not apparent under these assay conditions. These results suggested that Muk1 interacts specifically with Vps21 and Ypt53, while Vps9 interacts with all three yeast Rab5 proteins.

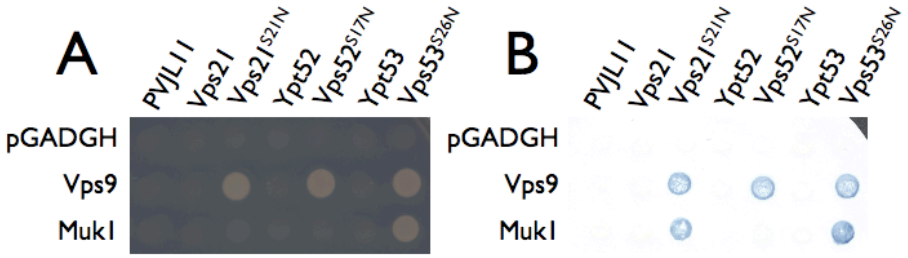

Figure 6. Two-hybrid interactions of the yeast Rab5 and Vps9 domain families. L40 yeast that were cotransformed with the indicated bait and prey plasmids were grown on selective media and monitored for growth on media lacking histidine (A) or transferred to nitrocellulose and lysed, with the presence of β-galactosidase determined using a colorimetric filter assay (B).

In an attempt to clarify the potential Rab specificity seen for Muk1 by the yeast two-hybrid system, we turned to a pull-down assay with recombinant proteins. GST-tagged Rabs were expressed and loaded with GDP, and their ability to interact with partially purified His_6MBP•Muk1 fusion protein was determined by western blot analysis. As seen in Figure 7, the Muk1 fusion was pulled down in similar quantities by GST-tagged Vps21, Ypt52 and Ypt53 but was not pulled

down by GST alone. These results indicated that Muk1 did not show specificity within the yeast Rab5 family *in vitro*. Additional experiments are needed to determine whether the inability of Muk1 to interact with Ypt52^{S17N} in the two-hybrid system is simply a false negative result or is a result of another factor preventing their association *in vivo*.

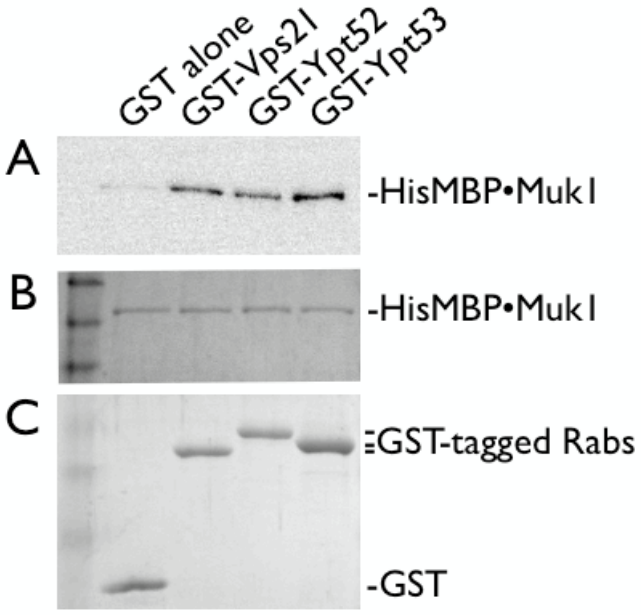

Figure 7. Interaction of Muk1 with GST-tagged Rabs. GST and the indicated GST-tagged Rab proteins were bound to glutathione sepharose beads and incubated with partially purified His6MBP•Muk1. Beads were isolated and the resulting complexes were analyzed by SDS-PAGE and Western blotting with αMBP antibody (A) or Coomassie staining (inputs, B and C).

GEF activities of Vps9 and Muk1 toward Vps21, Ypt52 and Ypt53

To further examine the functional interplay between Vps9, Muk1 and the yeast Rab5 proteins, the GEF activities of Vps9 and Muk1 were determined. The

function of a GEF is to stimulate release of GDP from inactive GTPases, allowing them to then bind GTP. Vps9 has previously been shown by our laboratory to stimulate the release of [^{3}H]-GDP from Vps21 using a filter-binding assay. Since that time, we have adopted a fluorescence-based assay utilizing N-methyanthraniloyl (mant)-tagged nucleotides. MantGDP and mantGTP are now commonly used in the study of GTPases, because their significant increase in fluorescence when bound to protein allows for easy observation of nucleotide binding or release events. Unlike the filter-binding assay used previously, which required time to take samples and wash filters between time-points, fluorescent assays can be followed in real time. Importantly, it has been demonstrated for a number of GTPases, including Rab5 (Simon, Zerial et al. 1996) and Vps21 (Esters, Alexandrov et al. 2001), that mantGDP and mantGTP have binding affinities similar to those of unmodified nucleotides(John, Sohmen et al. 1990).

Protein expression in *E. coli* and affinity chromatography were used to isolate Vps9 and Muk1 for analysis. A truncated form of Vps9 (aa 158-347) was previously identified as the minimal domain necessary and sufficient to interact with Vps21 and drive nucleotide exchange (G. Tall, unpublished). A number of similar constructs of Muk1 were made but found to be largely insoluble when expressed alone as His_6- or His_6MBP-fusions. Full length Muk1 was found to be suitably stable as a His_6MBP-fusion, but became insoluble after cleavage of the His_6MBP tag. For this reason, His_6MBP-fusions of full length Vps9 and Muk1

were used in the following analyses. Although Vps21, Ypt52, and Ypt53 are extremely soluble, they were also expressed as His_6MBP-fusions to allow for uniform cloning, expression and purification procedures. Rab constructs were truncated immediately before their carboxy terminal Cys residues to avoid an apparent dimerization of full length constructs during purification. The His_6MBP tag was cleaved and removed before the Rab proteins were used in exchange assays. Vps21, Ypt52 and Ypt53 were loaded with mantGDP, and the intrinsic rate of nucleotide release was monitored by the decrease in fluorescence in the presence of excess GTP. As seen in Figure 8, Vps21 showed an 8% loss of fluorescence over 10 minutes. Ypt53 showed a slightly faster release (11%), while the intrinsic rate of release from Ypt52 was twice as fast as Vps21 (16%).

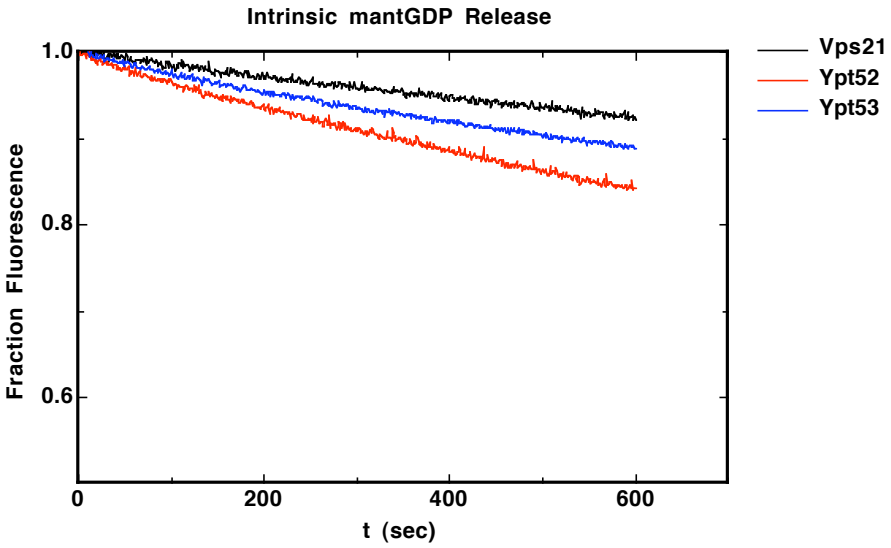

Figure 8. Intrinsic nucleotide release of yeast Rab5 proteins. Purified Rab proteins (1μM) were loaded with mantGDP. At time=0, GTP was added to 100μM, and the intrinsic release of nucleotide in the presence of buffer alone was monitored via fluorescence resonance energy transfer (FRET) measuring emission at 440nm with excitation of Rab tryptophan at 290nm.

We next tested the ability of His_6MBP•Vps9 and His_6MBP•Muk1 to stimulate mantGDP release from these Rabs. Figure 9 shows that both His_6MBP•Vps9 and His_6MBP•Muk1 exhibit GEF activity toward Vps21, Ypt52 and Ypt53. Neither of these Vps9 domain proteins stimulated mantGDP release from the unrelated Rab Ypt7 (data not shown). The faster intrinsic release rate of Ypt52 mandated the use of less GEF in order to observe the effect. In all cases, significantly more His_6MBP•Muk1 was needed to achieve the same stimulation as

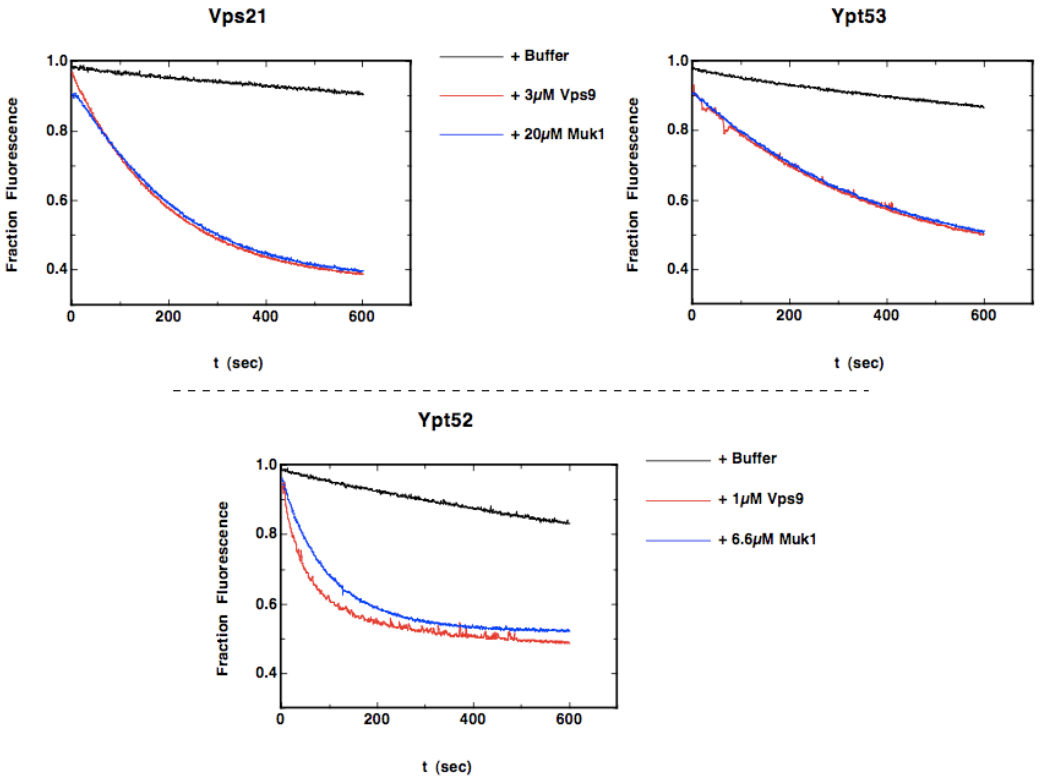

Figure 9. Vps9 and Muk1 stimulate nucleotide release from Vps21, Ypt52 and Ypt53. Purified Rab proteins (1μM) were loaded with mantGDP and incubated with buffer alone (black) or the indicated amount of His_6MBP•Vps9 (red) or His_6MBP•Muk1 (blue). At time=0, GTP was added to 100μM and release of nucleotide was monitored via FRET measuring emission at 440nm with excitation of Rab tryptophan at 290nm.

His_6MBP•Vps9. We used full length fusions of both Vps9 domain proteins to make comparisons as direct as possible, but the disparity in activity could be a consequence of the different degrees of interaction with the His_6MBP tag required for the solubility of Muk1, rather than a true indication of the relative activities of Muk1 and Vps9. Regardless, these data clearly indicate that Vps9 and Muk1 are GEFs for all three yeast Rab5 family members *in vitro*. This result was consistent with the ability of Muk1 to bind all three Rabs in pull-down assays and the ability of Vps9 to interact with all three in the yeast two-hybrid system.

Roles of Vps9, Muk1, Vps21, Ypt52 and Ypt53 in biosynthetic vacuolar protein trafficking

The contributions of Ypt52, Ypt53 and Muk1 to biosynthetic vacuolar protein sorting were examined. Most vacuolar hydrolases are synthesized as zymogens and are transported through the early stages of the yeast secretory pathway en route to the vacuole. Glycosylation and cleavage events that occur during this transportation process provide a convenient way to monitor traffic through the various stages of this localization pathway. Carboxypeptidase Y (CPY) is an excellent transportation marker. Upon entry to the endoplasmic reticulum (ER), CPY is core-glycosylated, yielding a distinct precursor (p1CPY). CPY then travels to and through the Golgi, where the core oligosaccharides are further modified by the addition of mannose residues, which yields the Golgi-

modified precursor (p2CPY). Finally, upon successful delivery to the vacuole, p2CPY is activated by an amino-terminal cleavage event, yielding the mature form of the protein (mCPY). These three forms of CPY can be separated using standard SDS-PAGE analysis. In the event that sorting to the vacuole becomes blocked or retarded, the Golgi-modified p2CPY is secreted from the cell (Stevens, Esmon et al. 1982). Vps21 (Horazdovsky, Busch et al. 1994) and Vps9 (Burd, Mustol et al. 1996) have previously been shown to be required for proper sorting of CPY and other hydrolases to the vacuole. To address whether Muk1, Ypt52 or Ypt53 played a role in this pathway, we examined CPY maturation in strains with these genes deleted.

Δvps9, *Δmuk1*, *Δvps21*, *Δypt52* and *Δypt53* strains were available in a collection of viable yeast deletion strains from Open Biosystems. These mutant strains and the wild-type parental strain (BY4742) were labeled with [^{35}S]-methionine and -cysteine for a 10 minute pulse followed by a 30 minute chase with unlabeled amino acids. CPY was then immunoprecipitated from intracellular and extracellular fractions of these cultures and immunoprecipitates were separated by SDS-PAGE. The labeled CPY was visualized using a phosphorimaging system (Figure 10). Wild-type yeast correctly sorted the vast majority of CPY to the vacuole as evidenced by the presence of the mature form of CPY inside the cell. In contrast, *Δvps9* and *Δvps21* strains showed significant accumulation of extracellular p2CPY, and only a small portion appears to have

been correctly loalized to the vacuole. Cells that lack Muk1 or Ypt53 showed no CPY sorting defect and phenocopied the wild-type cells. However, a small but reproducible defect was observed in cells that lacked Ypt52, with roughly twice as much secreted precursor detected, compared to wild-type cells. Similar results were obtained following the maturation of membrane-bound hydrolase carboxypeptidase S (CPS).

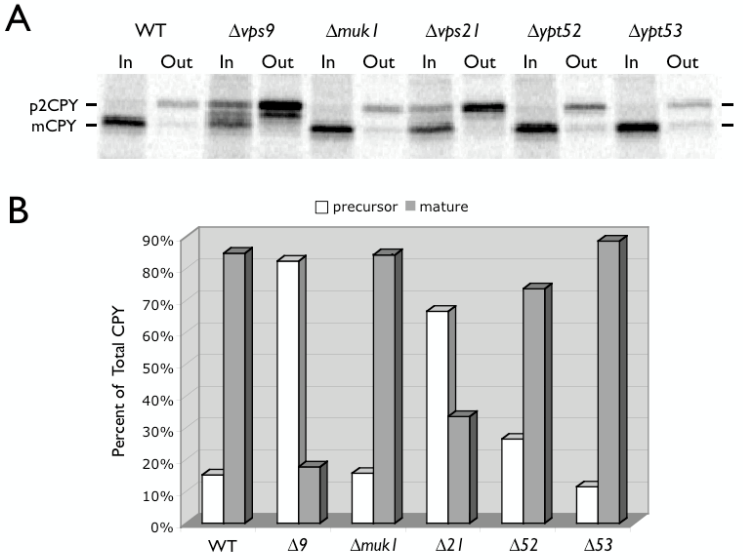

Figure 10. CPY sorting in strains lacking Rab5 orthologs or their GEFs. Wild-type (RGα) yeast or strains lacking Vps9 (Δ9), Muk1 (*Δmuk1*), Vps21 (Δ21), Ypt52 (Δ52), or Ypt53 (Δ53) were pulse labeled with ^{35}S-Pro-Mix for 10 minutes and chased with unlabeled methionine and cysteine for an additional 30 minutes at 30˚C. CPY was then immunoprecipitated from either the intracellular (In) or the extracellular (Out) fractions and resolved by SDS-PAGE and phosphorimagery (A). The positions of mature vacuolar (m) and Golgi-modified precursor (p) forms of CPY are indicated. (B) Bands were quantitated using ImageQuant, and the percentages of CPY found in the mature and precursor forms for each sample are graphically represented.

In an effort to investigate any potential redundancy within this system, a series of combination mutants were made. Haploid mutant strains were mated to obtain diploids for sporulation. The resulting tetrads were dissected, and spores were tested for 2:2 segregation of the kan^r gene marking the deletions. These mutants were then examined using a pulse/chase time-course assay to allow detection of kinetic defects in the vacuolar delivery of CPY and CPS. Deletion strains were labeled with [^{35}S]-methionine and cysteine as indicated above and the chase was terminated at specific times, without separating intracellular and extracellular fractions. Cell lysates were prepared and CPY and CPS were

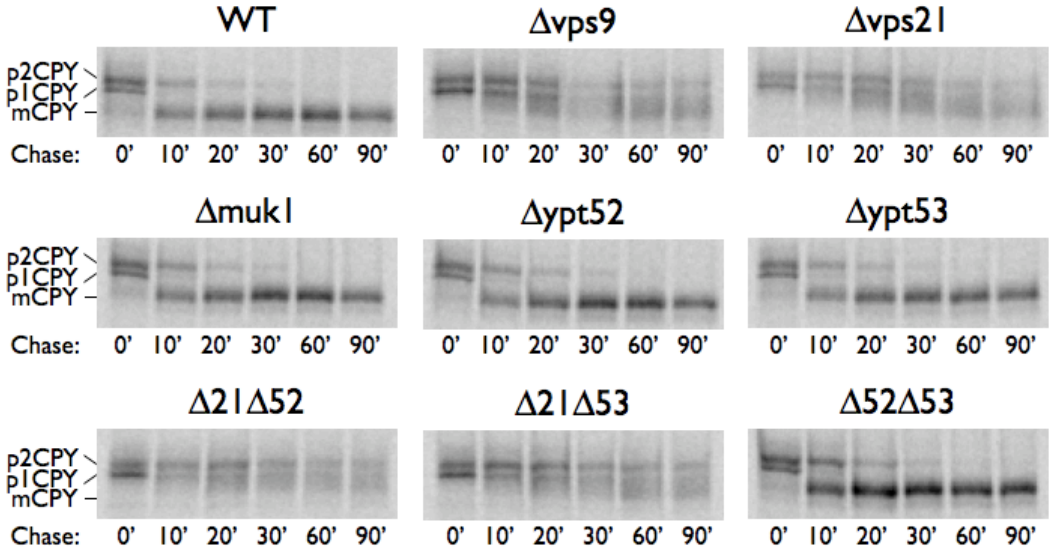

Figure 11. Maturation of CPY in strains lacking Rab5 family members or their GEFs. Wild-type RGα yeast or strains lacking Vps9, Muk1, Vps21, Ypt52, Ypt53, or the indicated combination of these were pulse labeled with ^{35}S-Pro-Mix for 10 minutes at 30°C before the addition of chase containing unlabeled cysteine and methionine. At time points indicated, the combined intracellular and extracellular fractions were precipitated with trichloroacetic acid (TCA). CPY was then immunoprecipitated and resolved by SDS-PAGE and fluorography. The positions of ER-modified (p1), Golgi-modified precursor (p2), and mature vacuolar (m) forms of CPY are indicated.

immunoprecipitated and the precipitated proteins were analyzed by SDS-PAGE and fluorography (Figures 11 and 12). In both cases, the kinetics of hydrolase maturation were identical in the *Δmuk1*, *Δypt52* and *Δypt53* and wild-type cells, with the vast majority of CPY being matured by 10 minutes of chase (Figure 11), and CPS at 20 minutes of chase (Figure 12). Cells that lacked Vps9 or Vps21 showed significant delays in the appearance of the mature forms of these enzymes. Very little mature CPY or CPS was seen even at the longest chase point. Analysis of the double mutants provided additional evidence that Ypt52 contributed to the sorting of these hydrolases, as the defect in cells lacking both

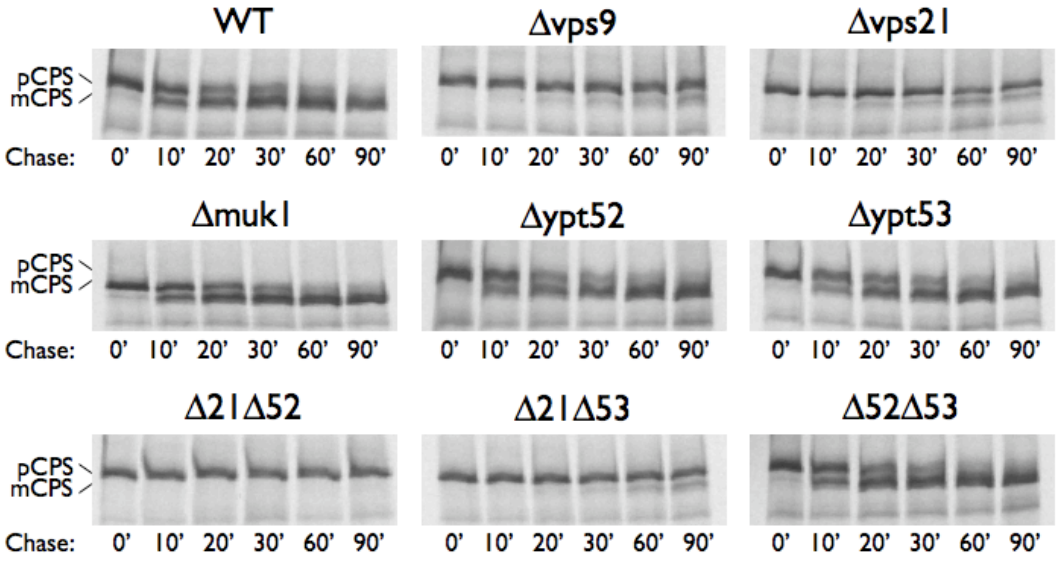

Figure 12. Maturation of CPS in strains lacking Rab5 family members or their GEFs. Wild-type RGα yeast or strains lacking Vps9, Muk1, Vps21, Ypt52, Ypt53, or the indicated combination of these were pulse labeled with ^{35}S-Pro-Mix for 10 minutes at 30°C before the addition of chase containing unlabeled cysteine and methionine. At time points indicated, the combined intracellular and extracellular fractions were precipitated with TCA. CPS was then immunoprecipitated, deglycosylated and resolved by SDS-PAGE and fluorography. The positions of precursor (p) and mature vacuolar (m) forms of CPS are indicated.

Ypt52 and Vps21 was more pronounced than that in cells lacking only Vps21. This exacerbation was best seen in the case of CPS where the small amount of mCPS seen in the later time-points in *Δvps21* cells was completely missing from all time-points in *Δvps21Δypt52* cells (Figure 12). In contrast no obvious role for Ypt53 was uncovered, as the phenotype of the *Δvps21Δypt53* double mutant was indistinguishable from that of *Δvps21*. This analysis is consistent with predominantly Vps21, and to a lesser extent Ypt52, being involved in mediating trafficking through the biosynthetic pathway, while a role for Ypt53 is not yet evident.

Roles of Vps9, Muk1, Vps21, Ypt52 and Ypt53 in endocytic vacuolar trafficking

The mammalian Rab5 family plays a well established role in the early stages of endocytosis, and Vps21 (Gerrard, Bryant et al. 2000) and Vps9 (Davies, Topp et al. 2003; Donaldson, Yin et al. 2003) have also been shown to be required for proper endocytic trafficking to the yeast vacuole. To determine whether Muk1, Ypt52 or Ypt53 also play a role in endocytosis, we examined the trafficking of green fluorescent protein (GFP)-tagged Ste3. The a-factor receptor Ste3 is a G protein-coupled receptor (GPCR) that is constitutively internalized, sorted into multivesicular bodies and delivered to the lumen of the vacuole for degradation through the endocytic pathway. Because GFP is relatively resistant to the

hydrolytic environment of the vacuole, successful endocytic sorting of the Ste3-GFP fusion results in an accumulation of GFP in the vacuole (Figure 13).

Deletion strains lacking Vps9, Vps21, Muk1, Ypt52, Ypt53 or a combination of these proteins were transformed with Ste3-GFP. The transformants were then labeled with the lipophilic fluorescent stain FM4-64, which demarks the limiting membrane of the vacuole (red). Prior to examining the localization of Ste3-GFP, cells were also treated with cyclohexamide to allow the reporter protein to clear the biosynthetic pathway and reach a final destination. Wild-type cells showed the expected accumulation of Ste3-GFP within the vacuole, along with some localization to the plasma membrane and a few large perivacuolar puncta (Figure 13). In contrast, almost no lumenal vacuolar signal was present in *Δvps9* and *Δvps21* cells, indicating a severe defect in endocytic trafficking. Instead there was an increased localization to the plasma membrane as well as to numerous small and disperse puncta. A third phenotype was present in *Δmuk1* and *Δypt53* cells. While some lumenal signal is observed, these cells consistently showed an increase in the number of bright perivacuolar puncta. Quantitation of the puncta indicated that *Δypt53* and *Δmuk1* cells contained approximately twice as many of these structures as wild-type cells (Table 1). The wild-type appearance of *Δypt52* cells suggested that Ypt52 was not involved in endocytosis. While quantitation found a similar number of puncta in *Δvps21* and *Δypt53* cells, the clear visual difference allowed an epistasis test. Cells lacking

both Vps21 and Ypt53 phenocopied cells lacking Vps21, suggesting that the defect in *Δvps21* cells may occur at an earlier step during endocytosis.

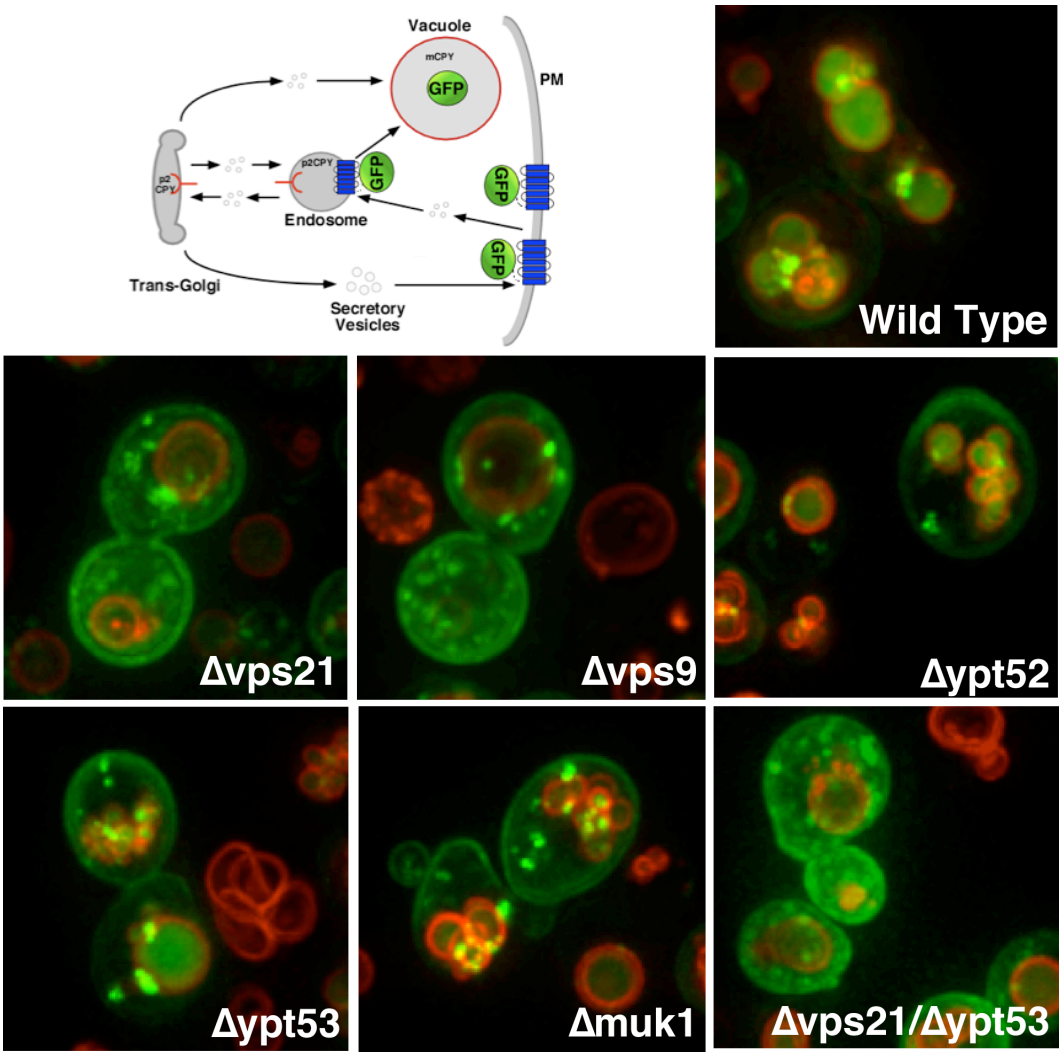

Figure 13. Ste3-GFP trafficking in strains lacking Rab5 orthologs or their GEFs. Ste3-GFP is trafficked from the plasma membrane through endosomal compartments to the lumen of the vacuole, where Ste3 is degraded but GFP is relatively stable (upper left). In panels, projections of deconvolved z-sections show Ste3-GFP trafficking in wild-type RGα yeast or the denoted deletion strain with FM4-64 (red) indicating the vacuolar membrane. Ste3-positive puncta were quantitated manually with results tabulated in Table 1.

Table 1. Quantitation of Ste3-GFP trafficking in strains lacking Rab5 orthologs or their GEFs.

Strain	Puncta/cell	Cells counted
WT	4.5 ± 2.1	83
Δvps21	10.6 ± 3.0*	59
Δvps9	15.1 ± 4.8*	85
Δypt52	4.6 ± 2.2	100
Δypt53	9.1 ± 3.6*	116
Δmuk1	9.2 ± 3.4*	64
Δvps21Δypt53	10.4 ± 4.7*	38

* $p < 0.001$.

To further characterize the nature of the compartments represented by the Ste3-GFP-positive puncta, Ste3 trafficking was analyzed with respect to the endosomal marker Pep12 (Figure 14). Pep12 is an endosomal t-SNARE, required for both biosynthetic (Becherer, Rieder et al. 1996) and endocytic (Holthuis, Nichols et al. 1998) transport to the vacuole. The Pep12-containing endosome has been proposed to act as the intersection of these two pathways (Lewis, Nichols et al. 2000). Deletion strains were transformed with Ste3-GFP and mCherry-tagged Pep12. In this experiment, mCherry-Pep12 was overexpressed and decorates both endosomal compartments and the limiting membrane of the vacuole. In wild type and *Δypt52* cells, Ste3-GFP is observed in the lumen of the vacuole and in Pep12-positive puncta, indicating that Ste3 passes through Pep12-positive endosomal structures en route to the vacuole. In *Δvps9* and *Δvps21* cells, Ste3-GFP was found on smaller, peripheral puncta that showed less colocalization with Pep12. In

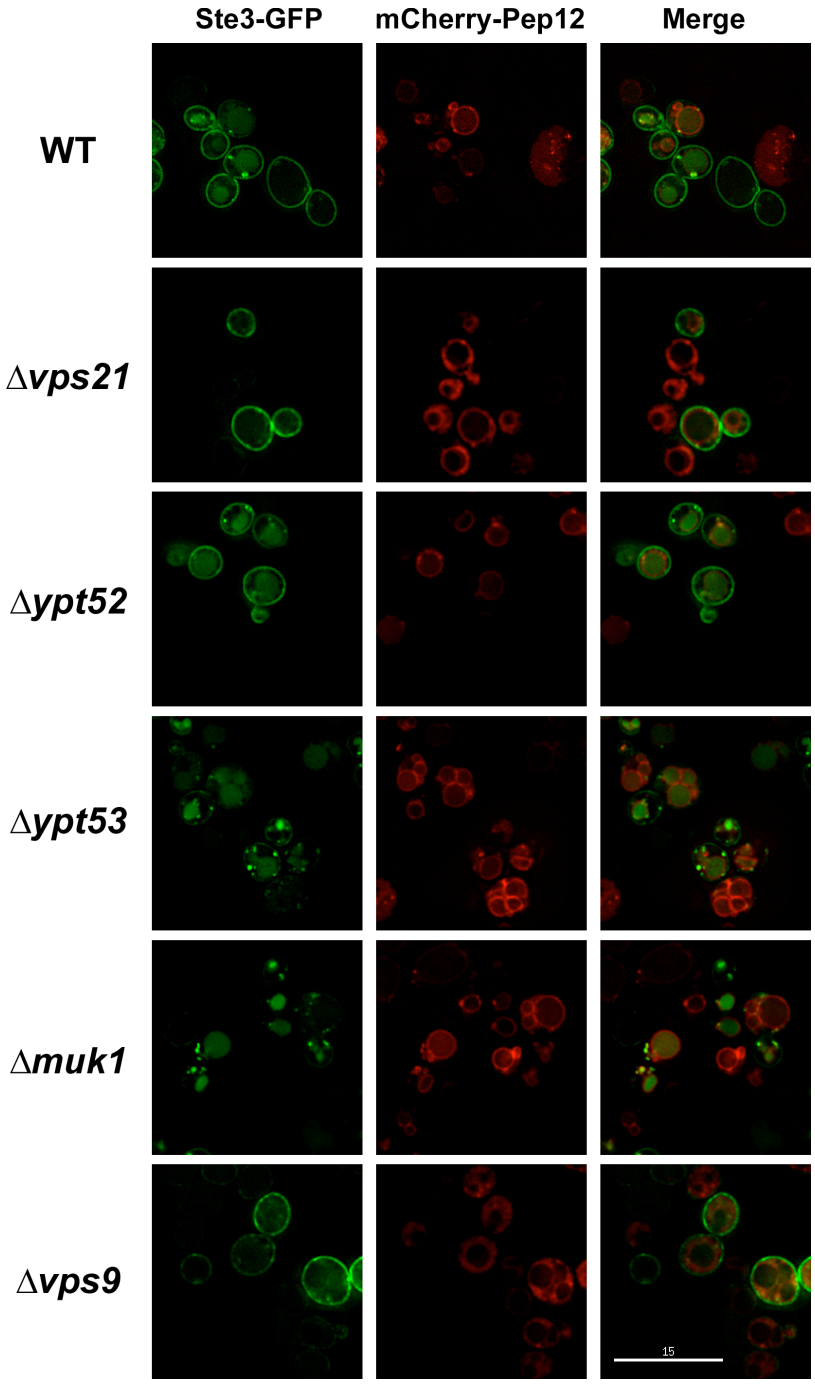

Figure 14. Ste3-GFP colocalization with Pep12 in yeast Rab5 or GEF deletions. Ste3-GFP and mCherry-Pep12 were coexpressed in wild-type RGα yeast or the denoted deletion strain. Shown are the green, red and merged channels of medial slices from deconvolved stacks of z-sections.

addition, the Pep12 structures themselves appeared more disperse, which could imply a role for Vps21/Vps9 function in the organization of these endosomes. This pattern suggested that Vps21 and Vps9 function were required for Ste3-GFP delivery to the Pep12-containing endosome; alternatively, the apparent reduced colocalization may be a byproduct of an altered morphology of the Pep12-containing endosome. In *Δypt53* and *Δmuk1* cells, the Ste3-GFP puncta tended to colocalize with mCherry-Pep12, suggesting that the compartments in which Ste3 accumulated in these mutants were similar to those seen in wild-type cells. This phenotype suggested that Muk1 and Ypt53 were not required for Ste3-GFP delivery to the Pep12-positive endosome. Together these data are consistent with a model in which Vps21 and Vps9 are involved in the trafficking of Ste3 to a Pep12-positive endosome, while Ypt53 and Muk1 are subsequently involved in the progression of this endosome onward to the vacuole (Figure 15). A role for Ypt52 was not evident in these assays.

Discussion

The yeast Rab5 ortholog Vps21 and its GEF Vps9 have been the subject of a number of studies. In contrast, Ypt52 and Ypt53 have only been examined once previously (Singer-Kruger, Stenmark et al. 1994). This disparity is presumably due to the lack of an obvious phenotype upon deletion and the ascription of a general role as “helpers” of Vps21. Similarly, Muk1, which has never been

examined, was ignored by our own laboratory for some time because an initial CPY sorting assay indicated that a *Δmuk1* mutation had no effect on this pathway (G. Tall, personal communication). In the first comprehensive analysis of the yeast Rab5 family and their GEFs, we find that Vps9 and Muk1 do not show specificity within this family *in vitro*, as both proteins show exchange activity for all three Rabs. However, we do observe a functional specificity, as only Vps9, Vps21 and Ypt52 contribute to biosynthetic sorting, while the Rab/GEF pairs Vps21/Vps9 and Ypt53/Muk1 show distinct involvement in endocytic trafficking. These observations indicate that the yeast Rab5 family and their GEFs do in fact show specialized involvement in different aspects of vacuolar delivery. This presents a scenario more in line with that seen in mammalian cells, where six Rab5 family members and at least nine Vps9 domain-containing proteins cooperate to specifically regulate many different trafficking events, suggesting that further examination of the coordination of the yeast Rab5 family and their exchange factors may ultimately provide insight into the complexity of the mammalian Rab5 system as well.

Muk1, the Rab5 family exchange factor

In this analysis, we demonstrate that Muk1 is an exchange factor for the yeast Rab5 family, but not the unrelated Rab Ypt7. Initial nucleotide release assays indicate that Muk1 may be a less potent GEF than Vps9, as greater than 6-

fold more Muk1 is required to similarly stimulate mantGDP release, but this may be related to the stability of the recombinant protein rather than a true reflection of its relative catalytic activity. While Muk1 did not show any specificity in *in vitro* experiments, the original yeast-two hybrid results hinted that Muk1 may prefer Ypt53 as a substrate. The connection between these two proteins was strengthened by analysis of deletion strains, in which *Δmuk1* and *Δypt53* cells show no defect in biosynthetic vacuolar sorting of CPY or CPS but display a similar Ste3 endocytic trafficking phenotype distinct from that seen for *Δvps9* and *Δvps21* or that seen for wild type cells.

Muk1 was originally given this name when the protein was *co**m**p**u**tationally linked to **K**ap95* in a predictive proteomics study, in which a computational analysis of available protein-protein interaction data was used to predict the function of uncharacterized genes (M Samanta, personal communication, (Samanta and Liang 2003)). This analysis clustered Muk1 with two nuclear pore components, Kap95 and Srp1, and a translation initiation factor, Gcd7. This led the authors to predict a role as either a transcription factor or a transporter of a transcription factor. The fourth protein clustered with Muk1 in this study is the GTPase Tem1, which has a known role in the termination of the M phase of mitosis. While not a Rab, Tem1 shows the highest sequence identity with Vps21 (Zhao, Chang et al. 2007) and has been identified as a Muk1 interactor by yeast two-hybrid (Ito, Chiba et al. 2001), raising the possibility that

Muk1 could act as a Tem1 GEF. We are currently preparing to investigate this possibility. Lte1 has been linked to Tem1 and may (Seshan and Amon 2005) or may not (Yoshida, Ichihashi et al. 2003) be responsible for its activation. Lte1 contains two domains homologous to CDC25, a RasGEF, suggesting that Lte1 may be the Tem1 GEF. A recent genetic interaction between Vps21 and Lte1 prompted the suggestion that Lte1 acts as a GEF for Vps21 (Zhao, Chang et al. 2007). While it seems highly unlikely that a protein with two Ras GEF domains and no Vps9 domain would be a GEF for a Rab5 family member, the finding of a second domain architecture with exchange activity on a Rab5 protein or that a Vps9 domain could activate a non-Rab5 GTPase would expand the knowledge of interactions on which models of Rab5/GEF specificity and the mechanism of nucleotide exchange are based. Therefore, we are in the process of examining Lte1 GEF activity toward Vps21 as well as Muk1 and Vps9 GEF activity toward Tem1.

Interestingly, Muk1 has been found associated with Vps5 and Vps35 by a tandem affinity purification/mass spectrometry analysis of protein complexes (Krogan, Cagney et al. 2006). Vps5 and Vps35 are part of the retromer complex required for the recycling of the CPY receptor Vps10 from endosomes to the Golgi, in which Vps5 forms a subcomplex with Vps17 (Horazdovsky, Davies et al. 1997) and Vps35 is part of a second subcomplex including Vps26 and Vps29 (Seaman, McCaffery et al. 1998). This association could be a simple case of

proteins being in proximity or part of a larger complex on an endosomal compartment. However, using the yeast two-hybrid assay we observed an interaction between Muk1 and Vps5 (data not shown), and Vps17 has been linked to Ypt53 by yeast two-hybrid as well (Vollert and Uetz 2004). This connection has not been tested *in vitro*, but an examination of the Vps10 degradation kinetics in *Δmuk1* and *Δypt53* cells indicates that these proteins do not regulate the function of the retromer complex (data not shown). An investigation into other binding partners and potential regulators of Muk1 has been initiated, and the possible association with the retromer complex may be revisited as part of this analysis.

The role of Ypt53 and Muk1 in endocytosis

We were unable to identify any role for Muk1 or Ypt53 in biosynthetic protein trafficking to the vacuole. However the increased number of intense Ste3-positive puncta seen by microscopy in deletions of *YPT53* or *MUK1* indicate that these proteins do play a role in endocytosis. Vps9 and Vps21 have previously been shown to be required for proper endocytic sorting, but the phenotype apparent in these cells is recognizably different from that seen in *Δmuk1* and *Δypt53* cells. The larger size and perivacuolar location of these puncta seen in the the *Δmuk1* or *Δypt53* suggest a block in endocytic trafficking at a later step than the Vps9/Vps21 site of action. This notion is supported by the epistasis

experiment, where the *Δvps21Δypt53* double mutant showed the smaller more disperse puncta of the *Δvps21* phenotype. The colocalization of Ste3 with the t-SNARE Pep12 in these deletions shed some light on the makeup of these puncta, as the *Δvps9* and *Δvps21* puncta show less colocalization with Pep12 than seen in *Δmuk1* and *Δypt53* or wild-type cells. These data support a model in which Vps9 and Vps21 are involved in trafficking Ste3 to a Pep12-positive endosomal compartment, where Muk1 and Ypt53 are then involved in the progression from this compartment to the vacuole or yet another intermediate structure (Figure 15).

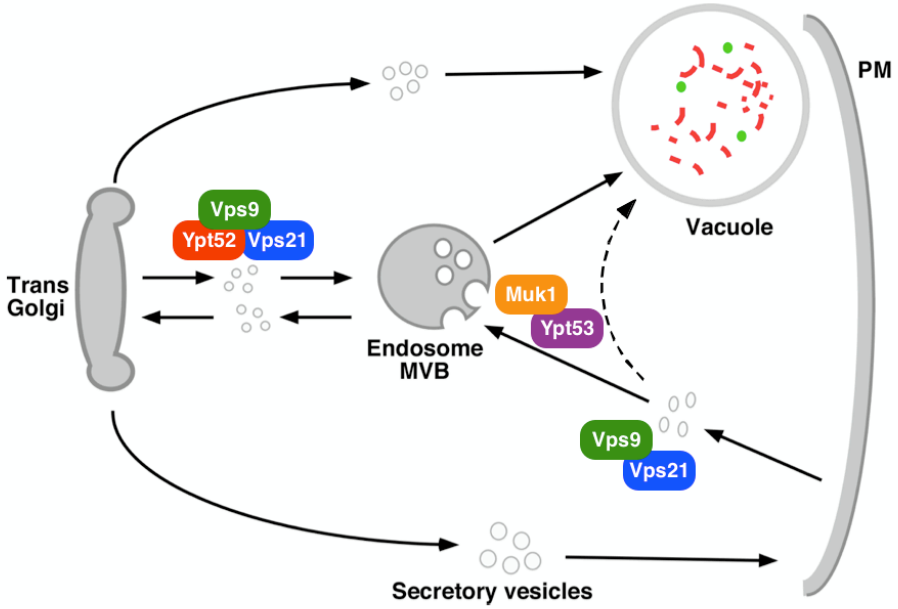

Figure 15. Roles of the yeast Rab5 family and their GEFs in vacuolar transport. Ypt53 and Muk1 act at a similar step in Ste3 trafficking downstream from Vps21 and Vps9. Ypt52 is not required for Ste3 trafficking but does offer minor contributions to biosynthetic transport with Vps21 and Vps9.

One potential issue with this model arises from the fact that Pep12 is required for both biosynthetic (Becherer, Rieder et al. 1996) and endocytic (Holthuis, Nichols et al. 1998) transport to the vacuole, and a Pep12-positive endosome has been proposed as the intersection of these two pathways (Lewis, Nichols et al. 2000). Muk1 and Ypt53 appear to have an endocytosis-specific involvement in transport from a Pep12 positive endosome to the vacuole. Reconciling this dual role for Pep12 with the specific endocytic role of Ypt53 requires either two methods of transport from a single Pep12-positive endosome to the vacuole or two populations of Pep12 endosomes. There is growing evidence to support additional endocytic compartments and/or pathways to the vacuole (A. Merz, personal communication), and the yeast endocytic compartments are poorly defined. Thus further study is required to delineate Muk1 and Ypt53 function with respect to the Pep12-containing endosome.

Interestingly, as the localization of Pep12 appears to be affected by the loss of Vps21 or Vps9. In *Δvps21* or *Δvps9* cells, Pep12-containing structures appear more diffuse than in wild-type cells, which suggests a role for Vps21 and Vps9 in the organization of these structures. The failure of Ste3 to colocalize with Pep12 in *Δvps21* or *Δvps9* cells could then result from either the failure to deliver vesicles containing Ste3 to the Pep12-positive structures or that these structures are incompetent for accepting delivery of Ste3-containing vesicles. The difference does not affect the placement of Ypt53 and Muk1 downstream of an earlier

requirement for Vps21 and Vps9, but it does affect the nature and the definition of the Ste3-positive and Pep12-positive compartments.

Both of the issues above relate to the fact that it is still unclear how many endosomal compartments exist in yeast, in what order cargo pass through these compartments, and in which compartment the endocytic and biosynthetic pathways converge. Further investigation into the differential function of of Vps21/Vps9 and Ypt53/Muk1 could not only solidify our model of their sequential action but help elucidate the relationships between endosomal compartments as well. To this end, the colocalization of Ste3 and other cargo with additional endosomal markers, such as the earlier or alternate t-SNARE Tlg1 or the phosphtidylinositol 3-phosphate (PI3-P)-binding FYVE doamin of early endosomal antigen 1 (EEA1), in these deletion strains will be examined in the future. In addition, the Horazdosvky lab will probe the time-dependent colocalization of a flourescently-tagged version of each yeast Rab5 protein with either cargo, endosomal markers, or the other members of the yeast Rab5 family.

The role of Ypt52 in biosynthesis

No specific function has been attributed toYpt52, and it may be redundant with Vps21. While deletion of Ypt52 alone does not show a significant effect on either biosynthetic or endocytic sorting, our data indicates that Ypt52 can supplement Vps21 activity to some degree in biosynthetic trafficking. We are

unable to assign Ypt52 a role in endocytosis, redundant or other wise, since *Δypt52* cells show no apparent defect in our assay and the severity of the *Δvps21* phenotype precludes the detection of any exacerbation in the *Δvps21Δypt52* double mutant. Singer-Kruger et al repeatedly observed a worsening of *Δvps21* phenotypes when combined with a deletion of *YPT52* (Singer-Kruger, Stenmark et al. 1994), and Chen et al. reported that *Δvps21Δypt52* cells showed synthetic lethality with a conditional allele of the GDI dissociation factor (GDF) Yip1, with which *Δvps21* or *Δypt52* cells were viable (Chen and Collins 2005).

In primary structure, Ypt52 is the most dissimilar of the yeast Rab5 proteins, with two insertions of 8 and 17 residues. The larger of these insertions maps to the G-4 loop of the guanine nucleotide-binding pocket, and may contribute to its increased intrinsic rate of nucleotide release seen in our exchange assays. Ypt52 has also been shown to have a rate of GTP hydrolysis 17 times faster than that of Vps21(Albert and Gallwitz 1999). Thus, Ypt52 inactivates itself (by hydrolysis) 17 times faster than Vps21 and reactivates itself (by releasing GDP to bind the more prevalent GTP) only twice as fast. In the absence of a GEF, Ypt52 would likely spend significantly more time in its inactive form. A more detailed kinetic analysis will be needed to determine whether Vps9 or Muk1 has an increased catalytic efficiency toward Ypt52 to overcome this inequity.

As Vps21 and Ypt52 have approximately equal expression levels (Ghaemmaghami, Huh et al. 2003), enhanced inactivation of Ypt52 may explain

the relative contributions of these two Rabs to biosynthetic protein sorting. It has been speculated that the increased hydrolysis rate of Ypt52 is due to an arginine at residue 32 in switch I where Vps21 and Ypt53 have a lysine (Esters, Alexandrov et al. 2000). If it is this accelerated nucleotide cycle that prevents Ypt52 from productively participating in trafficking events, expressing a Ypt52 mutant with a R32K mutation to match Vps21 or the standard Q70L hydrolysis-deficient mutant may answer the question of whether Ypt52 is properly localized and/or equipped to complement *Δvps21* or *Δypt53* phenotypes.

In summary, Vps21, Ypt52 and Ypt53 appear to be functionally discrete in the yeast biosynthetic and endocytic pathways to the vacuole. While Vps9 and Muk1 can bind to and stimulate nucleotide release in vitro for all three yeast Rab5 proteins, some level of specificity appears to exist in vivo with Muk1 appearing to be responsible for Ypt53 activation. This work has identified a novel role for Muk1 and Ypt53 in the intermediate or late endocytic pathway. Further studies are now required to establish the mechanisms driving this functional specificity.

Materials and Methods

Strains and reagents

E. coli was grown in Luria-Bertani (LB, 1 % tryptone, 0.5 % yeast extract, 1 % NaCl) medium supplemented with 100 μg/ml ampicillin or 50 μg/ml kanamycin as required. *E. coli* strains used were DH5α (Invitrogen, for cloning)

and BL21(DE3) (Stratagene, for protein expression). *S. cerevisiae* was grown in either YPD medium (1 % yeast extract, 2 % peptone, 2 % glucose) or synthetic minimal medium (0.67 % yeast nitrogen base, 2 % glucose) supplemented with appropriate amino acids (40 μg/ml each histidine, tryptophan, methionine, adenine and uracil, 60 μg/ml each leucine and lysine). *S. cerevisiae* single deletion strains are from the Saccharomyces Genome Deletion Project (Winzeler, Shoemaker et al. 1999) (purchased from Open Biosystems, Huntsville, AL), marked by the kan^r gene in the BY4741 (MATa his3Δ1 leu2Δ0 met15Δ0 ura3Δ0) and BY4742 (MATα his3Δ1 leu2Δ0 lys2Δ0 ura3Δ0) backgrounds. To create double deletion strains, pairs of single deletions were mated on YPD medium before selecting for diploids on synthetic medium lacking methionine and lysine. Diploids were then grown on YPD medium overnight, transferred to YPD liquid medium for growth overnight at 22˚C, and rinsed with H_2O before being transferred to CSH sporulation medium (1 % KOAc, 0.1 % yeast extract, 0.05 % glucose, supplemented with 2x amino acids) for 72 – 96 hours at 22˚C. Tetrads were dissected after partial digestion with Zymolyase 100T using a Singer Series 300 MSM System. After growth on YPD plates, spores were tested for 2:2 segregation of the kan^r gene by growth on plates containing G418. Potential double deletions were confirmed by PCR. L40 (MATa trp1 leu2 his3 LYS2::(lexAop)4-HIS3 URA3::(lexAop)-lacZ (Vojtek, Hollenberg et al. 1993)) was used in two-hybrid analyses.

MBP antiserum was purchased from New England Biolabs (Beverly, MA). HRP-conjugated anti-mouse antibody and SuperSignal West Maximum Sensitivity Substrate were purchased from Pierce Biotechnology Inc. (Rockford, IL). iTaq DNA polymerase was purchased from Biorad Laboratories, Inc. (Hercules, CA). The TOPO TA cloning kit was purchased from Invitrogen (Carlsbad, CA). *N*-methylanthraniloyl (mant)-GDP was purchased from Molecular Probes, Inc (Eugene, OR). Glutathione sepharose beads, Redivue PRO-MIX [^{35}S] cell labeling mix and all FPLC columns were purchased from Amersham Biosciences (Piscataway, NJ).

Plasmid construction

Full-length *VPS9, MUK1*, *VPS21*, *YPT52*, and *YPT53* and truncations of *VPS21*, *YPT52*, and *YPT53* encoding all but the c-terminal cysteine residues (to prevent apparent dimerization *in vitro* by these residues that are normally prenylated *in vivo*) were amplified with iTaq DNA polymerase using 5' oligos containing a BamHI site before the start codon and 3' oligos containing a SalI site after a stop codon. PCR products were cloned into pCR2.1 TOPO using the TOPO TA cloning kit and fully sequenced before subcloning into expression plasmids. Fragments were then subcloned into the BamHI and SalI sites of pET28MBP, described by Davies et al. (Davies, Carney et al. 2005), to yield pET28MBP-Vps9, -Muk1, -Vps21ΔC, Ypt52ΔC, Ypt53ΔC. The same fragments

of *VPS21*, *YPT52*, and *YPT53* were subcloned into the BamHI and SalI sites of pGST to yield pGST-Vps21ΔC, -Ypt52ΔC, Ypt53ΔC. Site directed mutagenesis was also performed with full-length Ypt52 and Ypt53 to generate $Ypt52^{S17N}$ and $Ypt53^{S26N}$ point mutants. The BamHI/SalI fragments of both WT and SN mutants were then subcloned into the two-hybrid plasmid pVJL11.

Protein expression and purification

pET28MBP-Vps9, -Muk1, -Vps21ΔC, -Ypt52ΔC, and -Ypt53ΔC were expressed in BL21(DE3) grown in LB medium supplemented with kanamycin to an OD_{600} of 0.6 - 1.0 and induced with 100 – 500 mM isopropyl β-d-thiogalactoside (IPTG) at 37˚C for 3 – 6 hours or at 22˚C for 16 – 20 hours. Cell pellets were harvested and frozen at -80˚C. After thawing, pellets were resuspended on ice in His Buffer A (25 mM $NaPO_4$, 300 mM NaCl, 5 mM $MgSO_4$, pH 7.5) supplemented with Complete EDTA-free protease inhibitors and 200 μM AEBSF, lysed using a French Press, and centrifuged. Supernatants were passed through 0.45 μm syringe filters and loaded into the AKTA FPLC for purification using a HiTrap Chelating HP column loaded with $NiSO_4$. After injection, the column was washed with 20 mM imidazole before proteins were eluted with a gradient of 20 – 250 mM imidazole. Relevant fractions were concentrated, adjusted to 1mM DTT, and cut overnight with His_6TEV at 16˚C to cleave the His_6MBP tag. Cleaved protein was buffer exchanged using a HiPrep

26/10 Desalting column to remove imidazole before a second pass through the HiTrap Chelating HP column to remove the His_6MBP tag and His_6TEV. Remaining contaminants were removed using a HiLoad 16/60 Superdex 75 gel filtration column.

In vitro binding assay

GST alone or fused to Vps21ΔC, Ypt52ΔC, or Ypt53ΔC were expressed in BL21(DE3) grown in LB supplemented with 100 μg/ml ampicillin to an OD_{600} of 0.6 before being induced with 500 μM IPTG for 6 hours at 30˚C. Pellets were harvested, resuspended in PBS (10 mM $NaPO_4$, 137 mM NaCl, 2.7mM KCl, pH 7.4), lysed by addition of 1mg/ml lysozyme for 30 minutes, sonicated and centrifuged. Supernatants were aliquoted and frozen at -80˚C. Glutathione sepharose beads were equilibrated with PBST (PBS with 0.5% Tween-20) before being incubated with GST or GST-fusions for 1 hour at 4˚C. Beads were washed with PBST and incubated with either partially purified HisMBP-tagged Vps9 or Muk1 for 1 hour at 4˚C. Beads were washed again with PBST before bound protein was eluted by addition of 5x Laemmli Sample Buffer (312 mM Tris, 10 % sodium dodecyl sulfate (SDS), 25 % β-mercaptoethanol, 0.05 % bromophenol blue, pH 6.8) and heating at 95˚C for 4 minutes. Eluted protein was separated by SDS-PAGE and detected by western analysis with MBP primary antiserum

(1:8000), HRP-conjugated anti-mouse secondary antibody (1:3000) and SuperSignal West Femto Maximum Sensitivity Substrate (1:2).

Nucleotide exchange assay

FRET-based nucleotide exchange assays were performed essentially as detailed previously (Davies, Carney et al. 2005). Purified Rab proteins were loaded with fluorescent nucleotide by incubation with equimolar mant-GDP and excess EDTA at 30˚C for 30 minutes. EDTA and unbound nucleotide were removed by desalting into exchange assay buffer (20mM HEPES, 5mM $MgSO_4$, pH 7.5). FRET signal (exciting Rab tryptophan at 290nm, measuring mant-GDP emission at 440nm) was monitored using a Photon Technology International fluorometer (model QM-2001–4) and the PTI Felix32 software. Mant-GDP-loaded Rabs was allowed to stabilize for 100 seconds before addition of varying amounts of HisMBP-Vps9 or -Muk1. After another 100 seconds, 100μM GTP was added and exchange was monitored for 15 minutes.

Immunoprecipitations

After *MET*$^+$ double and triple deletion strains were identified, ^{35}S-CPY and -CPS immunoprecipitations from wild-type and deletion mutant strains were carried out essentially as detailed previously (Davies, Carney et al. 2005). Cultures were grown in synthetic medium lacking methionine and buffered with

25 mM KPO_4 (pH 5.4) to an OD_{600} of 0.6 - 0.8. 5 OD_{600} per planned time-point was labeled with ^{35}S-methionine for 10 minutes and incubated with excess unlabeled methionine for 30 - 90 minutes. At time-points, 5 OD_{600} was harvested, precipitated with TCA and processed for immunoprecipitation with αCPY or αCPS antisera. Isolated material was then resolved by SDS-PAGE and labeled proteins were detected by fluorography or phosphorimagery. Quantitation was performed using ImageQuant.

Fluorescence microscopy

Images were acquired using a Zeiss inverted microsocope equipped with a Photometrix Coolsnap HQ digital camera and deconvolved using Delta Vision software from Applied Precision. Cells were grown in minimal media at 30˚C to a OD_{600} of ~ 0.5. For analysis of cells expressing Ste3-GFP and mCherry-Pep12, cells were directly analyzed. For comparison of Ste3-GFP and FM4-64, cells were resuspended in YPD containing FM4-64 for 15 minutes and then diluted with an excess of YPD for >1 hour. 45 minutes before harvesting samples, cyclohexamide was added.

CHAPTER THREE

Mutational Analysis of the Vps9 Domain and an Interdependence between the Vps9 and CUE domains

Overview

Vps9 is the founding member of a family of Rab5 guanine nucleotide exchange factors (GEFs) that share a conserved domain by the same name. A mutational analysis of Vps9's catalytic domain was undertaken for the purpose of identifying residues critical for GEF activity. Mutations of seven residues significantly impacted Vps9 GEF activity or *in vivo* function, including a potentially catalytic aspartate residue. Analysis of these mutants uncovered an interdependence between the Vps9 domain and the CUE domain that may serve to auto-inhibit both.

Introduction

Comprising the largest class of Ras-like small GTPases with 11 members in yeast and at least 60 in humans (Bock, Matern et al. 2001), Rab proteins are charged with the task of regulating vesicular trafficking events between the many

organelles within the cell (Zerial and McBride 2001). As GTPases, they accomplish this task by interacting with various effector proteins in a manner dependent on their nucleotide state (Grosshans, Ortiz et al. 2006; Novick, Medkova et al. 2006), which is governed by GTPase activating proteins (GAPs) and guanine nucleotide exchange factors (GEFs). GAPs inactivate Rabs by accelerating the rate of hydrolysis from GTP to GDP. GEFs then reactivate Rabs by promoting the dissociation of GDP, allowing the more prevalent GTP to bind and thus reactivating the Rab. Unlike Rab GAPs, which are relatively promiscuous, Rab GEFs show strict specificity for their cognate Rab or Rab family (Segev 2001).

The Rab5 family regulates trafficking through the early endocytic pathway (Gorvel, Chavrier et al. 1991; Bucci, Parton et al. 1992). Rabex5 (Horiuchi, Lippe et al. 1997)and Vps9 (Hama, Tall et al. 1999)were identified as GEFs for Rab5 and its yeast ortholog Vps21. A centrally located conserved region of these proteins, now known as the Vps9 domain, was proven to be necessary and sufficient for this activity (G. Tall, unpublished). The Vps9 domain demonstrated no significant sequence similarity with any other classes of GTPase GEFs, including the CDC25 domain of Ras GEFs, the Dbl homology (DH) domain of Rho GEFs, and the Sec7 domain of Arf GEFs. However, it was similar in both its overall size and its predicted mostly helical secondary structure to these other GEF domains.

As structural and mutational analyses began to elucidate the mechanisms of nucleotide exchange employed by these GEFs, a common theme appeared to be the insertion of a acidic residue into the nucleotide binding pocket (Cherfils and Chardin 1999). In the case of the Sec7 domain, a series of ARF/Sec7 domain structures confirmed the predicted insertion of an invariant glutamate residue known as the 'glutamate finger' (Beraud-Dufour, Robineau et al. 1998) into a position to interact with the phosphate-binding loop and prevent the coordination of Mg^{2+} and GDP (Goldberg 1998; Mossessova, Corpina et al. 2003; Renault, Guibert et al. 2003). A Ras/CDC25 domain structure implicated the insertion of both a glutamate residue and a leucine residue into the nucleotide binding pocket (Boriack-Sjodin, Margarit et al. 1998), and mutagenesis of DH domains had identified at least two sites where either an acidic residue or a serine/threonine residue might act in a similar manner (Aghazadeh, Zhu et al. 1998; Soisson, Nimnual et al. 1998).

Vps9 also contains a carboxy-terminal ubiquitin-binding motif known as the CUE domain (Ponting 2000), which is necessary and sufficient for Vps9's interaction with ubiquitin and facilitates its ubiquitination (Davies, Topp et al. 2003; Donaldson, Yin et al. 2003; Shih, Prag et al. 2003). The binding of ubiquitin by the CUE domain is required for proper endocytosis of the mating factor receptor Ste3 (Davies, Topp et al. 2003), but deletion of the CUE domain impacts neither the Vps9-dependent biosynthetic sorting of the vacuolar hydrolase

carboxypeptidase Y (CPY) nor the GEF activity of the protein. In fact, a Vps9 construct lacking the carboxy-terminal region including the CUE domain exhibited greater GEF activity than wild-type Vps9 in vitro (G. Tall, unpublished).

One of my goals was to use structural information about the Vps9 domain/ Rab5 family complex to infer a model for the mechanism of nucleotide exchange, which would then be tested by mutagenesis. While pursuing this structural information (see Chapter 4) a mutational analysis was initiated to identify critical residues of the Vps9 domain for the purpose of predicting an exchange mechanism. Through this analysis, we identified seven residues important for Vps9 function, including a prospective catalytic aspartate residue. In addition, we uncovered a potential regulatory mechanism through which the CUE domain affects GEF activity of the Vps9 domain and the Vps9 domain affects ubiquitin binding by the CUE domain.

Results

Alignment of available Vps9 domain sequences showed two universally conserved acidic residues corresponding to Vps9 Asp251 and Glu288 (Figure 16). As aspartate and glutamate residues had previously been implicated in the exchange mediated by GEFs for Ras, Arf, Rho, and Ran, we began our analysis with these two residues. $Vps9^{D251A}$ and $Vps9^{E288A}$ cassettes were generated

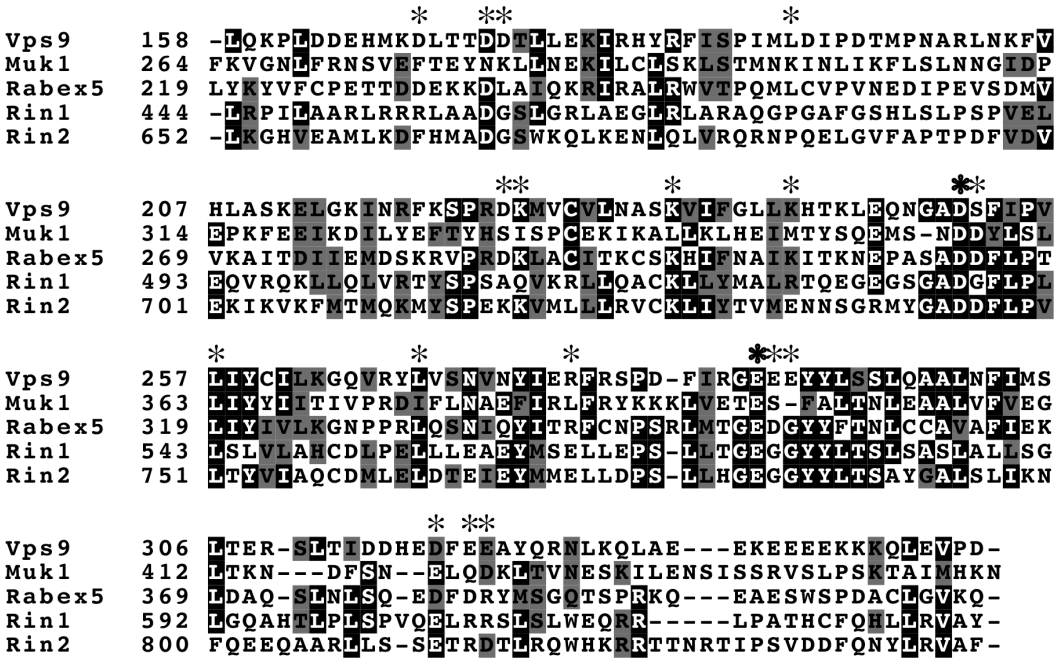

Figure 16. Conservation of mutated Vps9 domain residues. The sequence alignment between the Vps9 domains of the yeast and mammalian Vps9 domain-containing proteins known at the inception of these studies obtained using ClustalW 1.8 from the Baylor College of Medicine Search Launcher and the BOXSHADE server is shown. Black boxes indicate amino acid identity, and shaded boxes indicate conservative amino acid substitutions. Asterisks indicate residues mutated in these analyses, and bold asterisks indicate the conserved acidic residues mutated first.

manually using a three-step PCR method. Wild-type Vps9 had previously been shown to interact preferentially with the GDP-bound or nucleotide free Vps21 mutant Vps21^{S21N} using the yeast two-hybrid system (see Chapter 1 for more detail). Prey constructs encoding Gal4 activation domain-fusions of these Vps9 mutants were cotransformed into the L40 reporter strain with a bait encoding a LexA DNA binding domain-fusion of Vps21^{S21N}. Their interaction was then scored by their ability to drive transcription of the *HIS3* gene under control of the

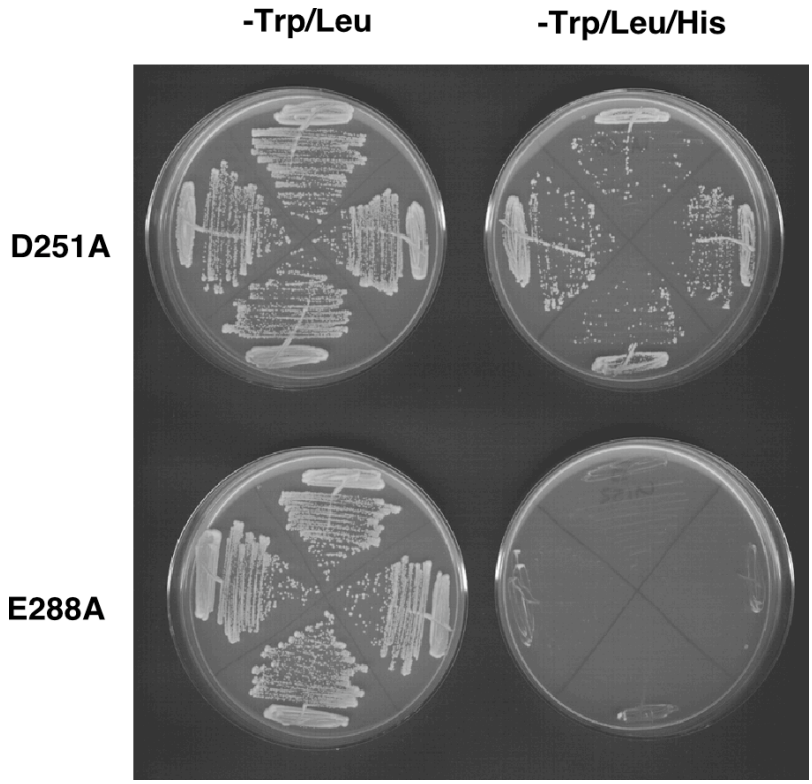

Figure 17. Two-hybrid interaction of Vps9^{D251A} and Vps9^{E288A} with Vps21^{S21N}. Two hybrid preys encoding Vps9^{D251A} or Vps9^{E288A} were cotransformed into L40 yeast with the Vps2l^{S21N} bait plasmid. Individual transformants were streaked onto YNB plates lacking either tryptophan and leucine as control or tryptophan, leucine and histidine to detect positive interactions between bait and prey.

LexA promoter and promote growth on media lacking histidine. As shown in Figure 17, Vps9^{D251A} retains the ability to interact with Vps21^{S21N}, while the E288A mutation ablates this interaction.

To assess the GEF activity of these mutant proteins, His_6-tagged versions of Vps9^{D251A} and Vps9^{E288A} were expressed along with wild-type Vps9 and tested for their ability to stimulate [^{3}H]-GDP release from Vps21 using a filter binding assay. In this method, Vps21 was loaded with [^{3}H]-GDP and incubated with

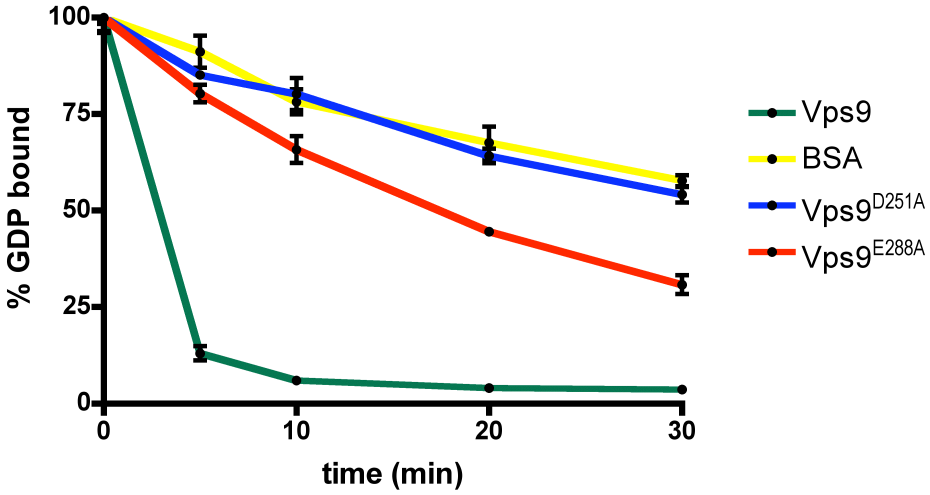

Figure 18. GEF activity of Vps9^{D251A} and Vps9^{E288A} toward Vps21. Vps21 (200 pmol) was preloaded with 15µM [^{3}H]-GDP then diluted into 200 µl assay mixtures containing 4 mM non-radioactive GDP and 200 pmol each of the following: BSA (yellow), His$_6$-Vps9 (green), His$_6$-Vps9^{D251A} (blue), and His$_6$-Vps9^{E288A} (red). At each time point, aliquots were removed, added to ice-cold quench buffer, and filtered through nitrocellulose membranes, which were then washed, dried, and counted. The percentage of [^{3}H]-GDP that remained protein-bound is presented as a function of time. Error bars are shown for three replicate experiments.

either BSA or one of the Vps9 proteins in the presence of excess unlabeled nucleotide. At time-points, samples were passed through a nitrocellulose filter to remove free nucleotide, and the [^{3}H]-GDP retained by Vps21 was quantitated by scintillation counting. As seen previously, wild-type Vps9 shows a significant stimulation of GDP release relative to the intrinsic rate represented by the BSA sample. Vps9^{E288A}, which did not interact with Vps21 in the yeast two-hybrid assay, did show a modest stimulation of GDP release, indicating that the E288A mutation allowed some level of association *in vitro*. Interestingly, Vps9^{D251A},

which did show a Vps21 interaction by yeast two-hybrid, showed a rate of GDP release indistinguishable from that of the BSA sample. The finding that the D251A mutation resulted in a Vps9 protein that could still bind its Rab but failed to stimulate nucleotide release suggested that Asp251 had a catalytic role in the GEF activity of Vps9.

To determine whether these mutations affected Vps9 function in vivo, we tested their ability to complement the CPY vacuolar sorting defect of cells that lacked wild-type Vps9 using the pulse-chase method as described in Chapter 2. Plasmids expressing wild-type or mutant Vps9 at the CEN level from the *VPS9* promoter were transformed into *Δvps9* yeast, labeled with ^{35}S-methionine and cysteine for 10 minutes and chased with unlabeled methionine and cysteine for 30 minutes. CPY was then immunoprecipitated from either the intracellular (I) or

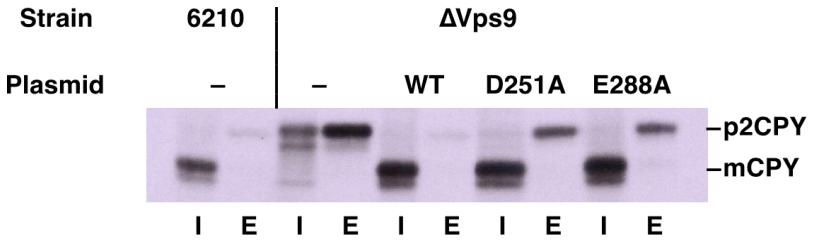

Figure 19. CPY sorting in yeast expressing Vps9^{D251A} and Vps9^{E288A}. pRS416-based plasmids expressing wild-type Vps9 or the indicated Vps9 point mutants from the *VPS9* promoter were transformed into CBY1 yeast (*Δvps9*). Alongside untransformed CBY1 and 6210 (wild-type), these yeast were pulse labeled with ^{35}S-Pro-Mix for 10 minutes at 30˚C. Chase solution with unlabeled methionine and cysteine was added and the cells were incubated for an additional 30 minutes. CPY was then immunoprecipitated from either the intracellular (I) or extracellular (E) fractions of these cells and resolved by SDS-PAGE. The positions of mature vacuolar (m) and Golgi-modified precursor (p2) forms of CPY are indicated.

extracellular (E) fraction. In *Δvps9* yeast, the vast majority of CPY was secreted from the cell in its Golgi-modified precursor form. Wild-type Vps9 complemented this phenotype almost entirely, as indicated by the majority of CPY being found in the intracellular fraction in its mature form, signifying delivery to the vacuole. $Vps9^{D251A}$ and $Vps9^{E288A}$, which exhibited no GEF activity and only modest GEF activity, respectively, in vitro, surprisingly showed similar yet modest missorting phenotypes. While neither of these mutations are as severe as the *Δvps9* deletion, these data indicate that both Asp251 and Glu288 play a role in Vps9 function in vivo, but are not essential.

Encouraged by these initial results, we expanded our mutational analysis. Seventeen additional residues that were largely conserved in available Vps9 domain sequences were targeted for mutation, and several double mutants were planned, including a combination of D251A and E288A. Our experience with these first two mutants had identified a number of steps where our procedures should be streamlined in order to increase the throughput of these analyses. The first such step was in the generation of the mutants themselves. This new round of mutations was generated using the Gene Tailor system (Invitrogen), which required only one PCR per mutation. In addition, these mutations were introduced into an excised fragment of the *VPS9* gene in pBS, which after verification could be reincorporated into Vps9 expression vectors. This both decreased cost and

effort involved in sequencing mutants and allowed for a uniform method of cloning Vps9 mutants into a new standardized set of plasmids.

The full set of Vps9 mutants were cloned into a yeast expression plasmid containing 100bp of the *VPS9* promoter and scored for their ability to complement the CPY sorting defect in *Δvps9* yeast. The ^{35}S-pulse/chase assay was performed as above, except that intracellular and extracellular fractions were not separated. In addition, Vps9 was immunoprecipitated from these samples to correlate potential sorting phenotypes with possible destabilization of the Vps9 protein by the harbored mutation. As seen in Figure 20 expressing wild-type Vps9 from the 100kb promoter resulted in a level of Vps9 equivalent to that seen using the longer 1kb promoter, and in both cases, wild-type Vps9 fully complemented the defect observed in cells transformed with empty vector. As seen above, Vps9^{D251A} and Vps9^{E288A} show a partial disruption of CPY delivery to the vacuole, though under these conditions, the E288A mutation appears slightly less severe than D251A. Neither of these two mutants show a decrease in protein level in the Vps9 immunoprecipitation, indicating that these mutations do not affect the stability of the protein in the time frame of these experiments. A combination of these two mutations showed a phenotype more severe than that of either alone. In fact, yeast expressing Vps9$^{D251A/E288A}$ show a level of CPY missorting similar to that of yeast transformed with empty vector, while this double mutation still does not have a significant impact on the stability of the protein.

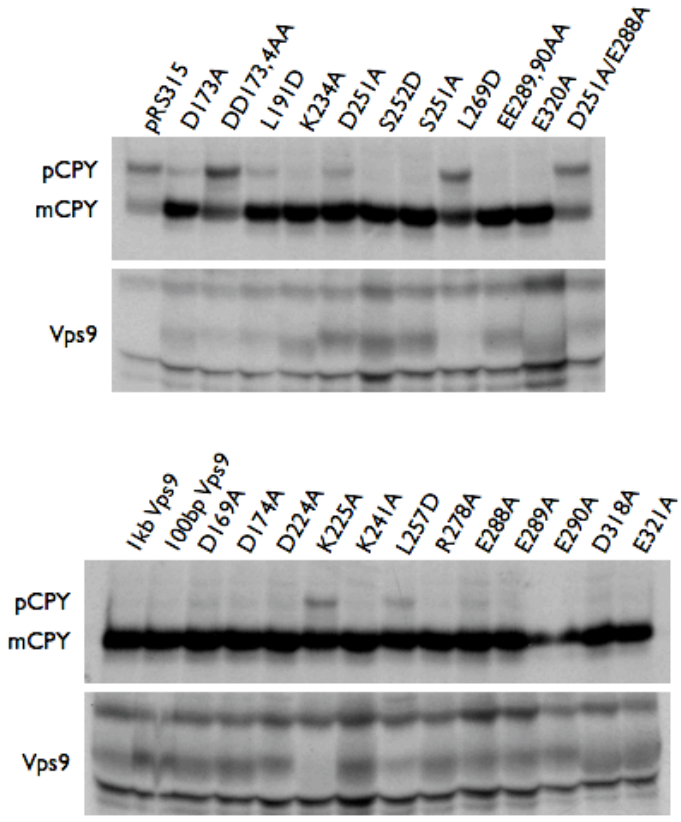

Figure 20. CPY sorting and Vps9 levels in yeast expressing Vps9 domain mutants. pRS315-based plasmids expressing wild-type Vps9 from the 1kb or 100bp Vps9 promoter or the indicated Vps9 point mutants from the 100bp Vps9 promoter were transformed into *Δvps9* yeast alongside empty vector. These yeast were pulse labeled with ^{35}S-Pro-Mix for 10 minutes and chased with unlabeled amino acids for an additional 30 minutes at 30˚C. CPY and Vps9 were then immunoprecipitated from the combined intracellular and extracellular fractions and resolved by SDS-PAGE. The positions of mature vacuolar (m) Golgi-modified precursor (p2) CPY and Vps9 are indicated. CPY bands were quantitated using GelEval, and the percent of CPY found in the p2 form for each sample is graphically represented below.

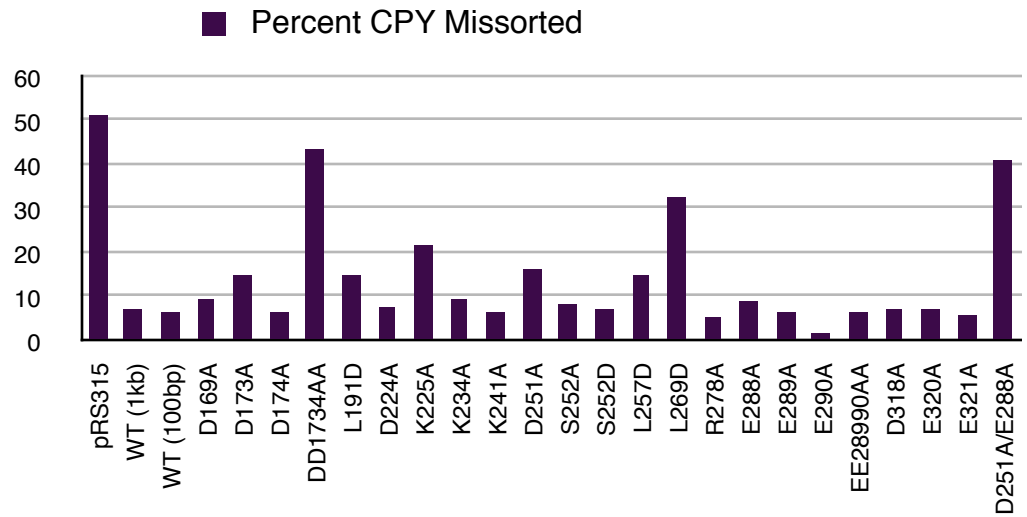

The most widely conserved residue mutated in this round of mutagenesis was Asp173, and yeast expressing Vps9^{D173A} did show an increased level of CPY missorting. Because Vps9 contains an aspartate in the next position, where most Vps9 domains do not, we mutated Asp174 as well and constructed a double mutant of these two (DD173,4AA). Unlike the Vps9^{D173A}, Vps9^{D174A} fully complemented the *Δvps9* phenotype. On the other hand, Vps9^{DD173,4AA} showed a level of missorting similar to that of Vps9$^{D251A/E288A}$, indicating that the effect of the D173A mutation may have been buffered by the ability to substitute Asp174 for the mutated Asp173. Both Vps9^{D173A} and Vps9^{DD173,4AA} show a reduction in Vps9 levels indicating that these mutants are less stable than wild-type Vps9. Mutation of either of two leucine residues (Leu191 or Leu257) to aspartate also results in a Vps9 protein that fails to fully complement the *Δvps9* phenotype but may be less stable than wild-type Vps9. Finally, yeast expressing Vps9^{K225D} or Vps9^{L269D} show a severe CPY missorting phenotype but contain almost no detectable Vps9 protein, suggesting that these mutants are highly unstable due to misfolding of the Vps9 domain. Other mutants examined show full complementation of the *Δvps9* phenotype, indicating that these residues are not critically involved in Vps9 function.

In order to determine how these mutations affected the GEF activity of Vps9 in vitro, each mutant was cloned into pET28MBP. Expressing these proteins as His_6MBP-tagged fusions allowed purification by affinity chromatography and

improved yield of several of the less stable mutants. Using this procedure, sufficient quantities of all but three mutants (Vps9^{K225A}, Vps9^{L257D}, and Vps9^{L269D}) were generated for analysis in the fluorescence-based nucleotide release assay described in Chapter 2. Vps21 was loaded with N-methylanthraniloyl GDP (mantGDP), whose fluorescence is quenched upon release from the nucelotide-binding pocket, and was incubated with purified wild-type or mutant Vps9 protein at either 25˚C or 30˚C. The resulting curves of fluorescence versus time (shown for the 30˚C experiment in Figure 21) were fit to

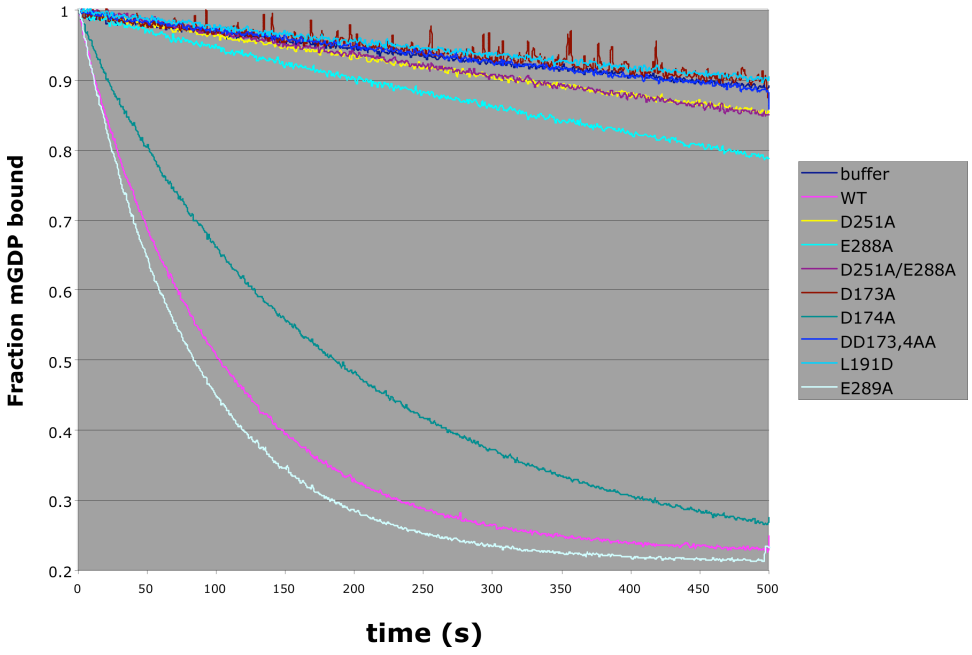

Figure 21. Stimulation of mantGDP release from Vps21 by Vps9 domain mutants at 30˚C. Vps21 (2μM) was preloaded with mantGDP and incubated with buffer alone or equimolar wild-type or mutant Vps9 at 30˚C. At time=0, GTP was added to 100μM, and the release of mantGDP was monitored by the FRET signal emitted at 440 with emission at 290. Curves of fraction mantGDP bound vs. time were fit to an exponential decay equation using proFit, and the rate constants (k_{obs}) and fold stimulation relative to buffer (Δk_{obs}) for the above experiment and an identical experiment at 25˚C are shown in Table 2.

Table 2. Stimulation of mantGDP release from Vps21 by Vps9 domain mutants.

Vps9 added	25˚C		30˚C	
	k_{obs} (s^{-1})	Δ k_{obs}	k_{obs} (s^{-1})	Δ k_{obs}
None (buffer)	1.73E-04	-	3.23E-04	-
Wild-type	3.91E-03	22.5	9.23E-03	28.6
D251A	2.11E-04	1.2	4.21E-04	1.3
E288A	2.76E-04	1.6	6.32E-04	2.0
D251A/E288A	1.98E-04	1.2	4.18E-04	1.3
D173A	1.68E-04	1.0	2.87E-04	0.9
D174A	2.59E-03	14.9	5.25E-03	16.2
DD173,4AA	1.74E-04	1.0	3.22E-04	1.0
L191D	1.59E-04	0.9	2.77E-04	0.9
E289A	5.81E-03	33.5	1.14E-02	35.3
D318A	3.04E-03	17.6	-	-
S252D	3.92E-03	22.7	-	-

an exponential decay equation to determine the observed rate constant and the fold stimulation for each (Table 2). At 30˚C, as seen above using the [^{3}H]-GDP release assay, wild-type Vps9 significantly increased the rate at which GDP is released from Vps21, with a rate constant nearly 30 times that of buffer alone. In contrast, Vps9^{D251A} and Vps9^{E288A} showed only 1.3- and 2-fold increases, respectively, in the rate of nucleotide release; hence, the D251A and E288A mutations reduce the activity by 99% and 93%, respectively. The severity of these mutations *in vitro* left little room for the exacerbating effect seen *in vivo* when combining these mutations and demonstrated a major difference between these two methods of assessing the function of Vps9 mutants. Three proteins, Vps9^{D173A}, Vps9^{DD173,4AA} and Vps9^{L191D}, failed to stimulate nucleotide release altogether. Each of these three showed decreased levels *in vivo* by Vps9 immunoprecipitation, and while the proteins are soluble enough for purification,

they may be incorrectly folded as a consequence of these mutations. Interestingly, while mutation of Glu288 has a strong negative effect on Vps9's activity, Vps9^{E289A} actually stimulates nucleotide release better than wild-type, a phenomenon that is even more pronounced at the lower temperature.

A link between the Vps9 domain and the CUE domain

Immunoprecipitation of Vps9 was used above to assess the protein level as an indicator of the stability of the mutant protein. As an alternative approach, protein levels were determined by western analysis of lysates from *Δvps9* yeast expressing wild-type or mutant Vps9 from the 100bp *VPS9* promoter. On the whole, this assay confirmed the immunoprecipitation data with respect to which mutants showed a decrease in protein level (data not shown), but analysis of a

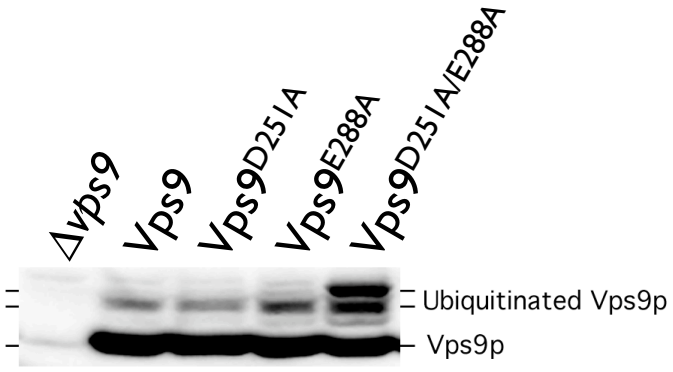

Figure 22. Ubiquitination of Vps9 domain mutants. pRS315-based plasmids expressing wild-type Vps9 or the indicated Vps9 point mutant from the 1kb *VPS9* promoter were grown to a density of ~0.6 OD_{600}/ml. Cells (2 OD600) were vortexed for 10 minutes with glass beads, and lysates were separated by SDS-PAGE. The presence of unmodified Vps9 and ubiquitinated Vps9 was detected by Western blotting with αVps9 antibody.

subset of these mutants expressed with the longer 1kb *VPS9* promoter revealed a curiosity. The major band detected with αVps9 antibody was identical in lysates from yeast expressing wild-type Vps9, Vps9^{D215A}, Vps9^{E288A} and Vps9$^{D251A/E288A}$. However, an upper band, which had earlier been characterized as a ubiquitinated form of Vps9 (Davies, Topp et al. 2003), was increased in Vps9^{E288A} and far more prevalent in Vps9$^{D251A/E288A}$., indicating that these mutants result in greater ubiquitination of Vps9.

Ubiquitination of Vps9 has been shown in the laboratory to be affected by defects in endosomal trafficking. Strains in which other Class D VPS proteins have been deleted, including *Δvps21*, *Δvps8*, *Δvps45*, *Δpep12*, *Δvac1*, *Δvps15*, *Δvps34*, and *Δvps3*, show higher levels of Vps9 ubiquitination than seen in wild-type yeast (B. Davies, unpublished). Though the source of this increase remains unclear, the elevated ubiquitination of these Vps9 mutants may similarly be a related to slowed endosomal delivery as a consequence of decreased Vps9 function. If the ubiquitination of these mutants were strictly a result of decreased activity of Vps9, however, it would be expected that Vps9^{D251A}, which showed a stronger defect than Vps9^{E288A} both in vitro and *in vivo*, would show at least the same level of ubiquitination as Vps9^{E288A}, rather than a level closer to wild type as seen.

Previous work in our laboratory and others established that the carboxy terminal CUE domain of Vps9 binds monoubiquitin(Davies, Topp et al. 2003;

Donaldson, Yin et al. 2003; Shih, Prag et al. 2003). To further investigate the connection between these mutants and ubiquitin, a series of GST pull-downs were performed. Purified wild-type or mutant Vps9 protein was incubated with either GST-Vps21 or GST-Ubiquitin, and their interaction was detected after isolation with glutathione sepharose beads by western blotting. The results were striking in that most proteins either bound Vps21 or ubiquitin. This dichotomy appears to correlate with Vps9 function, as wild-type Vps9, Vps9^{D174A}, and others with normal Vps9 activity bound Vps21 while Vps9^{E288A}, Vps9^{D173A} and several others with reduced Vps9 activity bound ubiquitin. Vps9^{D251A} was the only mutant to bind both Vps21 and ubiquitin, and it did so, in both cases to a lesser degree than proteins that bound one or the other. These results suggest an inverse relationship

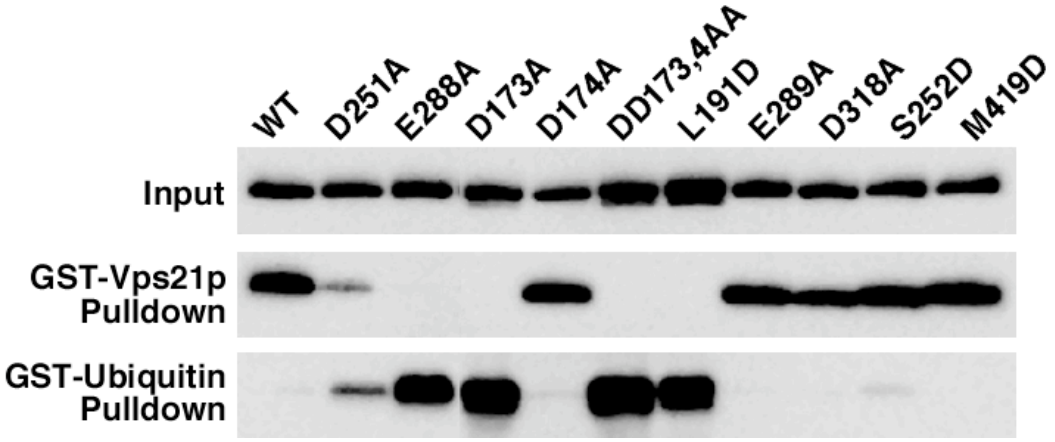

Figure 23. Binding of Vps9 mutants to Vps21 and ubiquitin. GST-tagged Vps21 or GST-tagged ubiquitin was conjugated to glutathione sepharose beads and incubated with purified wild-type Vps9 or the indicated Vps9 point mutant. Beads were isolated and washed, and the resulting complexes were analyzed by SDS-PAGE and Western blotting with αVps9 antibody. Inputs were identical for both experiments.

between Vps21 binding and ubiquitin binding by Vps9 mutants. One model is that the Vps9 domain and CUE domain interact to auto-inhibit their respective activities, such that mutations that perturb the Vps9 domain release the auto-inhibition of the CUE domain.

To further explore this model, we examined whether CUE domain mutants would potentiate Vps9 domain activity. A previous structure/function analysis of the Vps9 CUE domain identified a number of residues that were critical to the binding of ubiquitin by this domain (Davies, Topp et al. 2003; Prag, Misra et al. 2003). To study the apparent link between ubiquitin binding and GEF activity, several of these mutants were analyzed in the fluorescent nucleotide release assay described above (Figure 24). Under the conditions used, wild-type Vps9 showed a nearly eight-fold stimulation of the intrinsic mantGDP release from Vps21 (Table X). The ubiquitin mutations of either Leu427 or Leu447 had minimal effect on Vps9 GEF activity. $Vps9^{M419D}$, on the other hand, showed a dramatic enhancement of GEF activity, to more than four times that of wild-type Vps9. These results suggested that specific residues involved in CUE domain ubiquitin binding may auto-inhibit Vps9 domain activity. Further analysis of the impact of additional CUE domain mutations on Vps9 domain activity will be required to confirm this model.

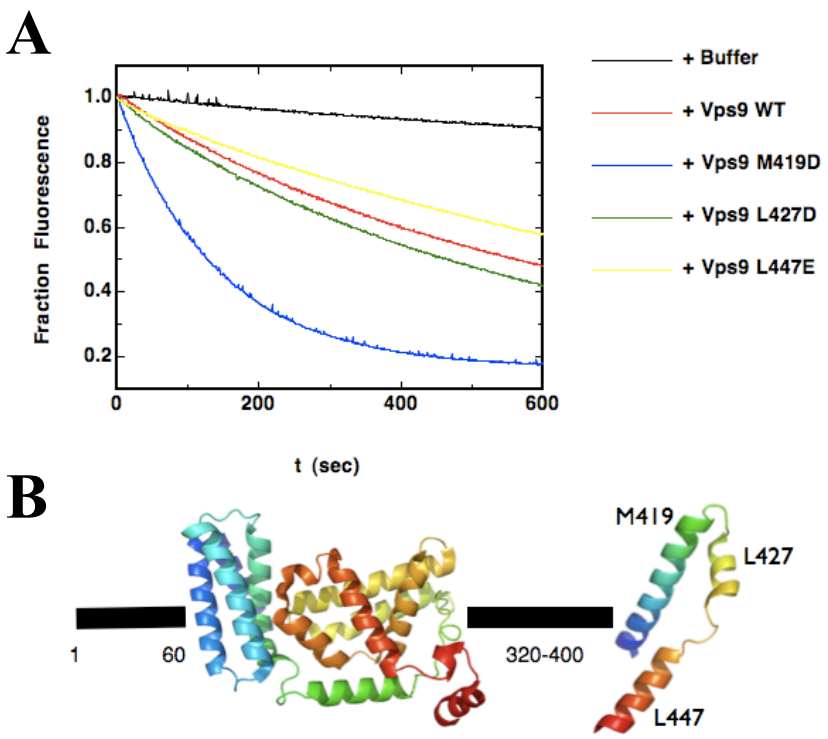

Figure 24. A CUE domain mutation increases GEF activity of the Vps9 domain. (A) Vps21 (2.5μM) was preloaded with mantGDP and incubated with buffer alone or equimolar wild-type or mutant Vps9 (0.5μM) at 25˚C. At time=0, GTP was added to 100μM, and the release of mantGDP was monitored by the FRET signal emitted at 440 with emission at 290. Curves of fraction mantGDP bound vs. time were fit to an exponential decay equation using proFit, and the rate constants (k_{obs}) and fold stimulation relative to buffer (Δk_{obs}) are shown in Table 3. (B) A structural map of Vps9 shows the location of the helix bundle and Vps9 domain (middle) and the CUE domain (carboxy-terminus), including the positioning of the three residues mutated in the proteins examined by the mantGDP release assay.

Table 3. Stimulation of mantGDP release from Vps21 by Vps9 CUE domain mutants.

Vps9 added	k_{obs} (s^{-1})	Δk_{obs}
none (buffer)	2.20E-04	-
wild-type	1.70E-03	7.7
M419D	7.10E-03	32.2
L427D	2.10E-03	9.5
L447D	1.40E-03	6.3

Discussion

Mutagenesis and the potential mechanism of nucleotide exchange

Our mutational analysis identified seven residues that when mutated significantly impacted Vps9 function. Of these, we suspected Lys225, Leu257, and Leu269 to contribute to the structural integrity of the Vps9 domain, as mutations of these residues not only showed the worst defects in CPY sorting but also exhibited markedly reduced levels of Vps9 in yeast cells and prevented isolation of soluble recombinant Vps9 protein from *E. coli*. Mutation of Asp173 and Leu191 also resulted in reduced cellular levels, but we were able to purify these proteins for biochemical assays. Finally, mutation of Asp251 and Glu288 showed no impact on cellular levels, even in combination as a double mutant, though both resulted in a CPY sorting defect and effectively abolish GEF activity *in vitro*. The inability of $Vps9^{E288A}$ to bind Vps21 by either two-hybrid or GST pull-down suggests that the effect of this mutation on Vps9 function arises from its inability to interact with the Rab. In contrast, $Vps9^{D251A}$ did interact with Vps21 in both assays yet had a stronger defect. These data, along with this residue's conservation throughout the Vps9 domain family, implied that Asp251 could have a catalytic role in Rab5 nucleotide exchange. However, the ability of yeast expressing $Vps9^{D251A}$ to correctly sort significantly more CPY than *Δvps9* cells may argue that the action of this aspartate is not the sole mechanism of nucleotide exchange and/or that proper sorting of CPY requires a function of

Vps9 in addition to the catalysis of nucleotide exchange. The former argument will be discussed further below and in Chapter 4, but evidence in support of the latter argument is provided by the finding that the amino terminus of Vps9, though not required for nucleotide exchange of Vps21 *in vitro*, is necessary to complement a *Δvps9* CPY sorting phenotype *in vivo* (G. Tall, unpublished.)

After these mutational analyses and while we were pursuing structural data on the Rab5/Vps9 domain interaction (see Chapter 4), the crystal structure of the Rabex-5 Vps9 domain was published by Lambright and colleagues (Delprato, Merithew et al. 2004). The structure consisted of a layered fold of six α-helices, with an additional carboxy-terminal helix that is missing from the Vps9-domain containing GEFs Alsin, ALS2CL and Rap6, and an amino-terminal bundle of four α-helices that is outside the conserved region identified as the Vps9 domain in databases and outside the minimal domain required for Vps9 function. Mapping our mutations to this structure allowed further interpretation of some of our observations (Figure 25). Leu191, Lys225, Leu257, and Leu269 are indeed buried within the layers of helices, where their mutation could plausibly destabilize the overall structure of the domain. Specifically, mutation of Lys225 may impact the nearby hydrogen bond formation between the backbone amide of Arg223 and the carboxylate group of Glu138 (analogous to Rabex5 Arg285 and Glu212, respectively), which Delprato et al. report is essential for the stabilization of the Rabex5 Vps9 domain by the helix bundle (Delprato, Merithew et al. 2004).

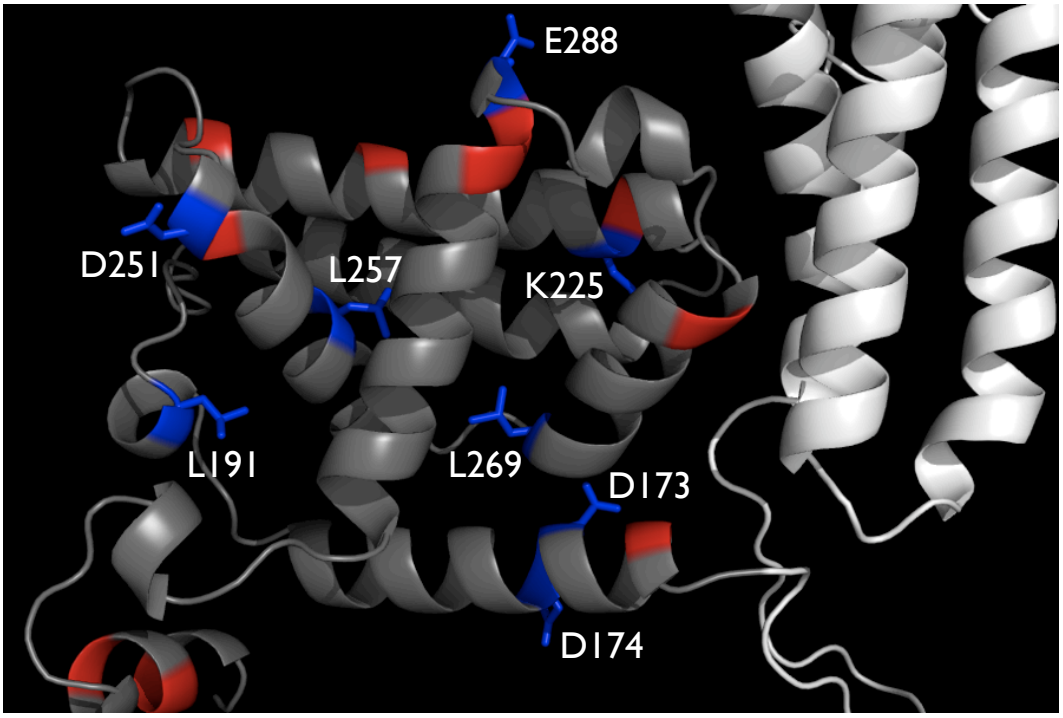

Figure 25. Structural position of Vps9 domain residues mutated. The Vps9 domain of Vps9 was modeled from the crystal structure of the Vps9 domain of Rabex5 (1TXU) using the Swiss-Model server. Residues discussed in this section are labeled and colored blue. The locations of other residues analyzed are indicated in red. The carboxy-terminal helix bundle is indicated in white. All structure figures were created using PyMol.

They also report a similar interaction between Asp173 and Ser271 of the adjacent helix (Rabex5 Asp235 and Ser333, respectively) is critical for Vps9 domain stability, though we were able to purify suitable quantities of $Vps9^{D173A}$ and $Vps9^{DD173,4AA}$ for analysis.

The highest concentration of conserved surface residues within Vps9 domains is located on and around a hydrophobic groove between αV4 and αV6 (Delprato, Merithew et al. 2004). Interestingly, despite the lack of sequence identity or overall similarity in tertiary structure between the Vps9 domain and

GEFs for different GTPase families, Delprato et al. recognized that this hydrophobic groove resembles an analogous substructure within the Sec7 domain of Arf GEFs (Mossessova, Gulbis et al. 1998; Mossessova, Corpina et al. 2003; Renault, Guibert et al. 2003). As seen in Figure 26, this parallel extends to the orientation of Asp251 (Rabex5 Asp313) in approximately the same position as the catalytic 'glutamate finger' in the Sec7 domain (reviewed in (Jackson and Casanova 2000)). These likenesses led Delprato et al. to the suggestion that the Vps9 domain may act through a mechanism of exchange similar to that of the Sec7 domain, wherein the aspartate of the Vps9 domain destabilizes Rab5 GDP binding by interacting with the P-loop and disrupting coordination of Mg^{2+} (Delprato, Merithew et al. 2004). This proposed mechanism is discussed further in Chapter 4.

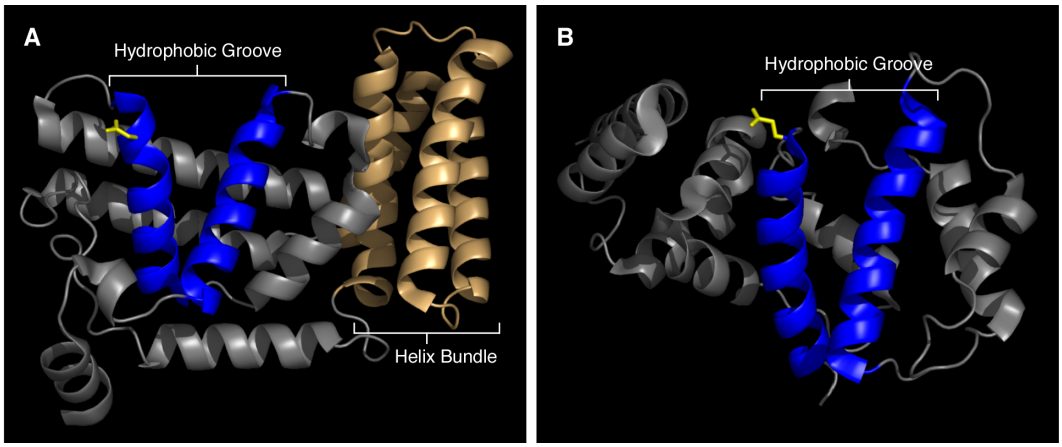

Figure 26. Structural comparison of the Vps9 and Sec7 domains. Shown are the crystal structures of the helix bundle (orange) and Vps9 domain of Rabex5 (1TXU, A) and of the Sec7 domain of the Arf GEF Gea1p (1RE0, B). The similarity of the hydrophobic grooves (blue) and the invariant acidic residue (yellow) indicate that the two might share a similar mechanism of stimulated nucleotide release.

Interdependence of the Vps9 and CUE domains

The uncovering of a link between the Vps9 domain and the CUE domain was an unexpected boon of these mutational analyses. Since the discovery that the CUE domain and its ability to bind ubiquitin were required for proper endocytosis of pheromone receptors, the question of how the CUE domain might regulate Vps9 function has gone unanswered. One possible mode of regulation is localization, as the CUE domain might localize Vps9 to endocytic compartments by interacting with ubiquitinated cargo or machinery. A second possibility is that the ubiquitination of Vps9, which requires ubiquitin binding by the CUE domain, actually affects Vps9 localization or activity. The data in the last section of this chapter shed light on a third means of regulation.

A number of mutants that impair Vps9 GEF activity were found to increase ubiquitin binding, while a mutation known to block ubiquitin binding increased GEF activity. Importantly, it was not a direct relationship between the lack of ubiquitin binding and increased GEF activity, as these experiments were performed with recombinant proteins from *E. coli* and only one of the three ubiquitin-binding mutants had this effect. Likewise, there was not a direct relationship between decreased GEF activity and ubiquitin binding, since Vps9^{D251A}, which is more defective than Vps9^{E288A}, bound less ubiquitin.

One speculative explanation of these data is an autoinhibitory intramolecular interaction between the CUE domain and the Vps9 domain, which

happens to be dependent on a methionine residue also required for ubiquitin binding. If one assumes that the D173A, DD173,4AA and L191D mutations affect the overall structure of the Vps9 domain, then this intramolecular interaction is also dependent on the structural integrity of the Vps9 domain, Glu288 and, to a lesser extent, Asp 251. This autoinhibitory mechanism helps explain a previous result wherein a construct of Vps9 lacking its carboxy-terminus showed increased GEF activity (G. Tall, unpublished). Testing this proposed mechanism should be straightforward and will include domain-mapping binding studies, additional mutagenesis, and perhaps interface-mapping by NMR, as described for the identification of the Vps21-binding surface of the Vps9 domain in Chapter 4.

If the intramolecular interaction between the Vps9 domain and the CUE domain is confirmed, the question of its functional significance remains. The requirement for ubiquitin binding goes beyond simply releasing an autoinhibitory interaction, as both ubiquitin-binding point mutants that do not stimulate GEF activity and constructs lacking this domain or Vps9^{M419D} which do stimulate GEF activity fail to properly sort endocytic cargo. Since preliminary evidence in our lab indicates that CUE domain-dependent ubiquitination of Vps9 does not affect GEF activity (B. Davies, J. Fendos, unpublished), this additional regulation is likely a result of localization of Vps9 through either binding of ubiquitin or subsequent ubiquitination. Further defining this interdependence between the

CUE domain and the Vps9 domain is a continuing area of research in the Horazdovsky Lab.

Materials and Methods

Plasmid construction and site-directed mutagenesis

pPS91 (pRS416 expressing Vps9 from the *VPS9* promoter) was constructed by Peg Scott (Burd, Mustol et al. 1996). The original D251A and E288A mutations were constructed by a three step PCR, in which fragment A was amplified using the 5' start oligo and a 3' oligo containing the mutation and overlapping sequence and fragment B was amplified using the 3' stop oligo and a 5' oligo containing the mutation and overlapping sequence. Fragments A and B were then mixed and amplified with the 5' start oligo and the 3' stop oligo. The resulting mutated VPS9 fragment was sequenced and swapped into pPS91. The larger set of mutants were constructed according to the GeneTailor mutagenesis system (Invitrogen) using a fragment of VPS9 in pBS that was then swapped into pRS315Vps9-1kb, pRS315Vps9-100bp, or pET28MBPVps9 (constructed by B. Davies)

Protein expression and purification

His_6- or His_6MBP- tagged Vps9 proteins were expressed in BL21(DE3) grown in LB medium supplemented with kanamycin to an OD_{600} of 0.6 - 1.0 and

induced with 500 mM isopropyl β-d-thiogalactoside (IPTG) at 37˚C for 22˚C for 16 – 20 hours. Cell pellets were harvested and frozen at -80˚C. After thawing, pellets were resuspended on ice in His Buffer A (25 mM $NaPO_4$, 300 mM NaCl, 5 mM $MgSO_4$, pH 7.5) supplemented with Complete EDTA-free protease inhibitors and 200 μM AEBSF, lysed using a French Press, and centrifuged. Supernatants were passed through 0.45 μm syringe filters and loaded into the AKTA FPLC for purification using a HiTrap Chelating HP column loaded with $NiSO_4$. After injection, the column was washed with 20 mM imidazole before proteins were eluted with a gradient of 20 – 250 mM imidazole. Relevant fractions were concentrated, adjusted to 1mM DTT, and cut overnight with His_6TEV at 16˚C to cleave the His_6MBP tag. Cleaved protein was buffer exchanged using a HiPrep 26/10 Desalting column to remove imidazole before a second pass through the HiTrap Chelating HP column to remove the His_6MBP tag and His_6TEV. Remaining contaminants were removed using a HiLoad 16/60 Superdex 75 gel filtration column.

In vitro binding assay

GST fused to Vps21 or Ubiquitin were expressed in BL21(DE3) grown in LB supplemented with 100 μg/ml ampicillin to an OD_{600} of 0.6 before being induced with 500 μM IPTG for 6 hours at 30˚C. Pellets were harvested, resuspended in PBS (10 mM $NaPO_4$, 137 mM NaCl, 2.7mM KCl, pH 7.4), lysed

by addition of 1mg/ml lysozyme for 30 minutes, sonicated and centrifuged. Supernatants were aliquoted and frozen at -80˚C. Glutathione sepharose beads were equilibrated with PBST (PBS with 0.5% Tween-20) before being incubated with GST-fusions for 1 hour at 4˚C. Beads were washed with PBST and incubated with purified Vps9 proteins for 1 hour at 4˚C. Beads were washed again with PBST before bound protein was eluted by addition of 5x Laemmli Sample Buffer (312 mM Tris, 10 % sodium dodecyl sulfate (SDS), 25 % β-mercaptoethanol, 0.05 % bromophenol blue, pH 6.8) and heating at 95˚C for 4 minutes. Eluted protein was separated by SDS-PAGE and detected by western analysis with Vps9 primary antiserum (Burd, Mustol et al. 1996) (1:1000), HRP-conjugated anti-rabbit secondary antibody (1:1000) and SuperSignal West Femto Maximum Sensitivity Substrate (1:2).

Nucleotide exchange assay

[^{3}H]-GDP-based exchange assays were performed as detailed previously (Hama, Tall et al. 1999). FRET-based nucleotide exchange assays were performed as described previously (Davies, Carney et al. 2005). Purified Vps21 proteins was loaded with fluorescent nucleotide by incubation with equimolar mant-GDP and excess EDTA at 30˚C for 30 minutes. EDTA and unbound nucleotide were removed by desalting into exchange assay buffer (20mM HEPES, 5mM $MgSO_4$, pH 7.5). FRET signal (exciting Rab tryptophan at 290nm, measuring mant-GDP

emission at 440nm) was monitored using a Photon Technology International fluorometer (model QM-2001–4) and the PTI Felix32 software. Mant-GDP-loaded Vps21 was allowed to stabilize for 100 seconds before addition of purified Vps9 protein. After another 100 seconds, 100μM GTP was added and exchange was monitored for 15 minutes.

CHAPTER FOUR

NMR Analysis of the Vps9 Domain and its Interaction with Vps21

Overview

Rab5 proteins and their Vps9 domain-containing GEFs regulate trafficking through the early stages of the endocytic pathway. Structural studies were undertaken to gain a better understanding of this critical interaction. We aimed initially to crystallize the Vps9 domain in complex with the yeast Rab5 protein Vps21 and then to solve the solution structure of the Vps9 domain alone. With the publication of a crystal structure of the Vps9 domain, we turned to the use of NMR analysis to model the complex with Vps21. Through HSQC perturbation mapping we identified the Rab-binding surface of the Vps9 domain. Attempts to map the Vps9 domain-binding surface of Vps21 yielded unexpected results with potential implications on the mechanism of Rab5 nucleotide exchange by this domain.

Introduction

The Rab5 family and other Rab proteins, are part of the Ras superfamily of small GTPases, which, through their guanine nucleotide cycles, regulate a vast array of cellular processes (Macara, Lounsbury et al. 1996; Zerial and McBride 2001). Active GTP-bound GTPases are inactivated by hydrolysis and re-activated by release of GDP and the loading of GTP in a notoriously slow cycle whose steps are accelerated by GTPase activating proteins (GAPs) and guanine nucleotide exchange factors (GEFs), respectively. Like all members of the Ras superfamily, Rab proteins share a significant amount of sequence homology and a common structural core of a six-stranded β-sheet surrounded by five α-helices (Sprang 1997; Pfeffer 2005). On top of this framework, five loops define the guanine binding-pocket (Figure 27). The loop between the β1 strand and the α1 helix (P-loop) interacts with the α- and β-phosphate groups of bound nucleotide and cooperates with the loops between the α1 helix and the β2 strand (switch I) and between the β3 strand and the α2 helix (switch 2) in the coordination of a Mg^{2+} ion and the γ phosphate group when present. The loops between the β5 strand and the α4 helix and between the β6 strand and the α5 helix recognize and stabilize the guanine base. As demonstrated in Figure 27, the switch I and switch II regions commonly show a significant conformational difference in GDP- and

GTP-bound forms, allowing nucleotide state-specific interaction with GEFs, GAPs, and effectors.

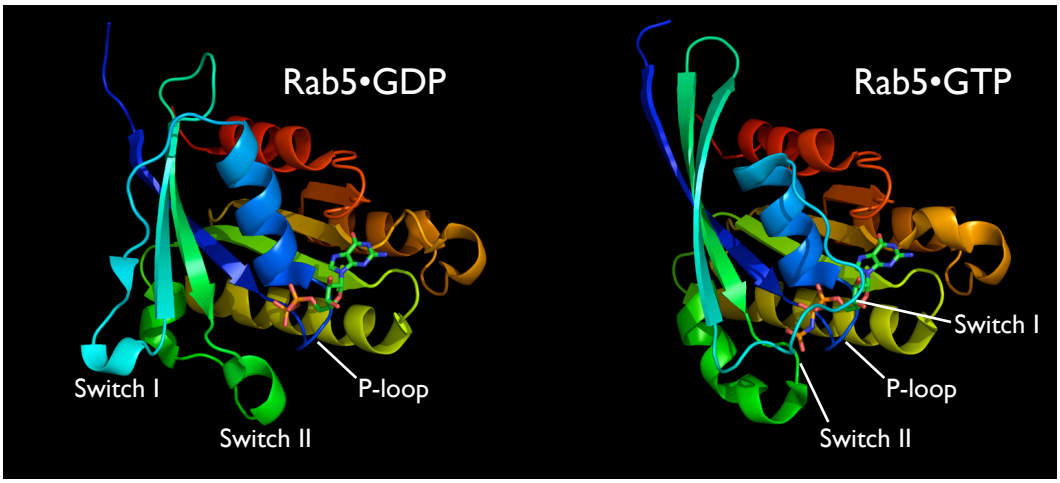

Figure 27. Conformational switch between Rab5•GDP and Rab5•GTP. Crystal structures of Rab5 in its GDP-bound (1TU4, left) and GTP-bound (1N6H, right) forms demonstrate the conformational differences that result from nucleotide binding. Structures are colored according to a spectrum with the amino-teriminus violet and the carboxy terminus red. The location of the P-loop (blue), switch I (teal) and switch II (green) are indicated.

GEFs for a given family of GTPases typically share an identifiable conserved catalytic domain. As examples, GEFs for the Rho family contain Dbl homology (DH) domains, GEFs for the Arf family contain Sec7 domains, and most GEFs for Ras contain CDC25 domains. While the different families of small GTPases are based on a common fold, the GEF domains for these different GTPase families are structurally unrelated (Cherfils and Chardin 1999). Though they use a common arsenal of mechanisms to effect GDP release, the structural differences of these GEF domains lead to differences in the degree to which they

interact with and remodel switch I and switch II, insert themselves into the Mg^{2+} and phosphate binding site, and distort the P-loop (Boriack-Sjodin, Margarit et al. 1998; Goldberg 1998; Worthylake, Rossman et al. 2000).

The Vps9 catalytic domain was established to be roughly similar in its size and helical composition to the GEF domains mentioned above. We initiated a series of structural studies aimed at defining the mechanisms used by the Vps9 domain to effect Rab5 nucleotide exchange as the framework of the molecular basis by which Rab5 GEFs regulate Rab5 function in response to specific environmental stimuli. As a result of these studies we uncovered evidence of conformational dynamics that result in an increased solvent accessibility of core Vps21 residues when bound to the Vps9 domain, laying the groundwork for additional studies into the impact these dynamics have on nucleotide exchange.

Results

Preliminary results and crystallization trials

A collaborative effort with the Sprang laboratory, which predates my tenure in the Horazdovsky laboratory, initially sought to crystallize the yeast Vps21/Vps9 complex and solve its structure. Vps21 (aa 1 – 178, lacking the carboxy-terminal prenylation site and a stretch that is unstructured in related structures) and Vps9ΔNΔC (aa 158 – 347, identified as a minimal domain necessary and sufficient for Vps21 exchange, G. Tall, unpublished.) were purified

separately using affinity chromatography, combined and isolated in complex using ion exchange and gel filtration chromatography. This purification strategy yielded adequate quantities of this complex for crystallization trials, but these trials were unsuccessful, primarily due to the high salt concentration (0.5M NaCl) needed to stabilize the complex. The group next turned to the Vps9 domain of human Rabex5 as a substitute for that of yeast Vps9.

Residues 239 – 439 of Rabex5 were shown to bind to and have exchange activity for yeast Vps21 (G. Tall, unpublished). Limited trypsin proteolysis of this Rabex5 fragment in complex with Vps21 indicated that Rabex5 residues 393 – 439 were not protected by this association and therefore extraneous. In addition, secondary structure predictions suggested the addition of residues 222 – 238 to this initial fragment would complete an α-helix. The resulting fragment consisting of aa 222 – 392 was termed Rabex5-T. It was at this point that I joined these structural efforts. Yields of a His_6-tagged version of Rabex5-T were inadequate for structural studies, mostly due to its insolubility. The solubility of this fragment was improved by expressing it as a maltose-binding protein (MBP)-fusion, but the total yield was still poor due to inefficient binding of the fusion protein to amylose resin during the purification process. Expressing Rabex5-T as a His_6-tagged MBP-fusion allowed both increased solubility and efficient affinity purification. Rabex5-T/Vps21 complex formation and isolation proceeded as described above, without the high salt requirement. When crystallization trials

using this complex failed to identify successful crystallization conditions, we turned to a series of Rabex5 constructs, Rabex5-11 through Rabex5-16, that were created by adding or subtracting amino-terminal sequences to reach predicted helix break points. Rabex5-11, -12, and -14 were quickly dismissed due to solubility issues, while Rabex5-13, -15, and -16 were incorporated into crystallization trials with Vps21, with the bulk of the effort being placed on Rabex5-15. Ultimately, however, no diffraction-quality crystals were obtained for any Rabex5 construct in complex with Vps21.

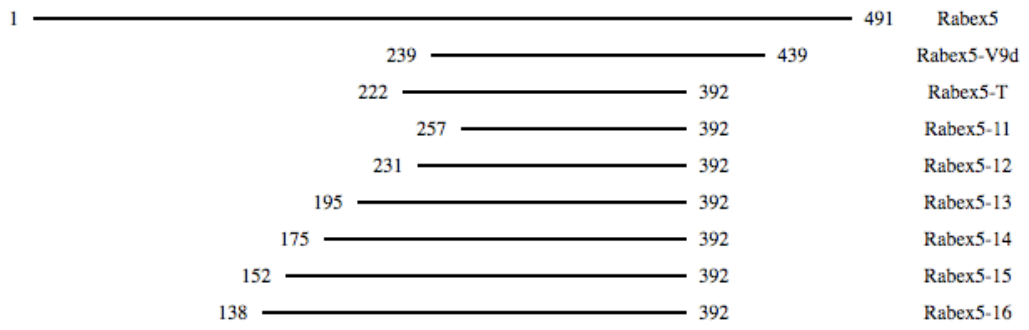

Figure 28. Rabex5 constructs used in crystallization trials. Graphical representation of the Rabex5 fragments referred to within the text. Briefly, limited proteolysis of Rabex5-V9d in complex with Vps21 suggested carboxy-terminal truncation at residue 392. The amino-termini of Rabex5-T and Rabex5-11 through Rabex5-16 were based on secondary structure predictions of helix break points.

Initialization of NMR studies

While pursuing a crystal structure of a Vps21/Vps9 domain complex, we began to investigate the use of NMR spectroscopy as a complementary approach

to obtaining structural information about this Rab, its GEF and their interaction. Though a Rab/GEF complex was too large for resolution by standard NMR methods (Evans 1995), Vps21 and Rabex5-T at 19.8 and 19.6 kDa, respectively, were both individually of an appropriate size for NMR analysis. Initial 2D $^{1}H/^{15}N$ HSQC spectra of ^{15}N-labeled Rabex5-T and Vps21 acquired with the help of Dr. Kevin Gardner showed approximately the correct number of fairly well-dispersed peaks (representing mostly backbone amides), indicating that both were suitable candidates for additional study by NMR (Figure 29).

Once the peaks in a $^{1}H/^{15}N$ HSQC spectrum have been assigned to specific residues this spectrum can be a valuable tool in the study of a protein's interactions with ligands or other proteins. Since the chemical shift of a particular peak is dependent on its local environment, peaks representing residues at or near

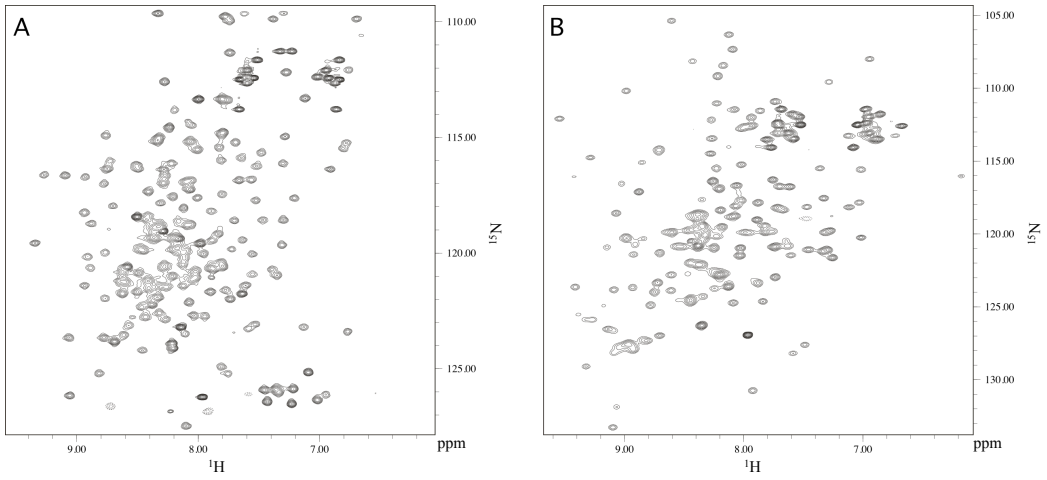

Figure 29. Rabex5-T and and Vps21 are suitable candidates for NMR analysis. 2D 1H/15N HSQC spectra of Rabex5-T (A) and Vps21 (B) show an expected quantitity of relatively well-dispersed peaks.

binding sites are likely to shift upon addition of the binding partner (Evans 1995; Cavanagh 1996). This principle would allow us to identify the residues at the Rab/GEF interface by comparing the $^{1}H/^{15}N$ HSQC of each protein (isotopically labeled) in the presence and absence of the other protein (unlabeled). At the inception of these studies, a crystal structure of Vps21 in its GTP-bound form had been published (Esters, Alexandrov et al. 2000), as well as four other Rab crystal structures including that of GDP-bound Sec4 (Dumas, Zhu et al. 1999; Ostermeier and Brunger 1999; Stroupe and Brunger 2000). Given the level of conservation within the Rab family, these structures would allow us to confidently map our HSQC data to a structural model. However, at the time, no structural information about the Vps9 domain was available, and the Vps9 domain showed no significant homology to any of the GTPase GEFs for which structures were known. Thus, mapping the Rab5/Vps9 domain complex interface by NMR would first require a Vps9 domain structure.

NMR-based structural analysis of Rabex5-T

Beginning with $^{1}H/^{15}N$ HSQC peaks, $^{1}H/^{15}N/^{13}C$ peaks were picked manually in a sequential manner from a standard set of 3D spectra, consisting of HNCO, HN(CA)CO, HN(CO)CA, HNCA, HNCACB, and CCONH spectra using the XEASY program (Bartels, Xia et al. 1995). These peaklists were used to assign backbone resonances automatically with the GARANT program (Bartels,

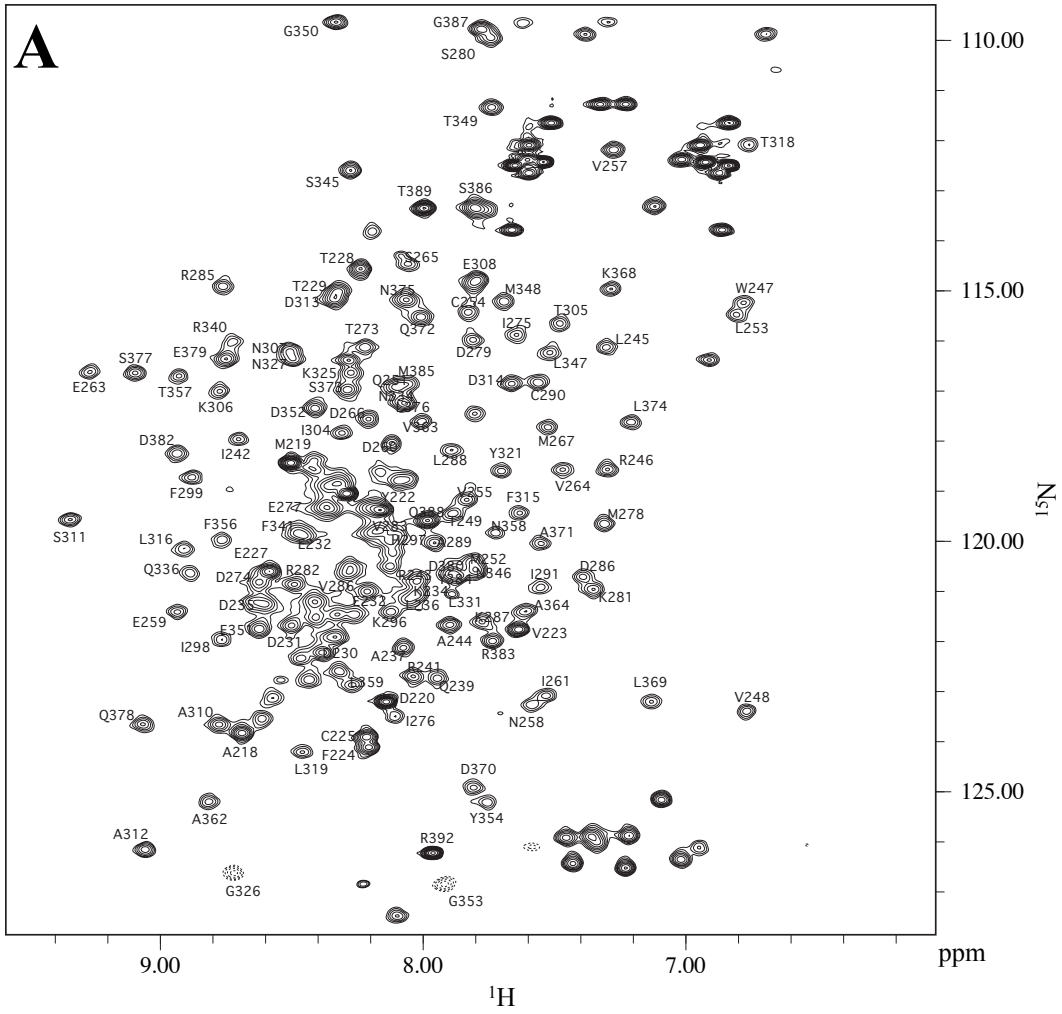

B

222 YVFCPETTDDEKKDLAIQKRIRALRWVTPQMLCVPVNEDIPEVSDMVVKAITDIIE

MDSKRVPRDKLACITKCSKHIFNAIKITKNEPASADDFLPTLIYIVLKGNPPRLQSNIQY

ITRFCNPSRLMTGEDGYYFTNLCCAVAFIEKLDAQSLNLSQEDFDRYMSGQTSPR 392

Figure 30. Backbone assignments of Rabex5-T. (A) 2D 1H/15N HSQC spectrum of 15N-Rabex5-T with the assigned backbone amide resonances indicated. (B) The sequence of Rabex5-T with assigned residues (black) and unassigned residues (gray) indicated.

Billeter et al. 1997), and these automated assignments were refined manually. This process allowed the assignment of 128 of 160 assignable backbone residues in the HSQC (Figure 30).

Spectra required to assign side chain resonances and eventually solve a solution structure of Rabex5-T were also acquired. Unfortunately, the ^{15}N and ^{13}C NOESY data sets, from which distance restraints necessary for structural determination would be generated, showed poor resolution, indicating an intrinsic intramolecular movement of this domain. Methods to stabilize the domain were considered, including the addition of Rab and revisiting other constructs such as Rabex5-15. None of these showed enough promise to warrant the acquisition of a new 3D data set, and ultimately a three-dimensional structure was not obtained. This outcome would have been a major setback in our effort to model the Vps9 domain/Rab5 family complex, except that shortly thereafter Delprato et al. published a crystal structure of the Rabex5 Vps9 domain (Delprato, Merithew et al. 2004). The impact of this structure will be discussed later in this chapter.

Identification of the Rab-binding surface of Rabex5-T

To identify the residues at the interface of Rabex5-T with Vps21, HSQC spectra of ^{15}N-labeled Rabex5-T were collected in the presence of increasing amounts of unlabeled GDP-bound Vps21. As shown in Figure 31, a number of resonances were altered upon the addition of Rab, indicative of a binding reaction.

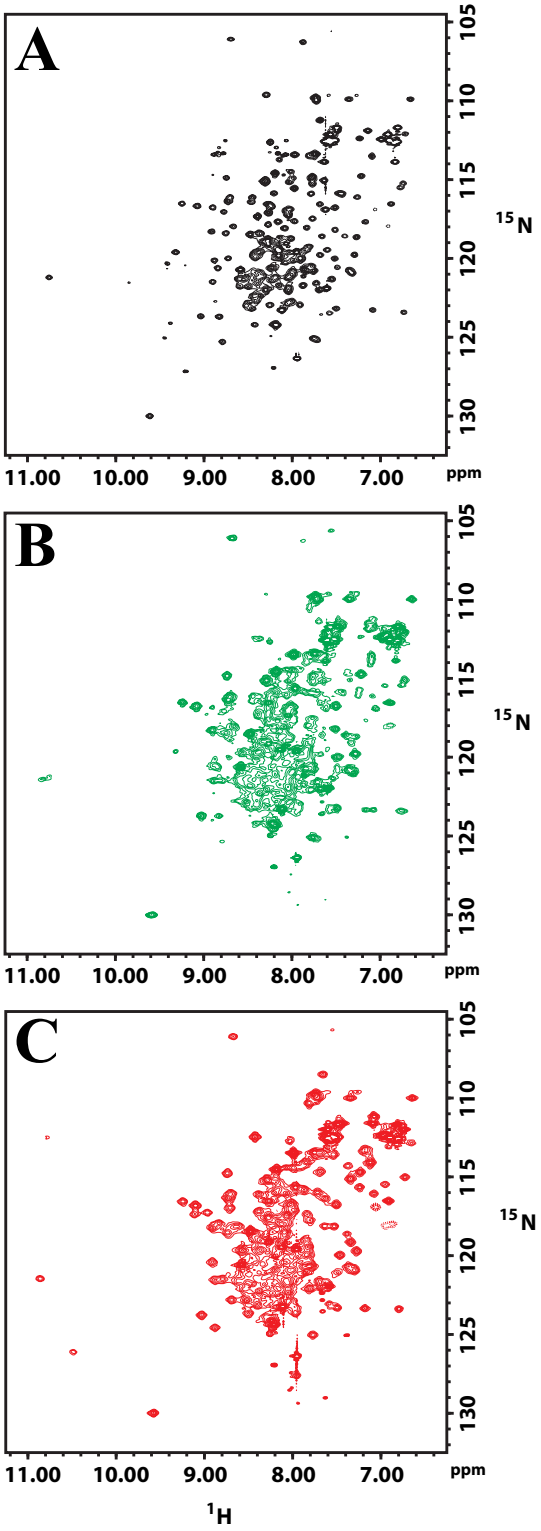

Figure 31. Chemical shift changes of the Vps9 domain upon binding of Vps21. 1H/15N HSQC spectra of 15N-labeled Rabex5-T alone (A) or in the presence of 1.5 molar equivalents (B) or 3 molar equivalents (C) of unlabeled Vps21.

The effect of binding on resonances is a function of the kinetics of the interaction. When an interaction rapidly exchanges between bound and free, peaks move linearly according to a population weighted average between the free peak location and the bound peak location. In the case of a slow exchange between bound and free, peaks disappear in their free position while appearing in their bound position (Cavanagh 1996). The finding that titration with Vps21•GDP caused some Rabex5-T signals to decrease in their original position and increase in another, rather than migrate between positions linearly, is evidence of the relatively slow exchange of the Rab/GEF complex in the absence of excess nucleotide. Because this peak movement is not continuous, quantitation of chemical shift perturbations would require assignment of Rabex5-T backbone in complex with Vps21, which was precluded by the poor resolution in the 3D spectra collected for this complex. However, affected residues can be identified.

When the residues perturbed by the binding of Rab were mapped to the Rabex5 crystal structure (Delprato, Merithew et al. 2004), they clearly indicated a single face of the Vps9 domain (Figure 32). This face contains the most highly conserved residues among Vps9 domains, both of the important residues identified by the mutagenesis of the Vps9 domain (described in Chapter 3), and a number of residues identified in a similar mutational analysis by Delprato et al. Together these data provide strong evidence that this is the Rab5-binding surface of the Vps9 domain.

A

R246	S311	G350
V248	D314	Y354
L253	F315	F356
C254	L316	T357
I275	T318	N358
D279	L319	C360
L288	Y321	A362
I291	N327	L369
T305	Q336	A371
K306	S345	Q372
N307	L347	L374
E308	M348	N375
A310	T349	

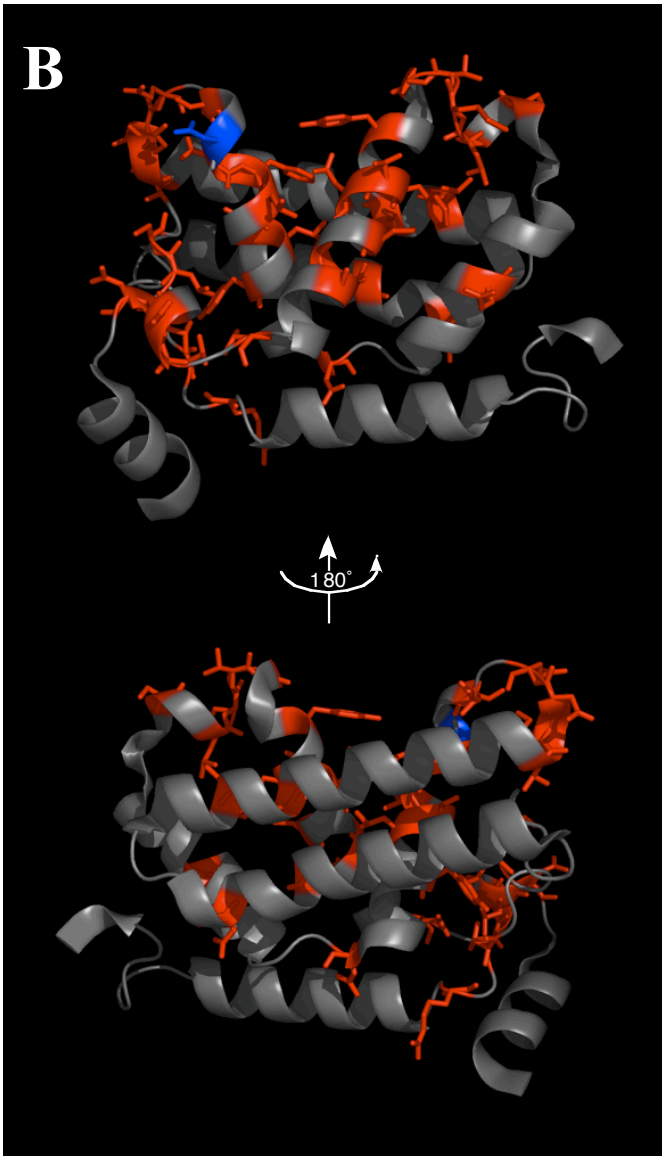

Figure 32. The Rab-binding surface of the Vps9 domain. (A) Rabex5-T residues whose HSQC peak was perturbed by the addition of unlabeled Vps21 in the experiment from Figure 31. (B) The structure of the Rabex5 Vps9 domain (1TXU) is used to demonstrate the location of Rabex5-T residues whose HSQC peaks were perturbed by the addition of unlabeled Vps21.

Identification of the Vps9 domain-binding surface of Vps21

Having established the Rab-binding surface of the Rabex5 Vps9 domain, we sought to identify the opposite side of the complex interface. This experiment required the assignment of the backbone residues of GDP-bound Vps21, which was accomplished using a standard set of 3D spectra by the same process described above for the assignment of the Vps9 domain backbone. Figure 33 shows the assignment 135 of 173 assignable residues.

HSQC spectra of ^{15}N-labeled Vps21•GDP were collected in the presence of increasing amounts of unlabeled Rabex5-T with unexpected results (Figure 34). Unlike the residue-specific changes observed for Rabex5, the Vps21 HSQC suffered from a more global loss of resolution upon complex formation. This large-scale spectral change was not simply attributable to the generation of a ~40 kDa Rabex5•Vps21 complex, since the Rabex5 titration was not similarly affected. Additionally, the distortion was not a result of the aggregation, precipitation or degradation of Vps21, as many of these changes could be reversed by the dissociation of the complex by addition of the nonhydrolyzable GTP analog GppNHp (Figure 35). Instead this result indicated that complex formation leads to Vps21 transitioning between two or more conformations. These conformational dynamics are probably on an intermediate time scale, since a rapid switch between conformations would result in a single peak for each residue averaged from the peak location in each conformation, and slow

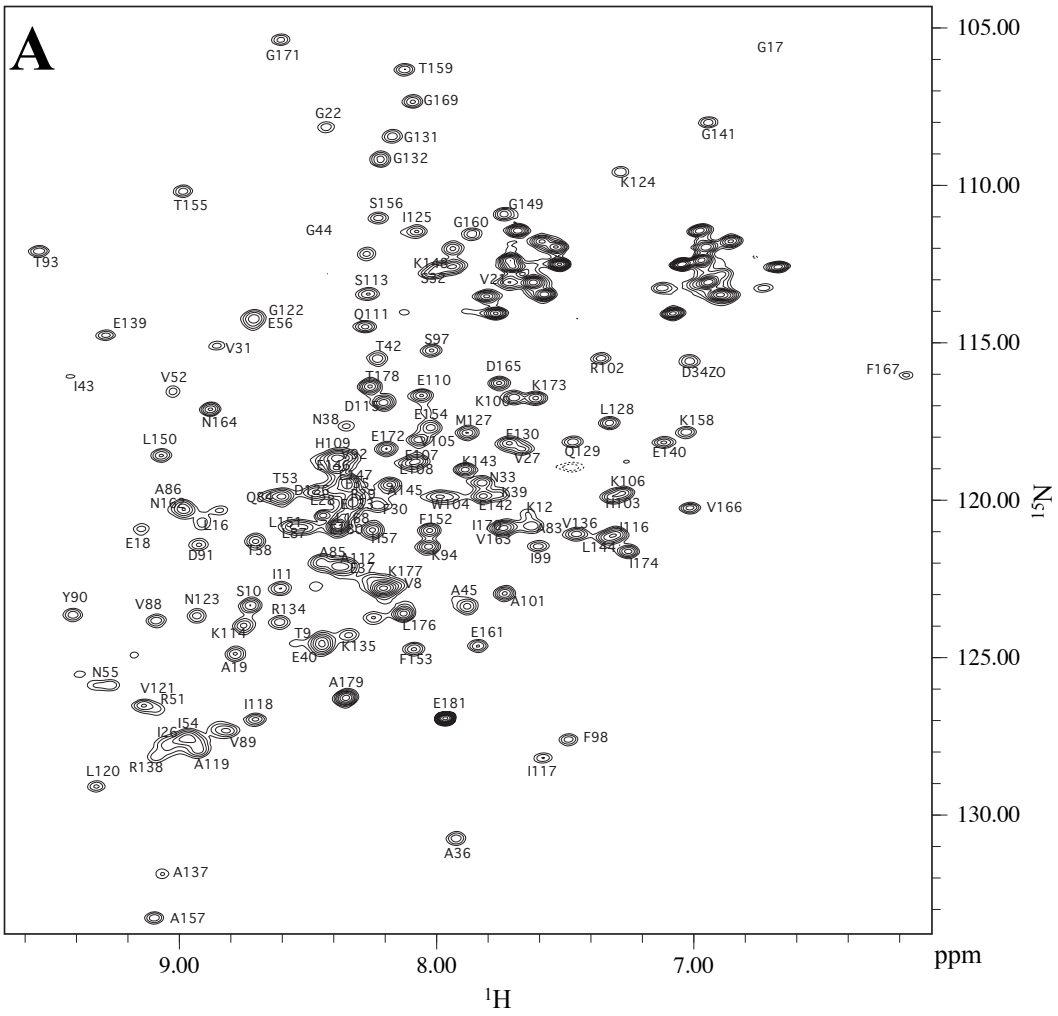

Figure 33. Backbone assignments of Vps21•GDP. (A) 2D 1H/15N HSQC spectrum of 15N-Vps21•GDP with the assigned backbone amide resonances indicated. (B) The sequence of Vps21•GDP with assigned residues (black) and unassigned residues (gray) indicated.

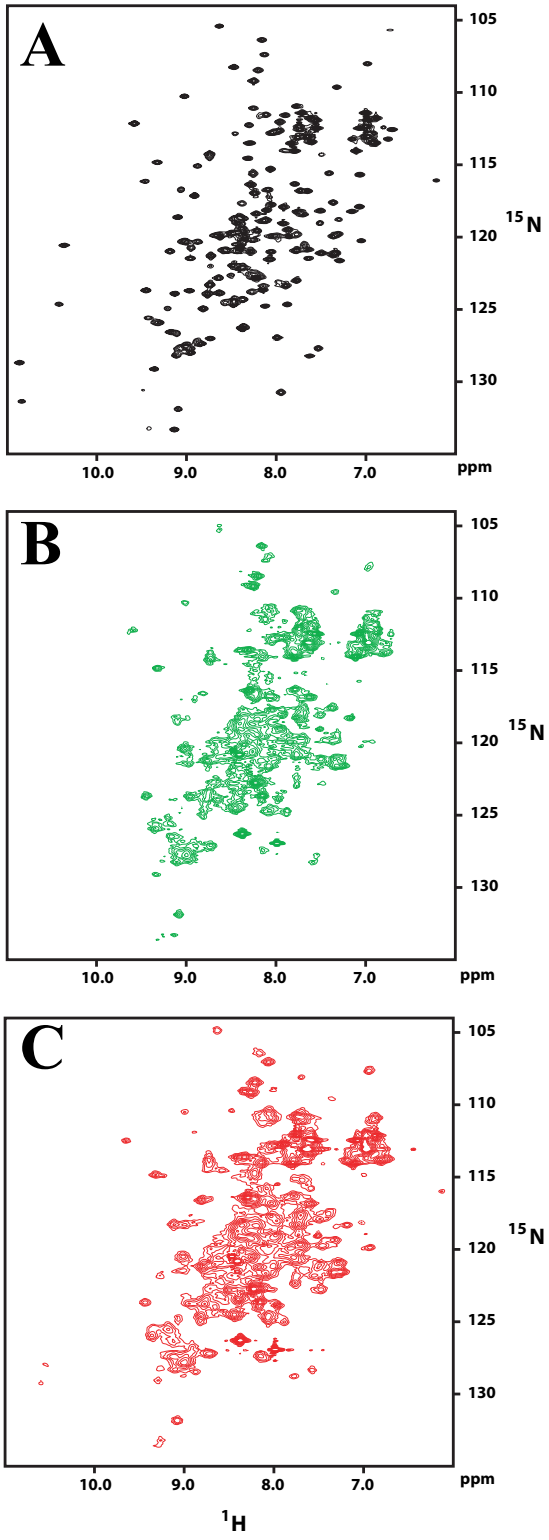

Figure 34. Chemical shift changes of Vps21•GDP upon binding of the Vps9 domain. 1H/15N HSQC spectra of 15N-labeled Vps21 alone (A) or in the presence of 1 molar equivalent (B) or 2 molar equivalents (C) of unlabeled Rabex5-T.

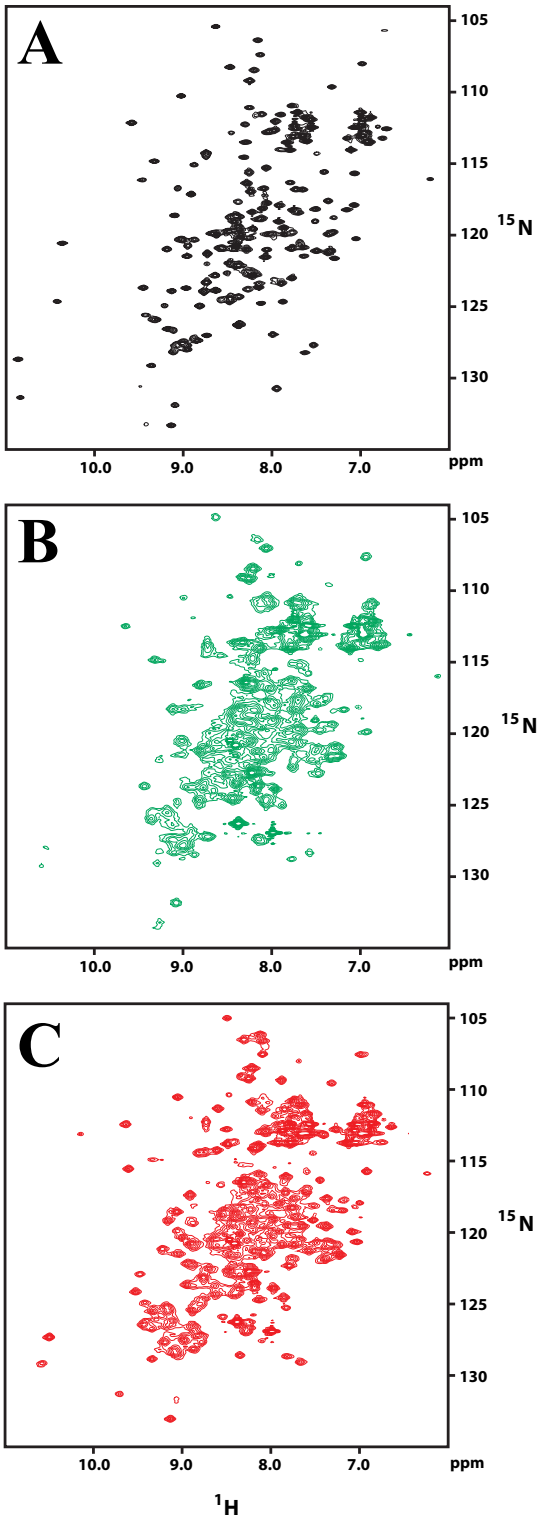

Figure 35. The GEF-induced disorder of Vps21 is reversible with GppNHp. The 1H/15N HSQC spectrum of 15N-labeled Vps21 alone (A) shows widespread changes and a loss of resolution upon addition of 2 molar equivalents of Rabex5-T (B), indicative of conformational heterogeneity. These effects are alleviated by the addition of excess GppNHp (C).

conformation switching will result in multiple peaks for each residue. Thus, while these results precluded the identification of the Rabex5-binding surface of Vps21 by this method, they provided unexpected insights into the behavior of Vps21 while in complex with the Vps9 domain and possibly into the mechanism of Rab5 nucleotide exchange.

Probing the GEF-induced dynamic disorder of Vps21

Mss4 has been reported to partially unfold Rab8 during binding (Itzen, Pylypenko et al. 2006). The possibility that the large spectral changes observed

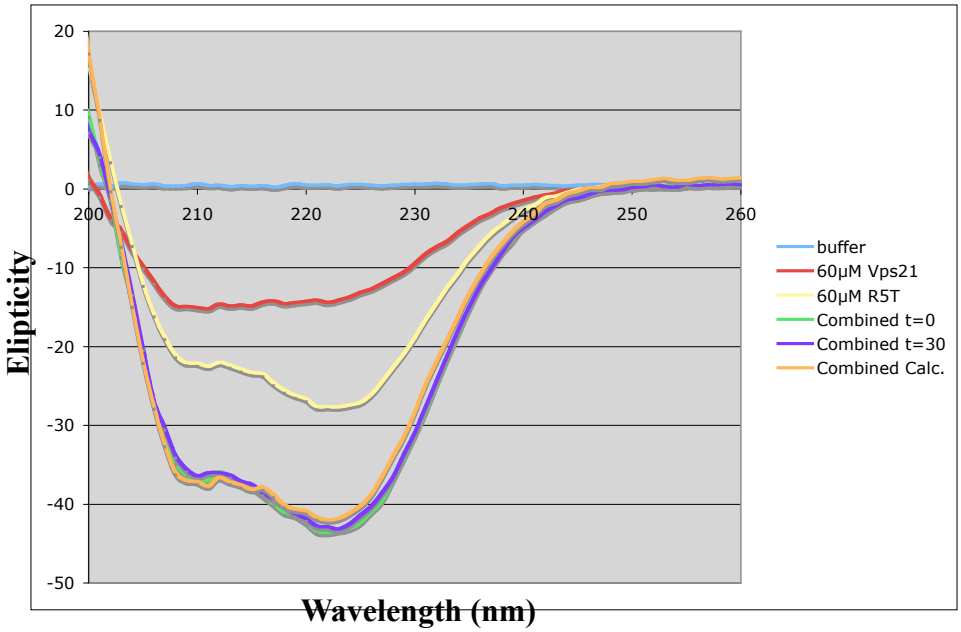

Figure 36. Vps21/Rabex5-T complex formation does not impact secondary structure. Far-uv CD scans of Vps21 (red) or Rabex5-T (yellow) agree with known secondary structures. Incubating Vps21 and Rabex5-T together under conditions known to allow complex formation for 0 minutes (green) or 30 minutes (blue) results in scans indistinguishable from a scan calculated from the addition of those for Vps21 and Rabex5-T.

for Vps21 upon Rab/GEF complex formation accompanied a similar unfolding event was addressed using circular dichroism (CD). Far-uv CD spectra were collected for Rabex5-T and Vps21 alone or together under conditions as similar to those used for NMR as the spectrometer would allow. The CD signal from the Rabex5/Vps21 complex was nearly identical to the combined signal of both proteins alone, indicating that complex formation has no significant effect on secondary structure at this level of resolution.

To test whether complex formation, either through unfolding or an induced conformational mobility, exposed additional hydrophobic surfaces, we first turned to the fluorescent hydrophobic probe 8-anilino-1-naphthalenesulfonic acid (ANS). The fluorescence of ANS increases upon binding hydrophobic patches and has been used extensively to detect molten globule intermediates in protein folding experiments (Semisotnov, Rodionova et al. 1991). Fluorescence of ANS was monitored in samples containing Vps21, Rabex5-T or the Rabex5/ Vps21 complex. Unfortunately, data from these experiments were largely uninterpretable, possibly due to the large amount of of ANS-binding by the individual proteins alone.

To further investigate the intramolecular changes that occur in Vps21 upon binding of the Vps9 domain, we turned to another implementation of NMR, hydrogen/deuterium exchange. In solution, amide protons are exchanged with protons from the surrounding solvent at some frequency. When present in

solution, deuterons are also exchanged for protons (Figure 37). Since a $^{1}H/^{15}N$ HSQC detects amide protons but not amide deuterons, incorporation of deuterons will result in a loss of signal, which will eventually reach an equilibrium at a fraction of the initial signal equal to the fraction of protons and deuterons in solution (Figure 37, Figure 39 f_H). Thus, the rate of decay for a residue is a measure of that residue's accessibility to the deuterated solvent (Cavanagh 1996; Mandell, Baerga-Ortiz et al. 2005).

The objective of this analysis was to determine hydrogen/deuterium exchange rates from HSQC spectra for Vps21 residues in the absence or presence of Rabex5-T in order to compare solvent accessibility of these residues while

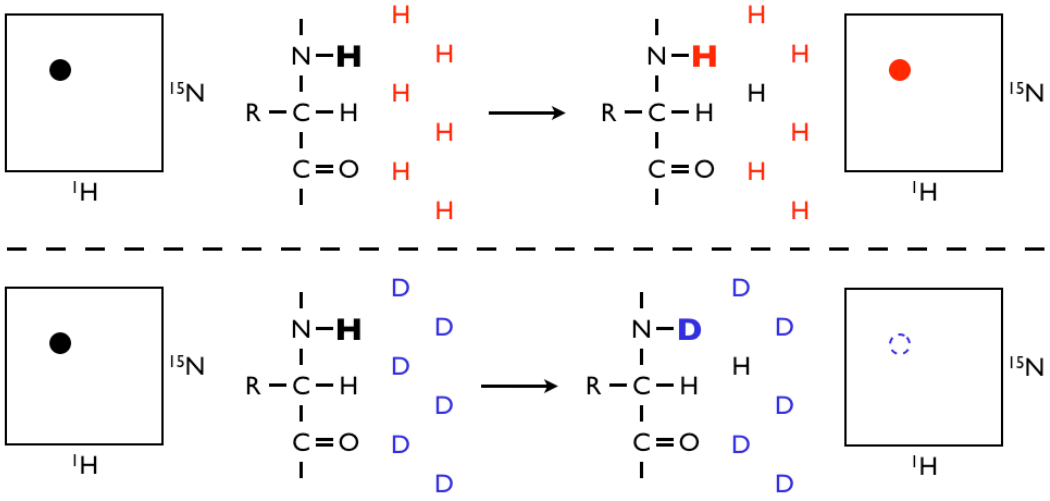

Figure 37. Deuterium Exchange and HSQC. Exchange of backbone amide protons for other protons from the solvent does not affect the amide signal of a given residue in a 1H/15N HSQC (top). However, exchange of backbone amide protons for deuterons from solution cause a loss of amide signal for that residue in a 1H/15N HSQC (bottom). This principle allows the monitoring of a residue's loss of HSQC signal over time in deuterated buffer as a means of measuring the solvent accessibility of that residue.

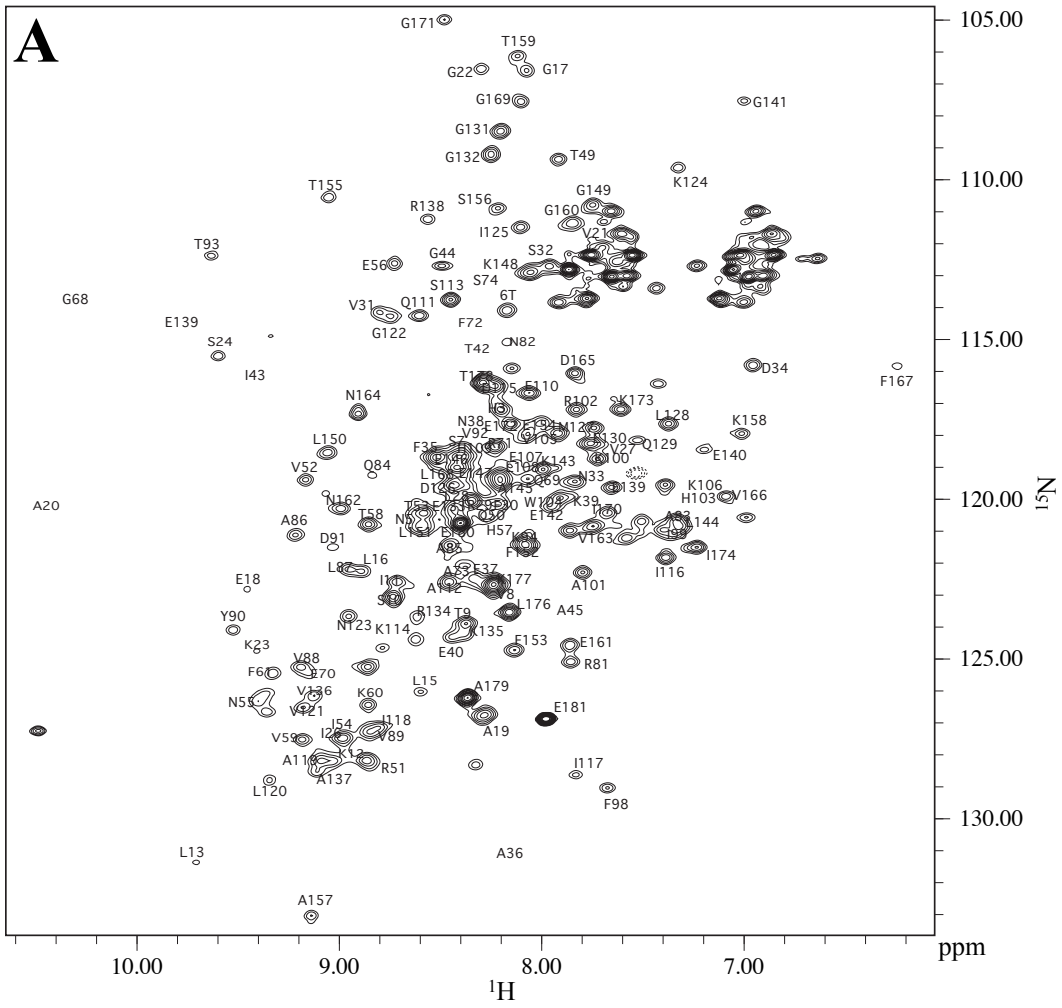

B

GSHMNTSVTSIKLVLLGEAAVGKSSIVLRFVSNDFAENKEPTIGAAFLTQRVTINEHTVK

Switch I

FEIWDTAGQERFASLAPMYYRNAQAALVVYDVTKPQSFIKARHWVKELHEQASKDIIIAL

Switch II

VGNKIDMLQEGGERKVAREEGEKLAEEKGLLFFETSAKTGENVNDVFLGIGEKIPLKTAEE

Figure 38. Backbone assignments of Vps21•GppNHp. (A) 2D 1H/15N HSQC spectrum of 15N-Vps21•GppNHp with the assigned backbone amide resonances indicated. (B) The sequence of Vps21•GppNHp with assigned residues (black) and unassigned residues (gray) indicated.

bound to nucleotide and while bound to the Vps9 domain. Because the HSQC of Vps21 in complex with Rabex5-T is uninterpretable, once this complex is formed, the Rab must first be dissociated from its GEF by the addition of GppNHp in order to detect the amount of deuterium incorporation while bound. This aspect of the experimental design mandated the assignment of the Vps21 backbone in its GppNHp-bound form. These assignments were made by analyzing a standard set of 3D spectra as described above. and Figure 38 shows the assignment of 138 of 178 assignable residues.

Protonated Vps21 loaded with either GDP or GppNHP was diluted from a 100% H_2O-based buffer into a 80% D_2O buffer, and sequential HSQC spectra were acquired overnight. Protonated Vps21•GDP was also mixed with Rabex5-T before dilution in deuterated buffer, with a single HSQC spectrum collected at time points after addition of excess GppNHp. The time from either dilution in

$$y = (1\text{-}f_H)A_0e^{(-xk_{ex})} + A_0f_H$$

A_0 = signal intensity at x=0

f_H = fraction H in buffer

k_{ex} = rate of H-D exchange

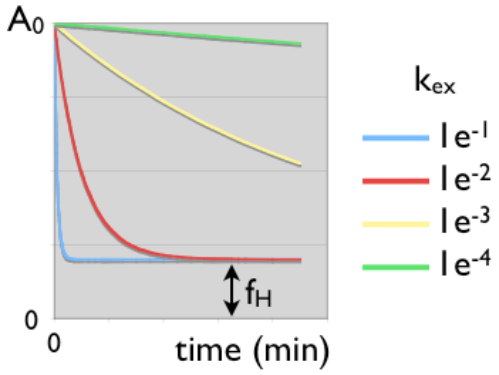

Figure 39. Exponential decay of HSQC signal during deuterium exchange. (A) The equation used to derive rate constants for the loss of hydrogen over time (x), where A_0 is the signal intensity (y) at time=0, f_H is the fraction of hydrogen vs deuterium in the buffer, and k_{ex} is the rate. (B) The dependence of curves with similar initial intensity in a 80% deuterium buffer on the rate constant.

deuterated buffer for Rab alone samples or the addition of GppNHp for Rab+GEF samples to the start of NMR data collection was maintained at eight minutes. Peaks within these three series of HSQC spectra were integrated in batches using the CARA program (Keller 2004). For each residue, a plot of signal intensity (remaining hydrogen) vs. time was then fit to an exponential decay equation (Figure 39) to determine the rate of amide exchange using pro Fit software (QuantumSoft).

One challenge in this analysis was distinguishing between very fast and very slow exchange rates. Some residues exchanged deuterium for hydrogen so quickly that they reached the equilibrium fraction before the first HSQC had been acquired. Thus the plots of signal intensity for these residues were essentially flat and difficult to differentiate from plots of residues with extremely slow exchange rates. Amide exchange is sensitive to pH and temperature, but lowering either of these conditions enough to slow the exchange of these residues would have required remapping all of our assignments for Vps21•GDP and Vps21•GTP. Because each peak has a unique starting intensity, signal intensity alone cannot be used to determine which residues have already reached this equilibrium. Instead, for each residue, the signal intensity of its peak in the first spectrum was compared to a reference spectrum of the same protein in a water-based buffer.

Because a residue's rate of amide exchange is sensitive to neighboring side chains (Bai, Milne et al. 1993), observed rates were divided by reference

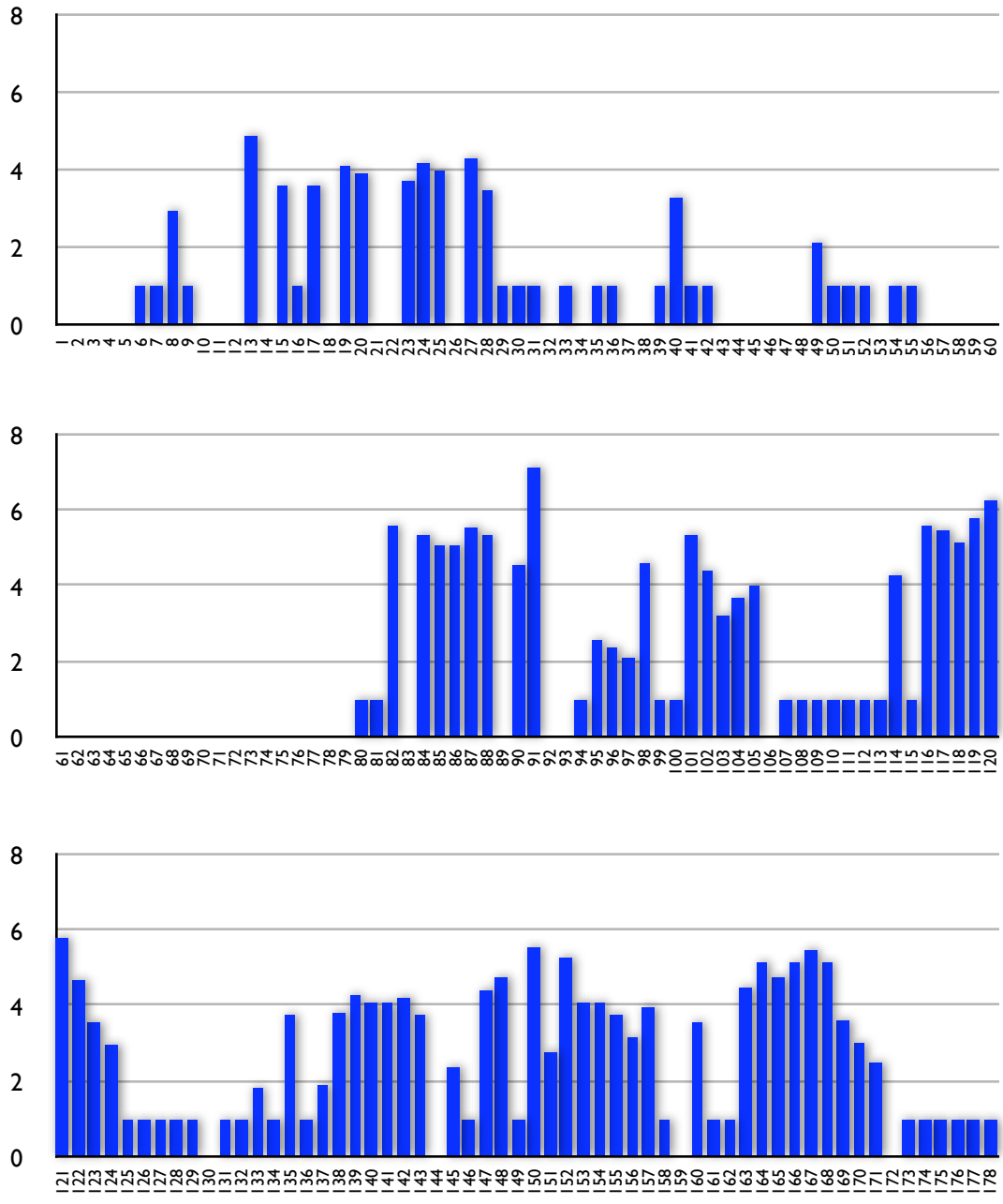

Figure 40. Hydrogen/deuterium exchange protection factors for GDP-bound Vps21. Rates of deuterium exchange were determined for individual residues by fitting curves of HSQC signal vs time to the equation described in Figure 39. Observed rates were divided by reference rates to account for primary structure effects, yielding protection factors. The log of each residue's protection factor is charted, with a value of 1 assigned to residues that exchanged too quickly to be detected and no value given to residues with unassigned or degenerate peaks.

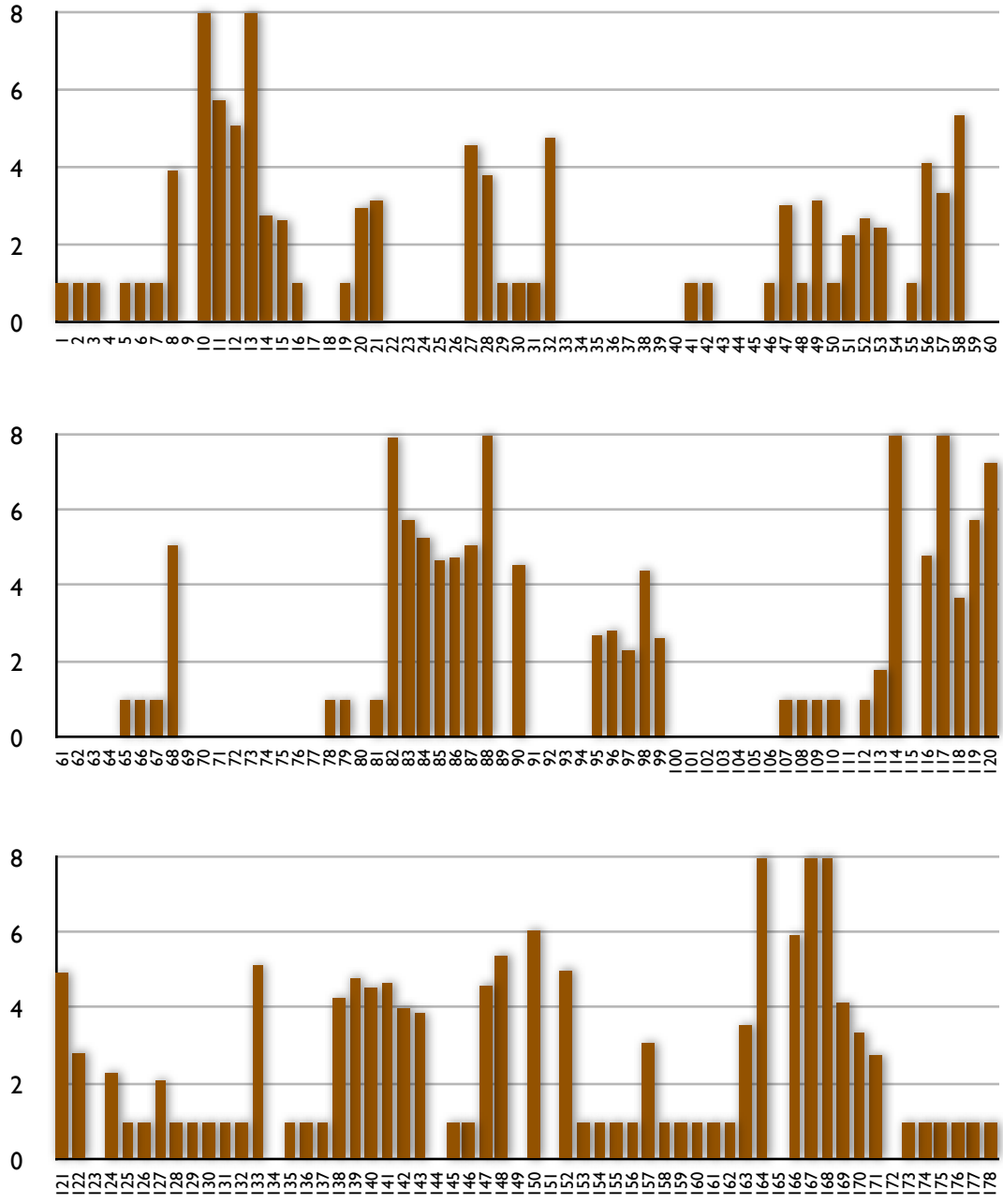

Figure 41. Hydrogen/deuterium exchange protection factors for Vps9 domain-bound Vps21. Rates of deuterium exchange were determined for individual residues by fitting curves of HSQC signal vs time to the equation described in Figure 39. Observed rates were divided by reference rates to account for primary structure effects, yielding protection factors. The log of each residue's protection factor is charted, with values of 1 and 8 assigned to residues that exchanged too quickly or too slowly to be detected and no value given to residues with unassigned or degenerate peaks.

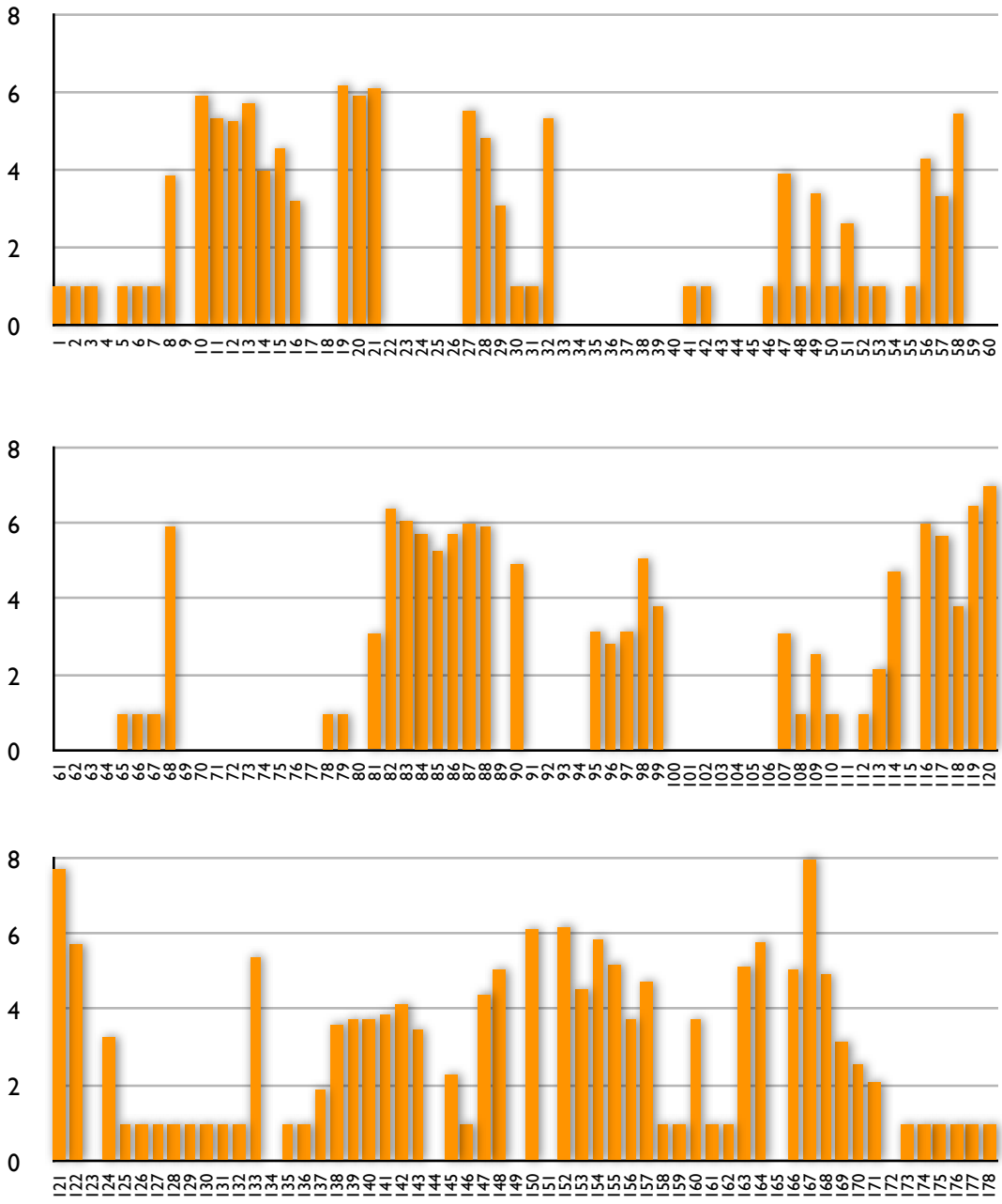

Figure 42. Hydrogen/deuterium exchange protection factors for GppNHp-bound Vps21. Rates of deuterium exchange were determined for individual residues by fitting curves of HSQC signal vs time to the equation described in Figure 39. Observed rates were divided by reference rates to account for primary structure effects, yielding protection factors. The log of each residue's protection factor is charted, with values of 1 and 8 assigned to residues that exchanged too quickly or too slowly to be detected and no value given to residues with unassigned or degenerate peaks.

rates that accounted for the Vps21 amino acid sequence to obtain protection factors, which could then be compared directly within and between data sets. Protection factors could not be calculated for residues that exchanged too fast for detection. Figures 40, 41 and 42 display the protection factors derived for GDP-, GEF- and GppNHp-bound Vps21, respectively. In Figure 43, these protection factors were compared to a mean value within each data set. As expected, in all cases, residues within the core of the protein are generally more protected from solvent than those residues on the exterior.

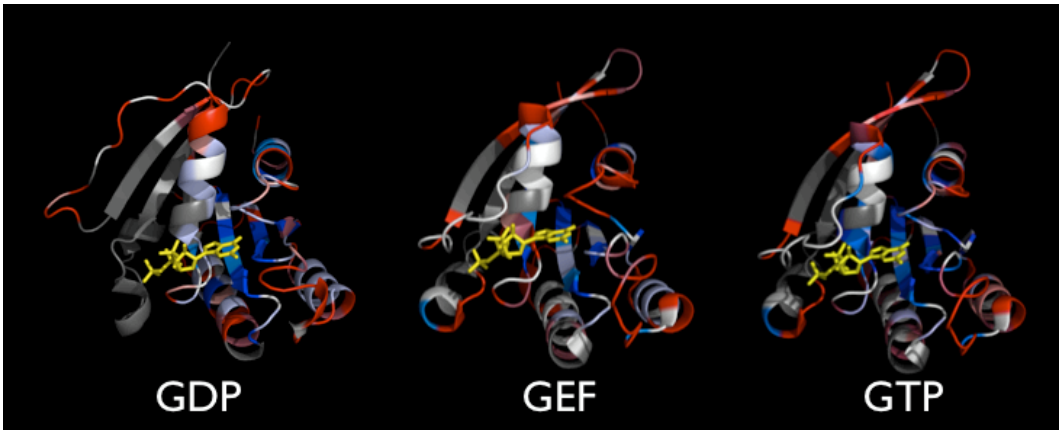

Figure 43. Relative rates of deuterium exchange for each nucleotide state of Vps21. Protection factors (F_p) for were compared within each of these data sets, and used to color appropriate crystal structures for GDP-bound, GEF-bound, or GTP-bound Vps21. (Since GEF-bound Vps21 was converted to the GppNHp bound for readout by HSQC and no GEF-bound structure is available, the GppNHp-bound structure is used to display the residues of this state.) Red indicates a residue with a log F_p >1 standard deviation lower (faster exchange) than the mean. Blue indicates a residue with a log F_p >1 standard deviation higher (slower exchange) than the mean. Lighter shades of red and blue indicate residues with log F_p values between 0.5 and 1.0 standard deviations lower and higher than the mean, respectively. Residues whose deuterium exchange was too fast or too slow to allow calculation of protection factors are included in the red and blue group, respectively.

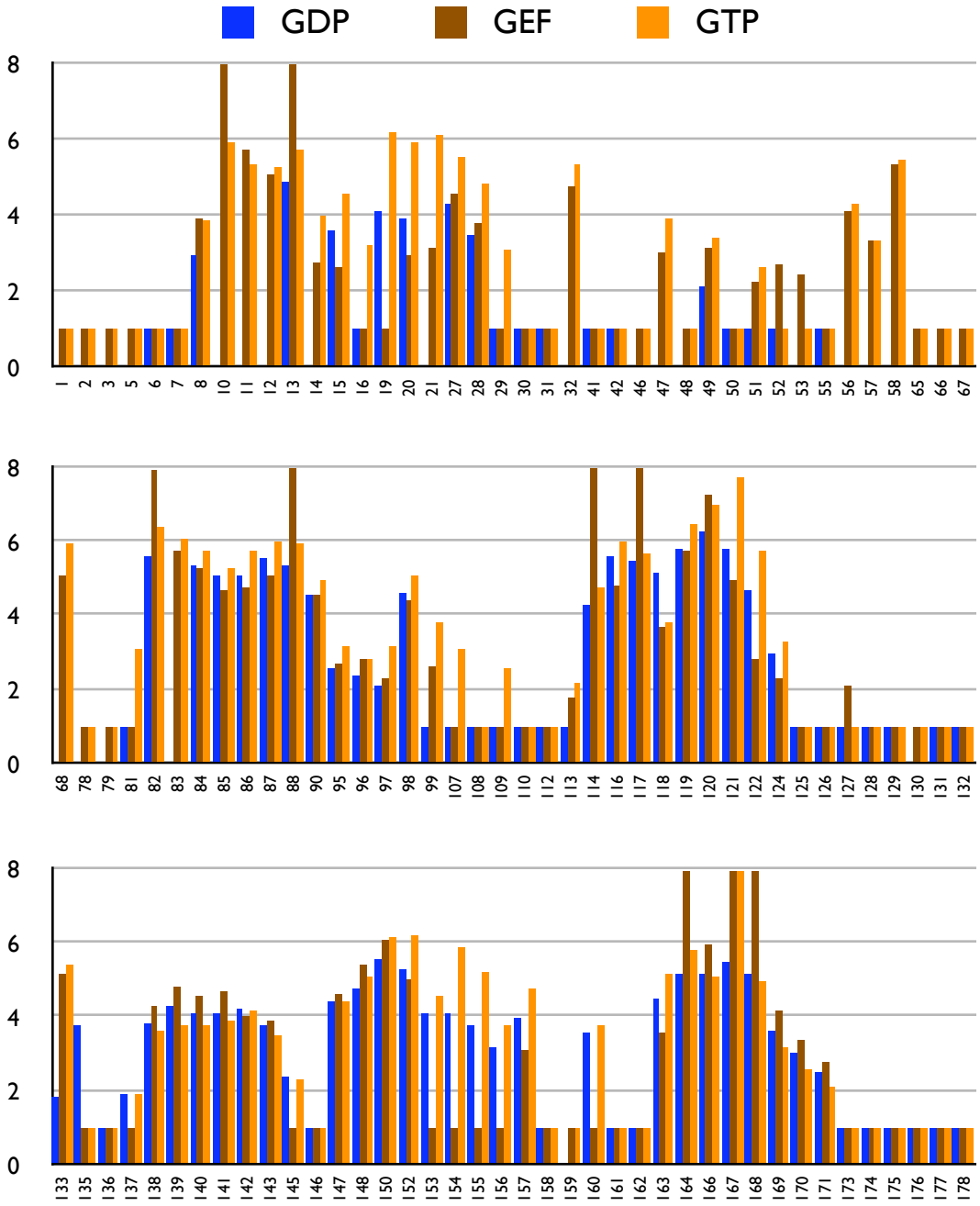

Figure 44. Comparison of hydrogen/deuterium exchange protection factors for GDP-, GEF- and GppNHp-bound Vps21. Protection factor values in each hydrogen/deuterium exchange data set (Figures 40-42) are compared for each residue, with values of 1 and 8 assigned to residues that exchanged too quickly or too slowly to be detected. Residues for which less than two protection factor values are available are not displayed.

Given the disorder observed in its HSQC upon complex formation, it was predicted that the dynamic mobility of Vps21 when bound to the Vps9 domain would lead to residues within the Rab becoming more solvent accessible. Figure 44 shows a comparison of the protection factors for each residue in these three data sets. Indeed, a number of residues are less protected while bound to Rabex5 than in either nucleotide-bound form (Figure 45, red, Table 4). Many of these more exposed residues surround the nucleotide binding pocket, which is to be expected, as this site becomes vacated during Rab/GEF complex formation. Of note, residues Lys121, Ile122, and Met124 of the β5 - α4 loop, which surrounds the guanine base, show a significant increase in exchange rate upon complex

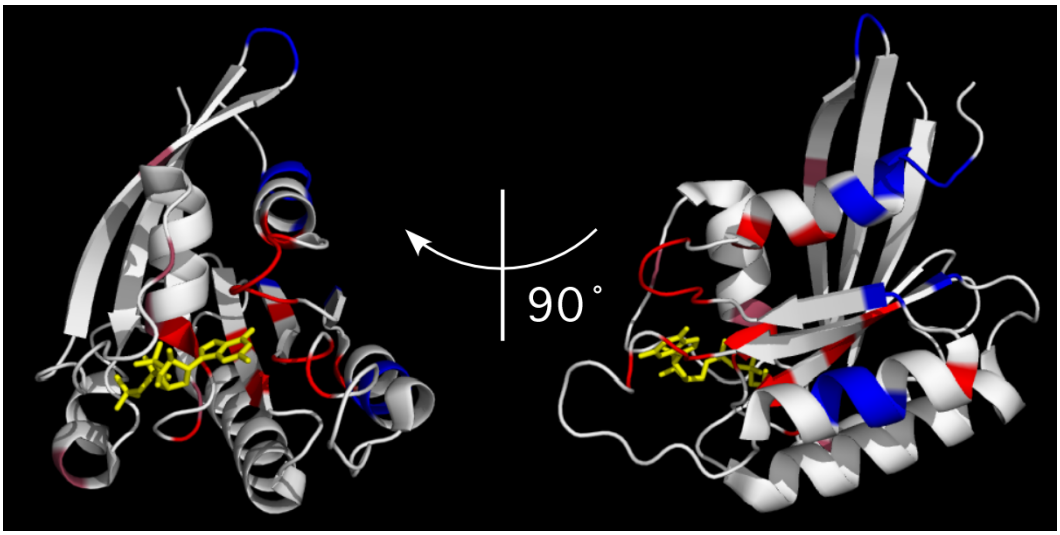

Figure 45. Effects of Vps9 domain binding on deuterium exchange rates of Vps21 residues. Exchange rates of each Vps21 residue were compared between GDP-bound, GEF-bound and GTP-bound states. Residues that showed faster or slower exchange in the GEF-bound state than in both GDP-bound and GTP-bound states (indicated in Tables 4 and 6, respectively) are shown in red and blue, respectively. Residues that showed faster exchange in GEF-bound state than in the GTP-bound state but could not be compared to the GDP-bound state due to unassigned or degenerate peaks (indicated in Table 5) are also colored (raspberry).

formation. We were unable to determine exchange rates for neighboring Asp123, which provides the guanine specificity of this binding pocket (Esters, Alexandrov et al. 2000), due to overlapping signal with Ile54. Glu15, Gly19 and Lys20 of the P-loop are also more solvent-accessible as a result of GEF binding. Ser21, which is involved coordination of the Mg^{2+} ion (Esters, Alexandrov et al. 2000), is among a list of residues that are more exposed in the presence of GEF than in the

Table 4. Residues exposed upon GEF-binding.

Residue	GDP F_P	GEF F_P	GTP F_P	Δk_{ex} GDP	Δk_{ex} GTP
E15	3.64	2.65	4.57	9.6	81.7
G19	4.11	F	6.18	-	-
K20	3.92	2.94	5.94	9.5	991.3
V85	5.12	4.72	5.30	2.5	3.9
V86	5.09	4.79	5.73	2.0	8.7
Y87	5.53	5.12	6.00	2.6	7.5
A116	5.65	4.80	6.04	7.1	17.5
K121	5.81	4.94	7.72	7.4	604.6
I122	4.67	2.82	5.77	70.4	882.5
M124	2.95	2.31	3.29	4.4	9.5
S153	4.09	F	4.59	-	-
A154	4.11	F	5.88	-	-
K155	3.77	F	5.22	-	-
T156	3.20	F	3.79	-	-
G157	3.95	3.09	4.74	7.3	44.6
V160	3.56	F	3.74	-	-
V163	4.49	3.55	5.19	8.8	43.6

F_P - protection factor, Δk_{ex} - fold difference in H-D exchange rate, F - too fast to detect.

Table 5. Residues potentially exposed upon GEF-binding.

Residue	GDP F_P	GEF F_P	GTP F_P	Δk_{ex} GDP	Δk_{ex} GTP
G14	D	2.80	3.98	-	15.1
S21	U	3.14	6.11	-	932.8
F32	D	4.78	5.35	-	3.7
Q47	U	3.01	3.92	-	8.2
R68	U	5.07	5.95	-	7.6
L83	D	5.75	6.08	-	2.2

U - unassigned residue, D - degenerate peak.

GTP-bound form but have unassigned or degenerate peaks in the GDP-bound form (Table 5). In addition, several residues deeper within the core of the protein, including Val85, Val86 and Tyr87 on β4, Ala116 on β5, and Val160 and Val163 on the interior side of α5, are also more exposed in the presence of Rabex5-T. These data indicate that binding of the Vps9 domain increases solvent accessibility of at least portions of the core of Vps21, as well as the nucleotide-binding pocket.

Surprisingly, a cluster of residues on the exterior of Vps21, opposite the switch regions, were relatively protected while bound to GEF (Table 6). This shielding could indicate a unique site of interaction between the Vps21 and the Vps9 domain (Figure 45, blue). This possibility is intriguing but also unlikely, since most proteins that specifically interact with one nucleotide-bound state of a Rab bind the region of switches I and II (Cherfils and Chardin 1999). Alternatively, the shielding could indicate a GEF-induced Rab conformation change that by itself reduces the solvent accessibility of this surface.

Table 6. Residues protected upon GEF-binding.

Residue	GDP F_P	GEF F_P	GTP F_P	Δk_{ex} GDP	Δk_{ex} GTP
A82	5.60	7.92	6.41	209.9	32.6
I114	4.31	S	4.74	-	-
G138	3.86	4.29	3.66	2.7	4.3
E139	4.30	4.83	3.76	3.3	11.8
K140	4.11	4.59	3.79	3.1	6.4
L141	4.10	4.67	3.89	3.7	5.9
L147	4.45	4.66	4.42	1.6	1.8
L148	4.74	5.39	5.10	4.4	1.9
F164	5.13	S	5.84	-	-
G166	5.15	5.93	5.07	6.0	7.2
G168	5.14	S	4.93	-	-
E169	3.64	4.14	3.17	3.2	9.3
K170	3.03	3.40	2.55	2.3	6.9
I171	2.54	2.78	2.12	1.7	4.5

Sec4 and Sec2

The possibility that the disordering effect on Vps21 seen upon binding by the Vps9 domain might represent a general Rab exchange mechanism led to the testing of another Rab/GEF pair. In yeast the only known such pair in which the exchange factor is not a heterodimer or part of a multiprotein complex is the Rab Sec4, required for transport of secretory vesicles from the Golgi to the plasma membrane (Novick, Goud et al. 1988), and its GEF Sec2 (Walch-Solimena, Collins et al. 1997). As a Rab, Sec4 has a size and overall structure similar to

other Rabs and Ras-like small G proteins (Stroupe and Brunger 2000) and suitable for NMR analysis. Sec2 is a protein of 759 amino acids and more than 84 kDa, but the amino terminal residues 1-160 have been shown to bind to and exhibit exchange activity for Sec4 (Ortiz, Medkova et al. 2002). In an effort to further

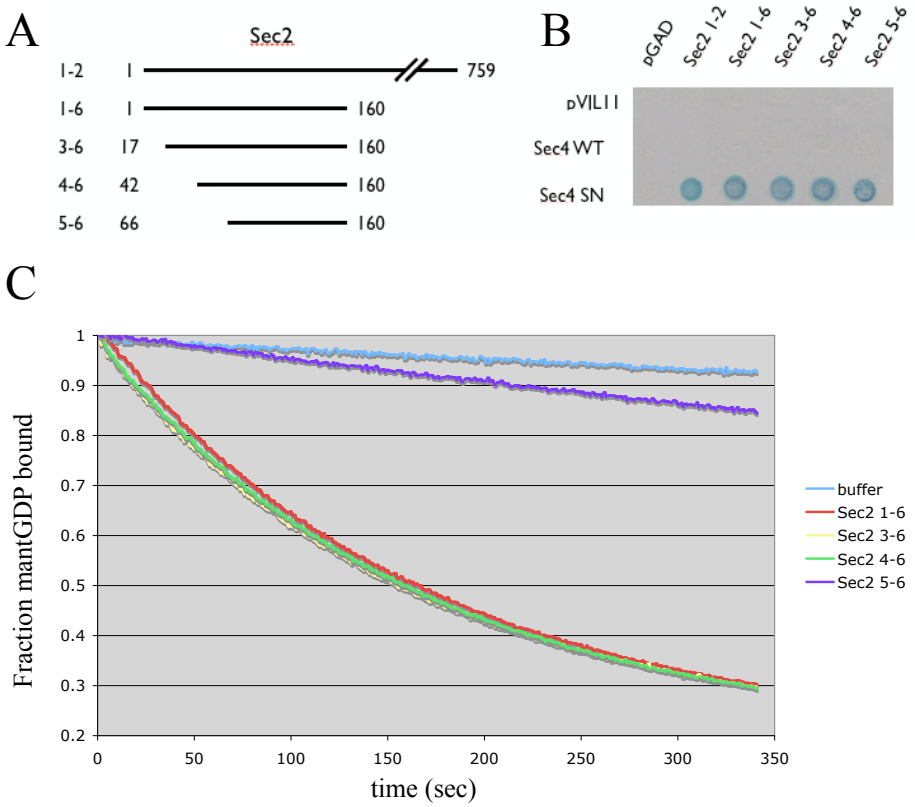

Figure 46. Sec2 residues 42-160 make up the minimal exchange domain for Sec4. (A) A series of Sec2 fragments were constructed based on the level of conservation between similar proteins and potential helix breaks. (B) L40 yeast that were cotransformed with the indicated bait and prey plasmids were grown on selective media, transferred to nitrocellulose and lysed, with the interaction of bait and prey gauged by the presence of β-galactosidase using a colorimetric filter assay. (C) Sec4 (1μM) was preloaded with mantGDP and incubated with buffer alone or the indicated purified Sec2 fragment (0.3μM) at 12°C. At time=0, GDP was added to 100μM, and the release of mantGDP was monitored by the FRET signal emitted at 440nm with Rab tryptophan excitation at 290nm.

limit the size of the exchange domain, a series of truncations were made based on secondary structure predictions and degree of conservation in homologous proteins. Figure 46 shows that all of the truncations bound Sec4 in a nucleotide state-specific manner, but Figure 46c shows that removing residues 42-65 significantly reduced the exchange activity of the domain indicating that residues 42-160 represent the minimal exchange domain.

^{15}N-labeled samples of Sec4 (aa 19 – 187, as used for crystallographic studies (Stroupe and Brunger 2000)) and Sec2 (aa 42 – 160) were analyzed by ^{1}H/^{15}N HSQC (Figure 47). The peaks of the Sec4 HSQC are of uniform size and well dispersed, suggesting that the assignment of these backbone amide peaks would be trivial upon collection of 3D spectra using ^{13}C/^{15}N-labeled protein. The Sec2 HSQC, however, shows almost no peak dispersion, indicative of an

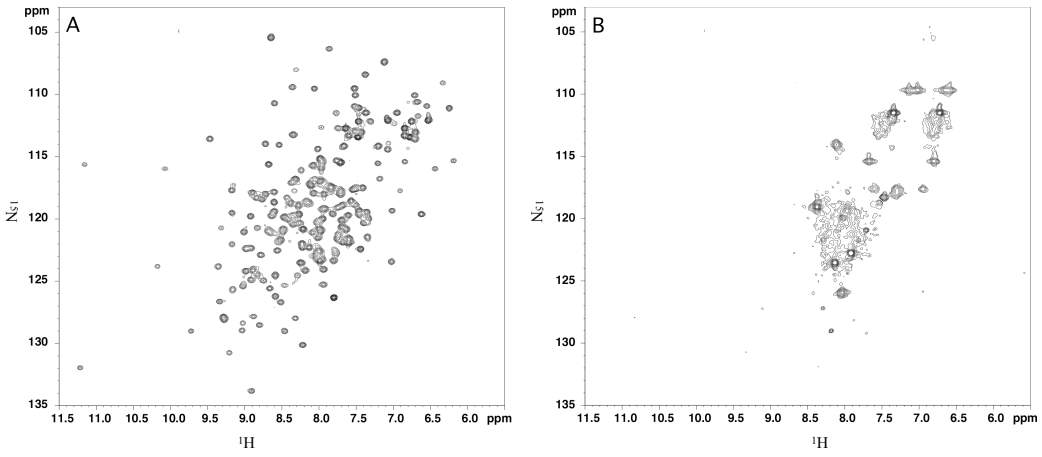

Figure 47. Suitability of Sec4 and Sec2 for NMR analysis. (A) A 2D 1H/15N HSQC spectrum of Sec4 demonstrates an appropriate number of well dispersed peaks. (B) A 2D 1H/15N HSQC spectrum of Sec2 aa 42-160 indicates that the protein likely forms a high molecular weight complex or aggregation.

aggregate or high molecular weight oligomer. Indeed, during gel filtration this fragment runs significantly faster than a 13kDa globular monomer should (data not shown), presumably due to Sec2 forming a multimer, as this region was predicted to form a coiled coil. A recent report confirms that residues 1-30 of Sec2 are not required for Sec4 binding or nucleotide exchange and shows by crystallography that residues 31-160 dimerizes in the form of an asymmetric coiled-coil (Dong, Medkova et al. 2007).

Discussion

Our efforts to obtain structural information about the Vps9 domain, either in complex with Vps21 by crystallography or alone by NMR, were ultimately unsuccessful. NOESY data for Rabex5-T suggest that the intramolecular dynamics of the Vps9 domain prevented our solving its solution structure, and this flexibility may have also hindered our crystallization attempts. Together these difficulties would have severely limited our ability to interpret data relating to the Vps9 domain and precluded us from modeling a Vps9 domain/Rab5 complex. Fortunately, crystal structure determination of the Rabex5 Vps9 domain alone by Lambright and colleagues allowed us to continue toward our goal (Delprato, Merithew et al. 2004). Interestingly, their structure (of a construct slightly longer than the longest of the constructs we examined, Rabex5-16)

contains a roughly conserved amino-terminal bundle of four α-helices. Delprato et al. reported that this helix bundle was required for soluble expression and propose the inclusion of this bundle as part of the catalytic core. Our own results expressing Vps9 domain constructs with and without an amino-terminal MBP-fusion echo the need for an additional structure to promote folding. Once folded, however, Rabex5-T can be separated from this fusion without sacrificing stability. In addition, exchange assays using the Vps9 domain with or without the inclusion of the helix bundle indicate that the helix bundle does not contribute to GEF activity (data not shown). Nevertheless, the requirement of the helix bundle for crystallization is not surprising given the intrinsic mobility of the Vps9 domain that likely prohibited our structural determination of Rabex5-T by NMR. While the inclusion of this additional domain might have benefitted our attempts at crystallizing a Vps21/Vps9 domain complex, nearly three years after the publication of the Vps9 domain, attempts by the Lambright group and others to crystallize the Rab5/GEF complex have thus far not benefited from the presence of the helix bundle alone. This objective has likely been complicated by the Rab's conformational dynamics that we observed by NMR upon complex formation. While the elusive constructs and/or conditions required for the crystallization of Rabex5 and Rab5 may still be discovered, with at least eleven separate Vps9 domain-containing proteins from a wide range of species showing various specificities for 9 different Rab5 family members, it seems equally likely that the

first structure of a Vps9 domain in complex with a Rab5 family member will be an alternate pair, such as the Vps9 domain of Varp in complex with Rab21 (Zhang, He et al. 2006) or that of Gapex5 in complex with Rab22b (Lodhi, Chiang et al. 2007).

The crystal structure of the Rabex-5 Vps9 domain revealed a novel layered fold of six α-helices, with an additional C-terminal helix that is missing from Alsin, ALS2CL and Rap6 (Delprato, Merithew et al. 2004). While most GEFs for the Ras, Rho, and Arf families of small GTPases contain easily identifiable nucleotide exchange domains -- Cdc25, Dbl homology (DH)/Pleckstrin homology (PH), and Sec7 domains respectively (Cherfils and Chardin 1999), Rab GEFs for different Rab subfamilies show almost no sequence similarity (Segev 2001). Available structures indicate that this difference extends to the structural frameworks these Rab GEFs use to accomplish nucleotide exchange. While the Vps9 domain consists of layered helices (Delprato, Merithew et al. 2004), the Sec4 GEF Sec2 is comprised of a linear coiled-coil (Dong, Medkova et al. 2007; Sato, Shirakawa et al. 2007). Mss4, though its relative promiscuity and unusual kinetics have led it to be described as a chaperone of nucleotide-free Rabs rather than a GEF (Nuoffer, Wu et al. 1997; Itzen, Pylypenko et al. 2006), promotes nucleotide release from a subset of Rabs with a structure made almost entirely from β-sheets (Yu and Schreiber 1995).

The residues most conserved within Vps9 domains are located on the Rab-binding surface of Rabex5 identified by our NMR titration analysis. The critical residues indicated by our mutational analyses (Chapter 3), as well as others (Delprato, Merithew et al. 2004), are found within this surface, on or around a hydrophobic groove between αV4 and αV6. Interestingly, in light of the lack of sequence homology or similarity in tertiary structure found for GEFs for different GTPase families, this important hydrophobic groove resembles an analogous substructure within the Sec7 domain of Arf GEFs(Mossessova, Gulbis et al. 1998; Mossessova, Corpina et al. 2003; Renault, Guibert et al. 2003). This parallel extends to the invariant aspartate residue in the Vps9 domain (Vps9 Asp251/ Rabex5 Asp313) that corresponds to the catalytic 'glutamate finger' in the Sec7 domain (reviewed in (Jackson and Casanova 2000)). Delprato et al. also found a number of Rab5 residues that are important for the Rab5/Vps9 domain interaction and noted that a similar triad of switch I and switch II residues within Arf were critical to its interaction with the Sec7 domain. These likenesses lead to the suggestion that the Vps9 domain may act through a mechanism of exchange similar to that of the Sec7 domain, wherein the aspartate of the Vps9 domain destabilizes GDP binding by interacting with the P-loop of Rab5 (Delprato, Merithew et al. 2004).

Though we had no substantial reason to doubt this proposed mechanism of Rab5 nucleotide exchange by the Vps9 domain, a number of aspects of this model

left us unsatisfied. While our own mutational analyses of yeast Vps9 were initiated with a similar possibility in mind and identified the same potentially catalytic aspartate residue, yeast expressing Vps9 with this aspartate mutated to alanine show a relatively mild missorting phenotype (Figure 19). Also, the model of this interaction presented by Delprato et al., from the limited visual representation, was clearly based on their structure of Rab5 in its active GTP-bound conformation, which differs significantly from the GDP-bound conformation and does not interact with the Vps9 domain. While a crystal structure of nucleotide-free Arf bound to the Sec7 domain does resemble that of Arf in its GTP-bound form (Goldberg 1998), Delprato et al. instead base their model on a structure which contains the inhibitor Brefeldin A (BFA) (Mossessova, Corpina et al. 2003), in which Arf is still bound to GDP. In addition, the compensatory mutations Delprato et al. presented to validate their model, while statistically significant, were fairly modest. Finally our initial NMR analyses with Rabex5-T indicated that the interaction of the Vps9 domain with Rab5 is a dynamic process, for which NMR might give us insight that could not be obtained from a crystal structure.

Our first indication that this could be true came when we attempted to map the Vps9 domain-binding surface of Vps21. Crystal structures of GTPases in complex with GEFs, GAPs and effectors have shown numerous static images of GTPases locked in various conformations. Given that the Vps9 domain catalyzes

a GEF reaction that begins with the Vps21•GDP conformation and eventually ends with the Vps21•GTP conformation, it would not have been surprising to see significant changes in the Vps21 HSQC upon binding of the Vps9 domain. However, our titration data did not indicate a change from a Vps21•GDP conformation to any single Vps21•GEF conformation. Rather, the data imply that GEF binding allows Vps21 to transition between at least two conformations, if not many, on a time scale that prevents resolution by HSQC. Future studies using using 15N relaxation measurements may shed light on the dynamics of this conformational heterogeneity.

In order to probe these dynamics further, we analyzed the effect that Vps9 domain binding had on hydrogen/deuterium exchange rates of Vps21 residues. These data confirmed that a number of residues, including residues at the core of Vps21 became more exposed to solvent during the interaction of Vps21 with the Vps9 domain. This result was intriguing in light of the extensive unfolding of Rab8 seen in the Mss4/Rab8 complex crystal structure that was proposed to play a key role in the mechanism of Mss4-induced GDP release (Itzen, Pylypenko et al. 2006) and raised the possibility that Vps9 domain-induced dynamic mobility of Vps21 could play a role in the mechanism of Rab5 nucleotide exchange. More recently, a crystal structure of nucleotide-free Sec4 in complex with its GEF Sec2 was published (Dong, Medkova et al. 2007). Dong et al. cite a reorganization of switches I and II of Sec4 and the resulting decrease in affinity for nucleotide as

the mechanism of exchange by Sec2. They do note additional unfolding of the nucleotide binding pocket, but this unfolding is less severe than that observed for Rab8 in complex with Mss4, and the authors suggest that this is likely to be a result of the loss of nucleotide, rather than the cause. A common feature in the Sec4/Sec2 and Rab8/Mss4 structures is that both Sec4 and Rab8 show a paucity of electron density in the β5 - α4 and β6 - α5 loops (Itzen, Pylypenko et al. 2006; Dong, Medkova et al. 2007), indicating the flexibility of these regions when in complex with their GEFs. While not a direct measure of flexibility, our deuterium exchange results directly demonstrate that residues in both of these loops in Vps21 are more accessible to solvent when bound to Rabex5-T. Thus, it is plausible that a crystal structure of a Rab5 family member in complex with a Vps9 domain may show a similar lack of electron density in these loops and that the flexibility of this region is indeed a common feature of all Rabs in the absence of nucleotide.

Our NMR analysis of Vps21 in complex with Rabex5-T suggests that the formation of this Rab/GEF complex results in a dynamic mobility that exposes the core of Vps21 to solvent. However, it is not yet clear whether this mobility facilitates the release of nucleotide from the nucleotide-binding pocket or is instead a result of the nucleotide-binding pocket being vacated as a result of another mechanism, such as the action of the identified aspartate residue. Additional analysis of nucleotide-free Vps21 will help distinguish between these

two possibilities. Since none of our data presented in this chapter directly refutes the mechanism proposed by Delprato et al., it is tempting to speculate that the Vps9 domain may actually utilize a combination of the insertion of the 'aspartate finger' and the dynamic unfolding of the Rab5 nucleotide pocket in order to accomplish nucleotide exchange. A bipartite mechanism such as this would help to explain why a point mutant of the catalytic aspartate could still exhibit functional levels of exchange *in vivo*, as found for $Vps9^{D251A}$ in Chapter 3.

Materials and Methods

Strains and reagents

E. coli strains used were DH5α (Invitrogen, for cloning) and BL21(DE3) (Stratagene, for protein expression). GDP and $^{2}H_2O$ were purchased from Sigma-Aldrich (St. Louis, MO). Bovine thrombin and GppNHp were purchased from Calbiochem (La Jolla, CA). $^{15}NH_4Cl$, [$^{13}C_6$]-glucose and 10x $^{15}N/^{13}C$-BioExpress cell growth media were purchased from Cambridge Isotope Laboratories, Inc. (Andover, MA). The plasmid encoding His_6-TEV[S219V]-Arg_5 was a gift from the Volkman laboratory (MCW).

Plasmid construction

All sequences were amplified with iTaq DNA polymerase, cloned into pCR2.1 TOPO using the TOPO TA cloning kit and sequenced before being subcloned into appropriate vectors. Unless otherwise noted, cloning was facilitated with a 5' Bam*HI* site and a 3' Sal*I* site. Limited trypsin proteolysis of a Rabex5/Vps21 complex and secondary structure predictions identified a fragment of Rabex-5 (aa 222 – 392), called Rabex5-T. The sequence encoding this fragment was cloned into pET28MBP, which encodes an amino terminal His_6-tagged MBP fusion and a TEV protease site (Davies, Carney et al. 2005), to yield pET28MBP-R5T. As a result of this cloning, after TEV cleavage, the Rabex5 fragment was appended at the amino terminus with a GAMDP pentamer. A fragment encoding residues 1 – 178 of Vps21 with a 5' Nde*I* site and a 3' Bam*HI* site was cloned into pET28a, which encodes a His_6-tag and a thrombin protease site, to yield pVps21-81. As a result of this cloning, after thrombin cleavage, the Vps21 fragment was appended at the amino terminus with a GSH trimer.

Protein expression and purification

pET28MBP-R5T and pVps21-80 were transformed into BL21(DE3). Unlabeled proteins were expressed in LB medium, and isotopically enriched samples were expressed in M9 minimal medium (48 mM $NaPO_4$, 22 mM KPO_4, 8.5 mM NaCl, 1 mM $MgSO_4$, 100 μM $CaCl_2$, 10 μg/ml each thiamine and biotin,

pH 7.4) containing 1 g/L $^{15}NH_4Cl$ for ^{15}N-labeled samples (and 3 g/L [$^{13}C_6$]-glucose as well as 0.1x $^{15}N/^{13}C$-BioExpress cell growth media for $^{15}N/^{13}C$-labeled samples). Cultures were supplemented with 50 μg/ml kanamycin and grown at 37˚C to an OD_{600} of 0.6 before induction with 500 μM IPTG at 22˚C for 16 hours. Cell pellets were harvested and stored at -80˚C until purification. When thawed, pellets were resuspended in HisA Buffer (25mM NaPO4, 300mM NaCl, 5mM MgCl2, pH 7.5) supplemented with Complete EDTA-free protease inhibitors and 200 μM AEBSF, lysed using a French Press, and centrifuged. Supernatants were passed through 0.45 μm syringe filters and loaded into the AKTA FPLC for purification using a HiTrap Chelating HP column loaded with NiSO4. After injection, the column was washed with 20 mM imidazole before proteins were eluted with a gradient of 20 – 250 mM imidazole. His_6MBP-R5T fractions were concentrated, adjusted to 1mM DTT and 0.5mM EDTA, and cut overnight with His_6TEV at 16˚C. Cleaved protein was buffer exchanged using a HiPrep 26/10 Desalting column to remove imidazole and EDTA before a second pass through the HiTrap Chelating HP column to remove the His_6MBP tag and His_6TEV. Remaining contaminants were removed by gel filtration. His_6Vps21 fractions were concentrated and cut over night with thrombin. After loading with either GDP or GppNHp by incubation with EDTA and an excess of desired nucleotide at 30˚C for 30 minutes, EDTA, unbound nucleotide, thrombin and the His_6 tag were removed by gel filtration. In both cases, gel filtration over a HiLoad 16/60

Superdex 75 column allowed buffer exchange into the NMR sample buffer (25 mM $NaPO_4$, 200 mM NaCl, 5 mM $MgCl_2$, pH 6.8).

NMR spectroscopy

NMR samples were prepared at 0.5 – 1.0 mM with 10% ^2H_2O. All NMR data were acquired at 25 °C on a Bruker 600 MHz spectrometer equipped with a triple-resonance CryoProbe and processed with NMRPipe software (Delaglio, Grzesiek et al. 1995). For each protein (or nucleotide state), a series of spectra including 2D $^1H/^{15}N$ HSQC and 3D HNCO, HNCACO, HNCA, HNCOCA, HNCACB and CCONH were collected. Peaks in the $^1H/^{15}N$ HSQC were picked automatically using SPSCAN (Glaser 1999). Peaks in the 3D spectra were picked manually using XEASY (Bartels, Xia et al. 1995), and backbone ^1H, ^{15}N and ^{13}C resonance assignments were obtained from the peak lists in an automated manner using the program GARANT (Bartels, Billeter et al. 1997) and confirmed or corrected manually.

Hydrogen-Deuterium exchange

Vps21 was expressed and purified in protonated buffers as described above. Rab loaded with either GDP or GppNHp was diluted into deuterated NMR sample buffer (80% ^2H_2O) alone, and $^1H/^{15}N$ HSQC spectra were collected continuously (20 minutes per spectrum) over night. The time between dilution in

deuterated buffer and the start of the first acquisition was 8 miniutes. GDP-loaded Rab was mixed with equimolar unlabeled Rabex5-T and diluted in deuterated buffer. At time points, excess GppNHp was added, and a single HSQC was acquired. Acquisition was initiated 8 minutes after the addition of GppNHp. Data sets were loaded into CARA, appropriate assigned peaklists were calibrated to the experimental data, and peaks were integrated in batch. Integration tables were exported into proFit, where curves of signal intensity vs time were fit to the equation

$$y = (1-f_H)A_0e^{(-xk}ex) + A_0f_H$$

where A_0 = signal at time=0, k_{ex} = rate of amide exchange and f_H = final fraction H. Protection factors were calculated from rate constants using a worksheet downloaded from the England laboratory (http://hx2.med.upenn.edu/).

CHAPTER FIVE

Discussion and Future Directions

From yeast to mammals

When I joined the Horazdovsky Lab, Greg Tall was just proving that the conserved region now known as the Vps9 domain conferred Vps21 and Rab5 nucleotide exchange activity. At the time, sequence alignments showed two Vps9 domain-containing proteins in fungi, Vps9 and YPL070w (Muk1), and three in mammals, Rabex5, Rin1, and JC265 (Rin2). Since then, that total has grown to at least 11 (Bateman, Coin et al. 2004; Letunic, Copley et al. 2004). Including the characterization of Muk1 as an exchange factor for the yeast Rab5 family in Chapter 2, Rab5 GEF activity has now been reported for 10 of these (Horiuchi, Lippe et al. 1997; Hama, Tall et al. 1999; Tall, Barbieri et al. 2001; Saito, Murai et al. 2002; Kajiho, Saito et al. 2003; Otomo, Hadano et al. 2003; Hadano, Otomo et al. 2004; Zhang, He et al. 2006; Lodhi, Chiang et al. 2007). Similarly the Rab5 family has expanded to include three yeast Rab proteins and six mammalian Rab proteins (Pereira-Leal and Seabra 2001; Delprato, Merithew et al. 2004). The multiplicity of these families begs the question of how these proteins specifically

interact to regulate the numerous individual trafficking events in which they participate.

In chapter 2, we analyzed the entire yeast Rab5 family with the entire yeast Vps9 domain family. This approach allowed direct comparison between data for proteins within a given family and identified a role for Muk1 and Ypt53 in endocytic trafficking distinct from that of Vps9 and Vps21. Expanding this type of analysis to the mammalian Rab5 and Rab5 GEF families grows exponentially more difficult. In addition to the size of these families, where for mammalian cells there are 54 possible combinations of 15 proteins, compared to the 6 combinations of 5 proteins for yeast, there are also many more signal transduction and trafficking pathways that would need to be considered (Di Fiore and De Camilli 2001; Sorkin and Von Zastrow 2002). This level of complexity may preclude a meaningful genome-wide analysis of functional specificity, but the Horazdovsky Lab is prepared to undertake a comprehensive in vitro analysis of all Rab5 family members and the Vps9 domains of all Vps9 domain family members, using similar constructs to test binding and GEF activity for each of the 99 possible combinations. This endeavor will demonstrate the specificity inherent in the interaction between members of these families and guide future studies into the regulation of this inherent specificity by localization or (auto)inhibition to effect functional specificity.

Regulation of the Vps9 domain

The carboxy-terminal CUE domain of Vps9 binds ubiquitin and facilitates the monoubiquitination of Vps9 and the ubiquitin-binding capacity is critical for the endocytic sorting of pheromone receptors (Davies, Topp et al. 2003; Donaldson, Yin et al. 2003; Shih, Prag et al. 2003). Our mutational analysis in Chapter 3 uncovered a potential regulatory mechanism whereby an intramolecular interaction between the CUE domain and the Vps9 domain appears to limit the GEF activity of Vps9. Though the details of this intramolecular interaction are still to be worked out, it seems to require some portion of the Rab-binding surface of the Vps9 domain and some portion of the ubiquitin-binding surface of the CUE domain. However, relief from this auto-inhibition is not sufficient for proper endocytic trafficking, as deletion of the CUE domain, which would mitigate any inhibition also results in defective endocytosis. It is likely that ubiquitin binding by the CUE domain simultaneously potentiates Vps9 function by both relieving this auto-inhibition and localizing Vps9 to an endosomal compartment for the activation of Vps21.

Like Vps9, Rabex5 contains its Vps9 domain approximately in the middle of the protein. Though little sequence identity is observed outside the Vps9 domains of these proteins, when the Vps9 CUE domain was discovered, a divergent CUE-like domain was also identified in the carboxy-terminus of Rabex5 (Davies, Topp et al. 2003; Donaldson, Yin et al. 2003). Since then Rabex5 has

been shown to both bind ubiquitin and become ubiquitinated, but these interactions with ubiquitin are through two amino-terminal ubiquitin-binding motifs, rather than the CUE-like domain (Lee, Tsai et al. 2006; Mattera, Tsai et al. 2006). These ubiquitin-binding motifs were shown to facilitate the interaction of Rabex5 with ubiquitinated EGFR receptors (Penengo, Mapelli et al. 2006), indicating that Rabex5 may be localized by binding ubiquitinated receptors as suggested for Vps9 above. In addition, the Vps9 domain of Rabex5 alone has a greater GEF activity than full-length Rabex5 (Delprato, Merithew et al. 2004). Though an inhibitory effect has not been attributed to either the amino- or carboxy-terminal portions of the protein, the GEF activity of full-length Rabex5 is enhanced by Rabaptin5 (Lippe, Miaczynska et al. 2001), which binds a carboxy-terminal coiled coil immediately upstream of the CUE-like domain (Mattera, Tsai et al. 2006). It is possible that the divergent CUE-like domain interacts with the Rabex5 Vps9 domain in a manner similar to that proposed for the CUE and Vps9 domains of Vps9, and that this interaction is disrupted by Rabaptin5 binding. Thus, Vps9 and Rabex5 may both be regulated by the combination of localization via ubiquitin-binding and relief of autoinhibition, though these regulatory mechanisms coincide within a single domain for Vps9 and are separated in Rabex5. Additionally, it will be interesting to examine whether the ubiquitin binding domains of Rabex5 influence the GEF activity of the Rabex5 Vps9 domain.

Though not employing ubiquitin-binding, at least one other Rab5 GEF has been demonstrated to exhibit similar dual regulation. Rin1 contains an amino-terminal SH2 domain and a carboxy-terminal Ras Association (RA) domain. The SH2 domain has been shown to facilitate Rin1's interaction with phosphorylated receptors (Barbieri, Kong et al. 2003), and binding of activated Ras to the RA domain potentiates the GEF activity (Tall, Barbieri et al. 2001). It is interesting to speculate that this potentiation of Rin1 may also occur through a release of auto-inhibtion between the Vps9 and RA domains upon Ras binding, and this possibility will be examined in the future. Rin2 and Rin3 have similar domain architectures (Saito, Murai et al. 2002; Kajiho, Saito et al. 2003), and although neither has yet been shown to bind a phosphorylated target or a Ras family member, it seems likely that they would be similarly regulated. As additional interaction data becomes available for Vps9 domain proteins, it will be interesting to see for how many of these proteins this trend of dual regulation holds true and how these modes of regulation contribute to functional specificity within the system.

Structure of the Rab5/Vps9 domain complex and the mechanism of Rab5 nucleotide exchange

We sought to determine the structure of the Rab5/Vps9 domain complex to infer a model for the mechanism of nucleotide exchange. As chronicled in

Chapter 4, these efforts were focused first on crystallography of this complex and then on NMR approaches. Using HSQC perturbation mapping, we identified the Rab-binding surface of the Vps9 domain. However, our attempts to use the same technique to map the opposite side of this complex interface met with unexpected results. Our data indicate that, upon Vps9 domain binding, Vps21 exhibits a conformational mobility that prevented the detection of Vps21 residues while in complex. While the observed dynamics prevented us from mapping the second binding surface needed to model this interaction, they offered unexpected insight into the behavior of Vps21 while in complex. We used a series of hydrogen/ deuterium exchange experiments to show that complex formation with Vps9 causes residues around the nucleotide binding-pocket and within the core of Vps21 to become more accessible to solvent. The major question remains whether the dynamics that expose the core help facilitate the release of GDP or simply result from the nucleotide-binding pocket being vacated through another mechanism. In order to address this question, we have initiated an examination of the nucleotide-free state of Vps21. Comparing an HSQC of nucleotide-free Vps21 to that of Vps21 in complex with Vps9 will tell us whether nucleotide-free Vps21 exhibits the same conformational dynamics we observed during our attempts to map the binding interface. As it is probable that nucleotide-free Vps21 will exhibit some level of dynamics, which we may not be able to distinguish from those seen for Vps21 in complex, we will also pursue an approach with higher

resolution. We will determine the rates of hydrogen/deuterium exchange for Vps21 residues in the nucleotide free state. Comparing these rates with those of Vps21 in complex with the Vps9 domain will allow us to differentiate the contributions of either GEF binding or the nucleotide-state in the solvent accessibility of residues both around the nucleotide-binding pocket and within the core. If the exposure of the Vps21 core is similar in the nucleotide-free state, it would argue that the mobility we observe is a consequence of nucleotide release by another mechanism, rather than a cause of this activity.

During the course of these studies, another mechanism of nucleotide release was proposed (Delprato, Merithew et al. 2004). With the publication of the Vps9 domain structure, Delprato et al. recognized a similarity between the framework of the Vps9 domain and the Sec7 Arf GEF domain and suggested that a conserved aspartate residue in the Vps9 domain may serve the same function as the similarly located 'glutamate finger' (Beraud-Dufour, Robineau et al. 1998). In our own mutational analysis (Chapter 3) we found that this aspartate residue was important for Vps9 function, but not critical. A Glu-to-Lys mutation of the Sec7 domain 'glutamate finger' allows binding to Arf without effecting nucleotide release (Beraud-Dufour, Robineau et al. 1998). Delprato et al. indicate that a similar Asp-to-Lys mutation in the Rabex5 Vps9 domain does not bind Rab5 (Delprato, Merithew et al. 2004). However, our data indicate that mutating this residue to alanine in Vps9 does allow binding to Vps21 without stimulating

release of GDP. If Rabex5-T^{D313A} shows the same ability to bind and inability to exchange Vps21, it may have interesting implications for further NMR analysis. First, A Rabex5-T^{D313A}/Vps21•GDP would represent an intermediate between the free Vps21•GDP and Rabex5-T/Vps21 complex and provide a second means of assessing the relative contributions of either Vps9 domain binding or release of nucleotide to the dynamic mobility we observed. Additionally, if it turns out that the mobility of Vps21 results from nucleotide release and not GEF binding, then HSQC perturbation mapping of Vps21 may not suffer the same consequences as our previous attempt with wild-type Rabex5-T. This may allow the detection of specific residues affected by the binding of the Vps9 domain, which could then allow us to model the interaction between these two proteins, as we intended.

Solution structures of Vps21

Considering that the Protein Data Bank currently lists 85 structures of 37 Rab proteins, including 28 structures of 7 Rab5 family members (Bhat, Bourne et al. 2001; Kouranov, Xie et al. 2006), it is somewhat surprising that there are no solution structures of Rabs. During the course of the NMR analyses described in Chapter 4, in which we assigned the backbone resonances of Vps21•GDP and Vps21•GTP, we have also collected the spectra necessary to assign side chain resonances and the NOESY data required for the generation of distance constraints used to solve structures for Vps21 in its GDP- and GTP-bound forms.

Initial examination of this data indicates that both of these data sets appear sufficient for successful structural determination (F. Peterson, personal communication). While working to complete this project, we may also pursue structural information about Ypt52 and Ypt53, as these now represent the only members of the Rab5 family without known structures.

Forthcoming crystal structures

As this document was being prepared, several structures that will undoubtedly impact future discussions of the interaction of the Rab5 family with their GEFs and the associated exchange mechanism were deposited into the RCSB Protein Data Bank (Bhat, Bourne et al. 2001; Kouranov, Xie et al. 2006). Each of these structures is currently on hold, awaiting publication for their release. The first, 2OT3, by Delprato and Lambright is a structure of the Rabex5 Vps9 domain in complex with nucleotide-free Rab21, which has been rumored for some time now. In addition, Uejima et al. deposited four structures of a Rab5/ Vps9 domain pair from *Arabidopsis*, Ara7 and AtVps9a. Though the titles of these structures have been removed, they were quite revealing for the brief time they were available:

2EFC Ara7-GDP/AtVps9a
2EFD Ara7/AtVps9a
2EFE Ara7-GDPNH2/AtVps9a
2EFH Ara7-GDP/AtVps9a(D185N)

I suspect that 2EFC and 2EFE are actually GDP- and GTP-bound forms of Ara7 alone, as it would be surprising to observe a wild-type Rab5 GEF forming a stable complex with a nucleotide-bound Rab5 protein. The presumably nucleotide-free complex of 2EFD should offer a cross-species comparison with the mammalian Rabex5/Rab21 structure. Finally, the Asp185 residue of AtVps9a corresponds to the Asp251 of Vps9 identified in our mutational analysis and the Asp313 of Rabex5 identified as the potential equivalent of the glutamate finger by Delprato et al (Delprato, Merithew et al. 2004). Assuming this residue is positioned in or around the nucleotide-binding pocket, the formation of an unsuccessful Rab/GEF complex as a result of this Asp-to-Asn mutation argues that wild-type exchange activity may result from the repulsive effect of the carboxylate group rather than a steric effect of the bulk of the side chain at this position. Together these structures may represent a collection similar to the structural snapshots of Arf activation by the Sec7 domain obtained several years ago (Goldberg 1998; Mossessova, Gulbis et al. 1998; Mossessova, Corpina et al. 2003; Renault, Guibert et al. 2003).

BIBLIOGRAPHY

Afar, D. E., L. Han, et al. (1997). "Regulation of the oncogenic activity of BCR-ABL by a tightly bound substrate protein RIN1." Immunity 6(6): 773-82.

Aghazadeh, B., K. Zhu, et al. (1998). "Structure and mutagenesis of the Dbl homology domain." Nat Struct Biol 5(12): 1098-107.

Albert, S. and D. Gallwitz (1999). "Two new members of a family of Ypt/Rab GTPase activating proteins. Promiscuity of substrate recognition." J Biol Chem 274(47): 33186-9.

Arnett, A. L., I. Bayazitov, et al. (2004). "Antisense oligonucleotide against GTPase Rab5b inhibits metabotropic agonist DHPG-induced neuroprotection." Brain Res 1028(1): 59-65.

Babst, M., D. J. Katzmann, et al. (2002). "Escrt-III: an endosome-associated heterooligomeric protein complex required for mvb sorting." Dev Cell 3 (2): 271-82.

Babst, M., D. J. Katzmann, et al. (2002). "Endosome-associated complex, ESCRT-II, recruits transport machinery for protein sorting at the multivesicular body." Dev Cell 3(2): 283-9.

Bai, Y., J. S. Milne, et al. (1993). "Primary structure effects on peptide group hydrogen exchange." Proteins 17(1): 75-86.

Bankaitis, V. A., L. M. Johnson, et al. (1986). "Isolation of yeast mutants defective in protein targeting to the vacuole." Proc. Natl. Acad. Sci. USA 83: 9075-9079.

Bar-Sagi, D. and J. R. Feramisco (1986). "Induction of membrane ruffling and fluid-phase pinocytosis in quiescent fibroblasts by ras proteins." Science 233(4768): 1061-8.

Barbieri, M. A., A. D. Kohn, et al. (1998). "Protein kinase B/akt and rab5 mediate Ras activation of endocytosis." J Biol Chem 273(31): 19367-70.

Barbieri, M. A., C. Kong, et al. (2003). "The SRC homology 2 domain of Rin1 mediates its binding to the epidermal growth factor receptor and regulates receptor endocytosis." J Biol Chem 278(34): 32027-36.

Barbieri, M. A., R. L. Roberts, et al. (2000). "Epidermal growth factor and membrane trafficking. EGF receptor activation of endocytosis requires Rab5a." J Cell Biol 151(3): 539-50.

Bartels, C., M. Billeter, et al. (1997). "Automated sequence-specific NMR assignments of homologous proteins using the program GARANT." J Biomol NMR 7: 207-213.

Bartels, C., T.-H. Xia, et al. (1995). "The program XEASY for computer-supported NMR spectral analysis of biological macromolecules." J Biomol NMR 6(1): 1-10.

Bateman, A., L. Coin, et al. (2004). "The Pfam protein families database." Nucleic Acids Res 32(Database issue): D138-41.

Becherer, K. A., S. E. Rieder, et al. (1996). "Novel syntaxin homologue, Pep12p, required for the sorting of lumenal hydrolases to the lysosome-like vacuole in yeast." Mol Biol Cell 7(4): 579-94.

Beraud-Dufour, S., S. Robineau, et al. (1998). "A glutamic finger in the guanine nucleotide exchange factor ARNO displaces Mg2+ and the beta-phosphate to destabilize GDP on ARF1." Embo J 17(13): 3651-9.

Bhat, T. N., P. Bourne, et al. (2001). "The PDB data uniformity project." Nucleic Acids Res 29(1): 214-8.

Bock, J. B., H. T. Matern, et al. (2001). "A genomic perspective on membrane compartment organization." Nature 409(6822): 839-41.

Bonifacino, J. S. (2004). "The GGA proteins: adaptors on the move." Nat Rev Mol Cell Biol 5(1): 23-32.

Boriack-Sjodin, P. A., S. M. Margarit, et al. (1998). "The structural basis of the activation of Ras by Sos." Nature 394(6691): 337-43.

Brambilla, R., N. Gnesutta, et al. (1997). "A role for the Ras signalling pathway in synaptic transmission and long-term memory." Nature 390(6657): 281-6.

Bucci, C., A. Lutcke, et al. (1995). "Co-operative regulation of endocytosis by three Rab5 isoforms." FEBS Lett 366(1): 65-71.

Bucci, C., R. G. Parton, et al. (1992). "The small GTPase rab5 functions as a regulatory factor in the early endocytic pathway." Cell 70(5): 715-28.

Burd, C. G., P. A. Mustol, et al. (1996). "A yeast protein related to a mammalian Ras-binding protein, Vps9p, is required for localization of vacuolar proteins." Mol Cell Biol 16(5): 2369-77.

Cavanagh, J. (1996). Protein NMR spectroscopy : principles and practice. San Diego, Academic Press.

Chen, C. Z. and R. N. Collins (2005). "Insights into biological functions across species: examining the role of Rab proteins in YIP1 family function." Biochem Soc Trans 33(Pt 4): 614-8.

Cherfils, J. and P. Chardin (1999). "GEFs: structural basis for their activation of small GTP-binding proteins." Trends Biochem Sci 24(8): 306-11.

Chiariello, M., C. B. Bruni, et al. (1999). "The small GTPases Rab5a, Rab5b and Rab5c are differentially phosphorylated in vitro." FEBS Lett 453(1-2): 20-4.

Davies, B. A., D. S. Carney, et al. (2005). "Ubiquitin regulation of the Rab5 family GEF Vps9p." Methods Enzymol 403: 561-83.

Davies, B. A., J. D. Topp, et al. (2003). "Vps9p CUE domain ubiquitin binding is required for efficient endocytic protein traffic." J Biol Chem 278(22): 19826-33.

Delaglio, F., S. Grzesiek, et al. (1995). "NMRPipe: a multidimensional spectral processing system based on UNIX pipes." J Biomol NMR 6(3): 277-93.

Delprato, A., E. Merithew, et al. (2004). "Structure, exchange determinants, and family-wide rab specificity of the tandem helical bundle and Vps9 domains of Rabex-5." Cell 118(5): 607-17.

Devon, R. S., J. R. Helm, et al. (2003). "The first nonsense mutation in alsin results in a homogeneous phenotype of infantile-onset ascending spastic paralysis with bulbar involvement in two siblings." Clin Genet 64(3): 210-5.

Devon, R. S., C. Schwab, et al. (2005). "Cross-species characterization of the ALS2 gene and analysis of its pattern of expression in development and adulthood." Neurobiol Dis 18(2): 243-57.

Dhaka, A., R. M. Costa, et al. (2003). "The RAS effector RIN1 modulates the formation of aversive memories." J Neurosci 23(3): 748-57.

Di Fiore, P. P. and P. De Camilli (2001). "Endocytosis and signaling. an inseparable partnership." Cell 106(1): 1-4.

Donaldson, K. M., H. Yin, et al. (2003). "Ubiquitin signals protein trafficking via interaction with a novel ubiquitin binding domain in the membrane fusion regulator, Vps9p." Curr Biol 13(3): 258-62.

Dong, G., M. Medkova, et al. (2007). "A catalytic coiled coil: structural insights into the activation of the Rab GTPase Sec4p by Sec2p." Mol Cell 25(3): 455-62.

Dumas, J. J., Z. Zhu, et al. (1999). "Structural basis of activation and GTP hydrolysis in Rab proteins." Structure 7(4): 413-23.

Esters, H., K. Alexandrov, et al. (2000). "High-resolution crystal structure of S. cerevisiae Ypt51(DeltaC15)-GppNHp, a small GTP-binding protein involved in regulation of endocytosis." J Mol Biol 298(1): 111-21.

Esters, H., K. Alexandrov, et al. (2001). "Vps9, Rabex-5 and DSS4: proteins with weak but distinct nucleotide-exchange activities for Rab proteins." J Mol Biol 310(1): 141-56.

Evans, J. N. S. (1995). Biomolecular NMR spectroscopy. Oxford ; New York, Oxford University Press.

Eymard-Pierre, E., G. Lesca, et al. (2002). "Infantile-onset ascending hereditary spastic paralysis is associated with mutations in the alsin gene." Am J Hum Genet 71(3): 518-27.

Farnsworth, C. L. and L. A. Feig (1991). "Dominant inhibitory mutations in the Mg(2+)-binding site of RasH prevent its activation by GTP." Mol Cell Biol 11(10): 4822-9.

Feig, L. A. and G. M. Cooper (1988). "Inhibition of NIH 3T3 cell proliferation by a mutant ras protein with preferential affinity for GDP." Mol Cell Biol 8 (8): 3235-43.

Gerrard, S. R., N. J. Bryant, et al. (2000). "VPS21 controls entry of endocytosed and biosynthetic proteins into the yeast prevacuolar compartment." Mol Biol Cell 11(2): 613-26.

Ghaemmaghami, S., W. K. Huh, et al. (2003). "Global analysis of protein expression in yeast." Nature 425(6959): 737-41.

Glaser, R. W. (1999). "SPSCAN (http://www.molebio.uni-jena.de/~rwg/spscan)."

Goldberg, J. (1998). "Structural basis for activation of ARF GTPase: mechanisms of guanine nucleotide exchange and GTP-myristoyl switching." Cell 95 (2): 237-48.

Gorvel, J. P., P. Chavrier, et al. (1991). "rab5 controls early endosome fusion in vitro." Cell 64(5): 915-25.

Gros-Louis, F., I. A. Meijer, et al. (2003). "An ALS2 gene mutation causes hereditary spastic paraplegia in a Pakistani kindred." Ann Neurol 53(1): 144-5.

Grosshans, B. L., D. Ortiz, et al. (2006). "Rabs and their effectors: achieving specificity in membrane traffic." Proc Natl Acad Sci U S A 103(32): 11821-7.

Hadano, S., C. K. Hand, et al. (2001). "A gene encoding a putative GTPase regulator is mutated in familial amyotrophic lateral sclerosis 2." Nat Genet 29(2): 166-73.

Hadano, S., A. Otomo, et al. (2004). "ALS2CL, the novel protein highly homologous to the carboxy-terminal half of ALS2, binds to Rab5 and modulates endosome dynamics." FEBS Lett 575(1-3): 64-70.

Haglund, K., P. P. Di Fiore, et al. (2003). "Distinct monoubiquitin signals in receptor endocytosis." Trends Biochem Sci 28(11): 598-603.

Hama, H., G. G. Tall, et al. (1999). "Vps9p is a guanine nucleotide exchange factor involved in vesicle-mediated vacuolar protein transport." J Biol Chem 274(21): 15284-91.

Han, L. and J. Colicelli (1995). "A human protein selected for interference with Ras function interacts directly with Ras and competes with Raf1." Mol Cell Biol 15(3): 1318-23.

Han, L., D. Wong, et al. (1997). "Protein binding and signaling properties of RIN1 suggest a unique effector function." Proc Natl Acad Sci U S A 94(10): 4954-9.

Hicke, L. and R. Dunn (2003). "Regulation of membrane protein transport by ubiquitin and ubiquitin-binding proteins." Annu Rev Cell Dev Biol 19: 141-72.

Hirst, J., W. W. Lui, et al. (2000). "A family of proteins with gamma-adaptin and VHS domains that facilitate trafficking between the trans-Golgi network and the vacuole/lysosome." J Cell Biol 149(1): 67-80.

Holthuis, J. C., B. J. Nichols, et al. (1998). "The syntaxin Tlg1p mediates trafficking of chitin synthase III to polarized growth sites in yeast." Mol Biol Cell 9(12): 3383-97.

Horazdovsky, B. F., G. R. Busch, et al. (1994). "VPS21 encodes a rab5-like GTP binding protein that is required for the sorting of yeast vacuolar proteins." Embo J 13(6): 1297-309.

Horazdovsky, B. F., B. A. Davies, et al. (1997). "A sorting nexin-1 homologue, Vps5p, forms a complex with Vps17p and is required for recycling the vacuolar protein-sorting receptor." Mol Biol Cell 8(8): 1529-41.

Horiuchi, H., R. Lippe, et al. (1997). "A novel Rab5 GDP/GTP exchange factor complexed to Rabaptin-5 links nucleotide exchange to effector recruitment and function." Cell 90(6): 1149-59.

Howe, C. L., J. S. Valletta, et al. (2001). "NGF signaling from clathrin-coated vesicles: evidence that signaling endosomes serve as a platform for the Ras-MAPK pathway." Neuron 32(5): 801-14.

Ito, T., T. Chiba, et al. (2001). "A comprehensive two-hybrid analysis to explore the yeast protein interactome." Proc Natl Acad Sci U S A 98(8): 4569-74.

Itzen, A., O. Pylypenko, et al. (2006). "Nucleotide exchange via local protein unfolding--structure of Rab8 in complex with MSS4." Embo J 25(7): 1445-55.

Jackson, C. L. and J. E. Casanova (2000). "Turning on ARF: the Sec7 family of guanine-nucleotide-exchange factors." Trends Cell Biol 10(2): 60-7.

John, J., R. Sohmen, et al. (1990). "Kinetics of interaction of nucleotides with nucleotide-free H-ras p21." Biochemistry 29(25): 6058-65.

Kajiho, H., K. Saito, et al. (2003). "RIN3: a novel Rab5 GEF interacting with amphiphysin II involved in the early endocytic pathway." J Cell Sci 116(Pt 20): 4159-68.

Kanekura, K., Y. Hashimoto, et al. (2005). "A Rac1/phosphatidylinositol 3-kinase/Akt3 anti-apoptotic pathway, triggered by AlsinLF, the product of the ALS2 gene, antagonizes Cu/Zn-superoxide dismutase (SOD1) mutant-induced motoneuronal cell death." J Biol Chem 280(6): 4532-43.

Kang, R. S., C. M. Daniels, et al. (2003). "Solution structure of a CUE-ubiquitin complex reveals a conserved mode of ubiquitin binding." Cell 113(5): 621-30.

Katzmann, D. J., M. Babst, et al. (2001). "Ubiquitin-dependent sorting into the multivesicular body pathway requires the function of a conserved endosomal protein sorting complex, ESCRT-I." Cell 106(2): 145-55.

Kauppi, M., A. Simonsen, et al. (2002). "The small GTPase Rab22 interacts with EEA1 and controls endosomal membrane trafficking." J Cell Sci 115(Pt 5): 899-911.

Keller, R. (2004). The Computer Aided Resonance Assignment Tutorial, Cantina Verlag.

Klionsky, D. J., P. K. Herman, et al. (1990). "The fungal vacuole: Composition, function and biogenesis." Microbiol. Rev. 54: 266-292.

Kouranov, A., L. Xie, et al. (2006). "The RCSB PDB information portal for structural genomics." Nucleic Acids Res 34(Database issue): D302-5.

Krogan, N. J., G. Cagney, et al. (2006). "Global landscape of protein complexes in the yeast Saccharomyces cerevisiae." Nature 440(7084): 637-43.

Lee, S., Y. C. Tsai, et al. (2006). "Structural basis for ubiquitin recognition and autoubiquitination by Rabex-5." Nat Struct Mol Biol 13(3): 264-71.

Letunic, I., R. R. Copley, et al. (2004). "SMART 4.0: towards genomic data integration." Nucleic Acids Res 32(Database issue): D142-4.

Lewis, M. J., B. J. Nichols, et al. (2000). "Specific retrieval of the exocytic SNARE Snc1p from early yeast endosomes." Mol Biol Cell 11(1): 23-38.

Li, G., C. D'Souza-Schorey, et al. (1997). "Uncoupling of membrane ruffling and pinocytosis during Ras signal transduction." J Biol Chem 272(16): 10337-40.

Lippe, R., M. Miaczynska, et al. (2001). "Functional synergy between Rab5 effector Rabaptin-5 and exchange factor Rabex-5 when physically associated in a complex." Mol Biol Cell 12(7): 2219-28.

Lodhi, I. J., S. H. Chiang, et al. (2007). "Gapex-5, a Rab31 guanine nucleotide exchange factor that regulates Glut4 trafficking in adipocytes." Cell Metab 5(1): 59-72.

Macara, I. G., K. M. Lounsbury, et al. (1996). "The Ras superfamily of GTPases." Faseb J 10(5): 625-30.

Mandell, J. G., A. Baerga-Ortiz, et al. (2005). "Measurement of solvent accessibility at protein-protein interfaces." Methods Mol Biol 305: 65-80.

Mattera, R., C. N. Arighi, et al. (2003). "Divalent interaction of the GGAs with the Rabaptin-5-Rabex-5 complex." Embo J 22(1): 78-88.

Mattera, R., Y. C. Tsai, et al. (2006). "The Rab5 guanine nucleotide exchange factor Rabex-5 binds ubiquitin (Ub) and functions as a Ub ligase through an atypical Ub-interacting motif and a zinc finger domain." J Biol Chem 281(10): 6874-83.

McBride, H. M., V. Rybin, et al. (1999). "Oligomeric complexes link Rab5 effectors with NSF and drive membrane fusion via interactions between EEA1 and syntaxin 13." Cell 98(3): 377-86.

Mesa, R., J. Magadan, et al. (2005). "Overexpression of Rab22a hampers the transport between endosomes and the Golgi apparatus." Exp Cell Res 304 (2): 339-53.

Mesa, R., C. Salomon, et al. (2001). "Rab22a affects the morphology and function of the endocytic pathway." J Cell Sci 114(Pt 22): 4041-9.

Mossessova, E., R. A. Corpina, et al. (2003). "Crystal structure of ARF1*Sec7 complexed with Brefeldin A and its implications for the guanine nucleotide exchange mechanism." Mol Cell 12(6): 1403-11.

Mossessova, E., J. M. Gulbis, et al. (1998). "Structure of the guanine nucleotide exchange factor Sec7 domain of human arno and analysis of the interaction with ARF GTPase." Cell 92(3): 415-23.

Nielsen, E., F. Severin, et al. (1999). "Rab5 regulates motility of early endosomes on microtubules." Nat Cell Biol 1(6): 376-82.

Novick, P., M. Medkova, et al. (2006). "Interactions between Rabs, tethers, SNAREs and their regulators in exocytosis." Biochem Soc Trans 34(Pt 5): 683-6.

Novick, P. J., B. Goud, et al. (1988). "Regulation of vesicular traffic by a GTP-binding protein on the cytoplasmic surface of secretory vesicles in yeast." Cold Spring Harb Symp Quant Biol 53 Pt 2: 637-47.

Nuoffer, C., S. K. Wu, et al. (1997). "Mss4 does not function as an exchange factor for Rab in endoplasmic reticulum to Golgi transport." Mol Biol Cell 8(7): 1305-16.

Odorizzi, G., C. R. Cowles, et al. (1998). "The AP-3 complex: a coat of many colours." Trends Cell Biol. 8: 282-288.

Orban, P. C., P. F. Chapman, et al. (1999). "Is the Ras-MAPK signalling pathway necessary for long-term memory formation?" Trends Neurosci 22(1): 38-44.

Ortiz, D., M. Medkova, et al. (2002). "Ypt32 recruits the Sec4p guanine nucleotide exchange factor, Sec2p, to secretory vesicles; evidence for a Rab cascade in yeast." J Cell Biol 157(6): 1005-15.

Ostermeier, C. and A. T. Brunger (1999). "Structural basis of Rab effector specificity: crystal structure of the small G protein Rab3A complexed with the effector domain of rabphilin-3A." Cell 96(3): 363-74.

Otomo, A., S. Hadano, et al. (2003). "ALS2, a novel guanine nucleotide exchange factor for the small GTPase Rab5, is implicated in endosomal dynamics." Hum Mol Genet 12(14): 1671-87.

Penengo, L., M. Mapelli, et al. (2006). "Crystal structure of the ubiquitin binding domains of rabex-5 reveals two modes of interaction with ubiquitin." Cell 124(6): 1183-95.

Pereira-Leal, J. B. and M. C. Seabra (2001). "Evolution of the Rab family of small GTP-binding proteins." J Mol Biol 313(4): 889-901.

Pfeffer, S. R. (2005). "Structural clues to Rab GTPase functional diversity." J Biol Chem 280(16): 15485-8.

Ponting, C. P. (2000). "Proteins of the endoplasmic-reticulum-associated degradation pathway: domain detection and function prediction." Biochem J 351 Pt 2: 527-35.

Prag, G., S. Misra, et al. (2003). "Mechanism of ubiquitin recognition by the CUE domain of Vps9p." Cell 113(5): 609-20.

Prescianotto-Baschong, C. and H. Riezman (2002). "Ordering of compartments in the yeast endocytic pathway." Traffic 3(1): 37-49.

Renault, L., B. Guibert, et al. (2003). "Structural snapshots of the mechanism and inhibition of a guanine nucleotide exchange factor." Nature 426(6966): 525-30.

Riccio, A., B. A. Pierchala, et al. (1997). "An NGF-TrkA-mediated retrograde signal to transcription factor CREB in sympathetic neurons." Science 277 (5329): 1097-100.

Rodriguez-Gabin, A. G., M. Cammer, et al. (2001). "Role of rRAB22b, an oligodendrocyte protein, in regulation of transport of vesicles from trans Golgi to endocytic compartments." J Neurosci Res 66(6): 1149-60.

Rothman, J. H. and T. H. Stevens (1986). "Protein sorting in yeast: Mutants defective in vacuole biogenesis mislocalization vacuolar proteins into the late secretory pathway." Cell 47: 1041-1051.

Rotin, D., O. Staub, et al. (2000). "Ubiquitination and endocytosis of plasma membrane proteins: role of Nedd4/Rsp5p family of ubiquitin-protein ligases." J Membr Biol 176(1): 1-17.

Saito, K., J. Murai, et al. (2002). "A novel binding protein composed of homophilic tetramer exhibits unique properties for the small GTPase Rab5." J Biol Chem 277(5): 3412-8.

Samanta, M. P. and S. Liang (2003). "Predicting protein functions from redundancies in large-scale protein interaction networks." Proc Natl Acad Sci U S A 100(22): 12579-83.

Sato, M., K. Sato, et al. (2005). "Caenorhabditis elegans RME-6 is a novel regulator of RAB-5 at the clathrin-coated pit." Nat Cell Biol 7(6): 559-69.

Sato, Y., R. Shirakawa, et al. (2007). "Asymmetric coiled-coil structure with Guanine nucleotide exchange activity." Structure 15(2): 245-52.

Schnatwinkel, C., S. Christoforidis, et al. (2004). "The Rab5 effector Rabankyrin-5 regulates and coordinates different endocytic mechanisms." PLoS Biol 2(9): E261.

Seals, D. F., G. Eitzen, et al. (2000). "A Ypt/Rab effector complex containing the Sec1 homolog Vps33p is required for homotypic vacuole fusion." Proc Natl Acad Sci U S A 97(17): 9402-7.

Seaman, M. N., J. M. McCaffery, et al. (1998). "A membrane coat complex essential for endosome-to-Golgi retrograde transport in yeast." J Cell Biol 142(3): 665-81.

Segev, N. (2001). "Ypt and Rab GTPases: insight into functions through novel interactions." Curr Opin Cell Biol 13(4): 500-11.

Semisotnov, G. V., N. A. Rodionova, et al. (1991). "Study of the "molten globule" intermediate state in protein folding by a hydrophobic fluorescent probe." Biopolymers 31(1): 119-28.

Seshan, A. and A. Amon (2005). "Ras and the Rho effector Cla4 collaborate to target and anchor Lte1 at the bud cortex." Cell Cycle 4(7): 940-6.

Shiba, Y., H. Takatsu, et al. (2002). "Gamma-adaptin interacts directly with Rabaptin-5 through its ear domain." J Biochem (Tokyo) 131(3): 327-36.

Shih, S. C., G. Prag, et al. (2003). "A ubiquitin-binding motif required for intramolecular monoubiquitylation, the CUE domain." Embo J 22(6): 1273-81.

Simon, I., M. Zerial, et al. (1996). "Kinetics of interaction of Rab5 and Rab7 with nucleotides and magnesium ions." J Biol Chem 271(34): 20470-8.

Simpson, J. C., G. Griffiths, et al. (2004). "A role for the small GTPase Rab21 in the early endocytic pathway." J Cell Sci 117(Pt 26): 6297-311.

Simpson, J. C. and A. T. Jones (2005). "Early endocytic Rabs: functional prediction to functional characterization." Biochem Soc Symp(72): 99-108.

Singer-Kruger, B., H. Stenmark, et al. (1994). "Role of three rab5-like GTPases, Ypt51p, Ypt52p, and Ypt53p, in the endocytic and vacuolar protein sorting pathways of yeast." J Cell Biol 125(2): 283-98.

Singer-Kruger, B., H. Stenmark, et al. (1995). "Yeast Ypt51p and mammalian Rab5: counterparts with similar function in the early endocytic pathway." J Cell Sci 108 (Pt 11): 3509-21.

Soisson, S. M., A. S. Nimnual, et al. (1998). "Crystal structure of the Dbl and pleckstrin homology domains from the human Son of sevenless protein." Cell 95(2): 259-68.

Sorkin, A. and M. Von Zastrow (2002). "Signal transduction and endocytosis: close encounters of many kinds." Nat Rev Mol Cell Biol 3(8): 600-14.

Sprang, S. R. (1997). "G protein mechanisms: insights from structural analysis." Annu Rev Biochem 66: 639-78.

Stenmark, H., R. G. Parton, et al. (1994). "Inhibition of rab5 GTPase activity stimulates membrane fusion in endocytosis." Embo J 13(6): 1287-96.

Stevens, T., B. Esmon, et al. (1982). "Early stages in the yeast secretory pathway are required for transport of carboxypeptidase Y to the vacuole." Cell 30 (2): 439-48.

Stroupe, C. and A. T. Brunger (2000). "Crystal structures of a Rab protein in its inactive and active conformations." J Mol Biol 304(4): 585-98.

Szabo, K., G. Jekely, et al. (2001). "Cloning and expression of sprint, a Drosophila homologue of RIN1." Mech Dev 101(1-2): 259-62.

Tall, G. G., M. A. Barbieri, et al. (2001). "Ras-activated endocytosis is mediated by the Rab5 guanine nucleotide exchange activity of RIN1." Dev Cell 1 (1): 73-82.

Topp, J. D., N. W. Gray, et al. (2004). "Alsin is a Rab5 and Rac1 guanine nucleotide exchange factor." J Biol Chem 279(23): 24612-23.

Tudor, E. L., M. S. Perkinton, et al. (2005). "ALS2/ALSIN regulates RAC-PAK signalling and neurite outgrowth." J Biol Chem.

Valsdottir, R., H. Hashimoto, et al. (2001). "Identification of rabaptin-5, rabex-5, and GM130 as putative effectors of rab33b, a regulator of retrograde traffic between the Golgi apparatus and ER." FEBS Lett 508(2): 201-9.

van der Sluijs, P., M. Hull, et al. (1992). "The small GTP-binding protein rab4 controls an early sorting event on the endocytic pathway." Cell 70(5): 729-40.

Vitale, G., V. Rybin, et al. (1998). "Distinct Rab-binding domains mediate the interaction of Rabaptin-5 with GTP-bound Rab4 and Rab5." Embo J 17 (7): 1941-51.

Vojtek, A. B., S. M. Hollenberg, et al. (1993). "Mammalian Ras interacts directly with the serine/threonine kinase Raf." Cell 74(1): 205-14.

Vollert, C. S. and P. Uetz (2004). "The phox homology (PX) domain protein interaction network in yeast." Mol Cell Proteomics 3(11): 1053-64.

Walch-Solimena, C., R. N. Collins, et al. (1997). "Sec2p mediates nucleotide exchange on Sec4p and is involved in polarized delivery of post-Golgi vesicles." J Cell Biol 137(7): 1495-509.

Wang, Y., R. T. Waldron, et al. (2002). "The RAS effector RIN1 directly competes with RAF and is regulated by 14-3-3 proteins." Mol Cell Biol 22(3): 916-26.

Weigert, R., A. C. Yeung, et al. (2004). "Rab22a regulates the recycling of membrane proteins internalized independently of clathrin." Mol Biol Cell 15(8): 3758-70.

Winzeler, E. A., D. D. Shoemaker, et al. (1999). "Functional characterization of the S. cerevisiae genome by gene deletion and parallel analysis." Science 285(5429): 901-6.

Worthylake, D. K., K. L. Rossman, et al. (2000). "Crystal structure of Rac1 in complex with the guanine nucleotide exchange region of Tiam1." Nature 408(6813): 682-8.

Wurmser, A. E., T. K. Sato, et al. (2000). "New component of the vacuolar class C-Vps complex couples nucleotide exchange on the Ypt7 GTPase to SNARE-dependent docking and fusion." J Cell Biol 151(3): 551-62.

Yang, Y., A. Hentati, et al. (2001). "The gene encoding alsin, a protein with three guanine-nucleotide exchange factor domains, is mutated in a form of recessive amyotrophic lateral sclerosis." Nat Genet 29(2): 160-5.

Yoshida, S., R. Ichihashi, et al. (2003). "Ras recruits mitotic exit regulator Lte1 to the bud cortex in budding yeast." J Cell Biol 161(5): 889-97.

Yu, H. and S. L. Schreiber (1995). "Structure of guanine-nucleotide-exchange factor human Mss4 and identification of its Rab-interacting surface." Nature 376(6543): 788-91.

Zerial, M. and H. McBride (2001). "Rab proteins as membrane organizers." Nat Rev Mol Cell Biol 2(2): 107-17.

Zhang, X., X. He, et al. (2006). "Varp is a Rab21 guanine nucleotide exchange factor and regulates endosome dynamics." J Cell Sci 119(Pt 6): 1053-62.

Zhao, X., A. Y. Chang, et al. (2007). "A role for Lte1p (a low temperature essential protein involved in mitosis) in proprotein processing in the yeast secretory pathway." J Biol Chem 282(3): 1670-8.

Zhu, G., P. Zhai, et al. (2004). "Structural basis of Rab5-Rabaptin5 interaction in endocytosis." Nat Struct Mol Biol 11(10): 975-83.

Zhu, Y., B. Doray, et al. (2001). "Binding of GGA2 to the lysosomal enzyme sorting motif of the mannose 6-phosphate receptor." Science 292(5522): 1716-8.

VITA

Darren Scott Carney was born in Newport Beach, California, on August 26, 1976, the son of Dr. Darrell Howard Carney and Margaret Anne Carney. Darren grew up in Dickinson, Texas, with his younger brother, Ryan. In 1994, after graduating as valedictorian at Dickinson High School, Darren enrolled at Trinity University in San Antonio, Texas. While at Trinity, he worked in the organic chemistry lab of Dr. Nancy Mills and played trombone in numerous ensembles. During the summers of 1996 through 1998, he worked for GalTech Wound Therapies and Chrysalis BioTechnology. In 1998, after receiving his Bachelor of Science with majors in Biology and Biochemistry, he entered the Graduate School of the Biomedical Sciences at the University of Texas Southwestern Medical Center at Dallas and worked under the guidance of Dr. Bruce Horazdovsky. From 2001 to 2002 he was awarded a DCMB training grant. In 2002, Darren moved with Dr. Horazdovsky and his lab from UT Southwestern to the Mayo Clinic College of Medicine in Rochester, Minnesota, where he finished his doctoral studies. After receiving his Ph.D., Darren will work with Dr. Horazdovksy and Dr. Brian Volkman at the Medical College of Wisconsin toward the completion of some of the subsequent NMR structural work discussed herein. Darren is an outspoken advocate of Macintosh computers and other Apple products. His amazing son, Landon Scott Carney, was born in 2002.

Permanent Address:

1125 Tallow Drive
Dickinson, Texas 77539